# A high-resolution hindcast of wind and waves for The North Sea, The Norwegian Sea and The Barents Sea



Mean Hs 1957-2002

**Magnar Reistad, Øyvind Breivik, Hilde Haakenstad, Ole Johan Aarnes and Birgitte R. Furevik**

# *report*

**Norwegian Meteorological Institute met.no**

| Title | Date |
|---|---|
| **A high-resolution hindcast of wind and waves for The North Sea, The Norwegian Sea and The Barents Sea** | 2009-12-22 |

| Section | Report no. |
|---|---|
| VV/FoU | 2009/14 |

| Author(s) | Classification |
|---|---|
| Magnar Reistad, Øyvind Breivik, Hilde Haakenstad, Ole Johan Aarnes, Birgitte R. Furevik | ☐ Free ☒ Restricted |
| | **ISSN** 1503-8025 |
| | **e-ISSN** |

| Client(s) | Client s reference |
|---|---|
| Norwegian Deepwater Programme | C06200-NDP |

**Abstract**

A combined high-resolution atmospheric downscaling and wave hindcast based on the ERA40 reanalysis covering the Norwegian Sea, the North Sea and the Barents Sea. The period covered is September 1957 to August 2002 with an extension to the end of 2008 using analyzed fields from ECMWF. The HIRLAM atmospheric downscaling is performed as a series of short prognostic runs initialized from ERA40 (later operational analyses) and the previous integration and with ERA40 on the boundary. The nested WAM wave model hindcast consists of an outer 50 km model covering the North Atlantic and an inner 10-11 km resolution model covering the same domain as HIRLAM . The ice edge is updated every 10-11 days.

A comprehensive comparison against coastal and open-ocean stations as well as co-located satellite observations of wind speed and significant wave height reveals a significant improvement of both mean values (mean absolute error, mean error) and the upper percentiles in both wind speed and the significant wave height. The probability distribution of the wind speed and the wave height is also found to correspond better with the observed distribution.

Trend analysis reveals an increase in both mean and upper percentiles of the significant wave height, statistically significant for limited geographical regions and generally consistent with the findings of other workers.

| Keywords |
|---|
| Wave hindcast, atmospheric downscaling, wave and wind climate |

| Disiplinary signature | Responsible signature |
|---|---|
| **Magnar Reistad** | **Karen H Doublet** |

# A high-resolution hindcast of wind and waves for The North Sea, The Norwegian Sea and The Barents Sea

## 1 Introduction

Reliable historical wind and wave data are important in designing offshore installations and in planning offshore operations. But often there are not sufficient measurements to make good estimates of the probability distribution for wind and wave parameters necessary to make accurate calculations of design loads on offshore structures. The measured time series are also too short to make realistic simulations of offshore operations, *e.g.* calculate the long-term probability of weather windows and threshold levels of wind and waves. Hindcast data are produced by running numerical models based on historical data. A hindcast archive properly evaluated against reliable measurements represents a powerful proxy for long instrument time series. Furthermore, a hindcast archive is area-covering and as such will yield statistics for whole regions and locations not specifically planned in advance. In previously unexplored areas like the Barents Sea where reliable measurement series are patchy or lacking entirely, a hindcast archive becomes even more important for assessing the climatology and the exceedence criteria for various geophysical parameters. The Arctic does however pose a particular challenge to hindcast and climate estimates as small-scale polar lows and the precise location of the ice edge demand high-resolution models of the atmosphere and the wave field.

An atmospheric reanalysis is a rerun of the past using a subset of available observations and a fixed model setup and data assimilation scheme to minimize the drift in error statistics (*i.e.* keep the error statistics as stationary as possible by keeping the set of observations as stable as possible) over the period (Bromwich *et. al*., 2007). The most commonly used global atmospheric reanalyses today are the European Reanalysis project (ERA40, see Uppala *et. al*., 2005), the 40-year reanalysis of the National Centers for Environmental Prediction/National Center (NCEP/NCAR) for Atmospheric Research Reanalysis (NRA), see Kalnay *et. al*. (1996) and the Japanese Reanalysis (JRA-25, see Onogi *et. al*., 2005). Of these, ERA40 has the highest resolution (together with JRA-25) and covers the longest period. The resolution of the ERA40 and JRA-25 is approximately 125 km, while the resolution of the NCEP/NCAR reanalysis is approximately 210 km. Although these reanalyses represent the best available long-term global statistics, none of these fields can resolve mesoscale phenomena nor can they come close to modelling coastal wind conditions. The aim of downscaling a reanalysis is to resolve the interaction of large-scale flow with regional physiographic details in the high resolution forecast model and thus form realistic mesoscale features.

Wave hindcast integrations are similar to atmospheric reanalyses in their attempt to recreate past conditions as accurately as possible. However, atmospheric reanalyses rely on the assimilation of observations, while the general scarcity of wave observations, especially before the advent of satellite altimetry, means that wave hindcast integrations usually rely only on wind forcing without data assimilation. With the notable exception of the wave field produced by ERA40 (Uppala *et. al.*, 2005), where a wave model was coupled to the atmospheric component, wave hindcast studies generally involve a one-way forcing of the sea state by the near-surface wind field. Several hindcast studies have been performed on 10 m wind fields ($U_{10}$) computed from estimates based on wind and pressure observations and atmospheric analyses (Cox *et. al.*, 1995, WASA-group, 1998, Günther *et. al.*, 1998, Wang and Swail, 2001 and Wang and Swail, 2002). These can produce good results, but the quality of the wind field estimates are limited by the amount of surface observations and tend to be rather coarse. With the advent of full atmospheric reanalyses, several studies have exploited the wind fields thus produced. Several coarse-resolution wave hindcast studies have exploited NRA winds (Swail and Cox, 2000 and Cox and Swail,

2001). Similarly, Sterl *et. al.* (1998) performed a global wave hindcast study based on the 15-year atmospheric reanalysis ERA15, the precursor to ERA40 (Gibson *et. al.*, 1996, 1997). More recently, Sterl and Caires (2005) reported 100-year return estimates for significant wave height based on ERA40.

Very few attempts have been made to date to produce long-term wave hindcasts on high resolution. Weisse and Gunther (2007) carried out a very-high (5.5 km) resolution wave hindcast integration based on a regional downscaling of the NCEP reanalysis (NRA). However, the model domain was limited to the Southern North Sea. Our study attempts to model the wave climate of the North Sea, the Norwegian Sea and the Barents Sea by resolving the most important features of the wind field, the ice cover and the topography that influence the wave field in the coastal zone and the open ocean by going to approximately 10 km resolution.

## 1.1 Previous hindcast projects at the Norwegian Meteorological Institute

The Norwegian Meteorological Institute has over the past 30 years carried out several hindcast projects to meet the need for long term time series of wind and waves from the oil industry. In the first extensive hindcast (Haug and Guddal, 1981), wind and wave data were estimated from air pressure fields in a 150 km grid using the first generation wave model NOWAMO. The air pressure fields were digitised from operational weather maps. To improve the estimates of atmospheric fields a new project was initiated in 1982 (Eide *et. al.*, 1985). Observations of air pressure were collected and used in an objective pressure analysis with the old pressure fields as first guess. However, the most significant improvement was the introduction of the second generation wave model WINCH. The second hindcast project established a data base of wind and waves for the years 1955-1981. This archive has since been regularly updated. The homogeneity of such long data series is always a problem. Even when the same methods are applied, different data coverage and data quality may create statistics with nonstationary error terms. There are several sources of inhomogeneities in the current hindcast data, among those the shift to pressure analyses from the numerical weather prediction introduced in 1982 (Reistad and Iden, 1998).

Since the previous Norwegian hindcast project was completed more than 20 years ago, great strides have been made in the field of numerical weather and wave prediction. Numerics, assimilation techniques and the spatial resolution have been much improved while computing power has grown exponentially. The advent of high quality boundary data through global reanalysis projects has now opened the possibility to build a new hindcast archive for Norwegian waters which resolves spatial scales an order of magnitude smaller than previous hindcast archives.

## 1.2 The ERA40 global reanalysis project

ERA40 is a global coupled atmosphere-wave reanalysis of the atmosphere covering the 45 years from September 1957 to August 2002. ERA40 was produced using the Integrated Forecasting System version T159L60 of The European Centre for Medium-Range Weather Forecasts (ECMWF). Atmospheric fields are available every six hours with approximately 1.125 degrees horizontal resolution. Wave fields were generated with the WAM model (WAMDI, 1988) coupled to the atmospheric component. The horizontal resolution of the wave model is 1.5 degrees. Angular resolution is 30 degrees (12 directional bins) and the frequency resolution is logarithmic, spanning the range from 0.0420 to 0.4137Hz. By keeping the model system and data assimilation system invariant over the 45-year integration period the error statistics are quite stationary, although the amount of observations is not constant over the period. In particular the amount of satellite data has increased dramatically during the last two decades. The ERA40 reanalysis was

completed in 2003, see Uppala *et. al.* (2005) for a comprehensive overview of ERA40. The archive is relatively coarse compared with operational high-resolution data assimilation systems, but gives a good reproduction of most large-scale dynamical features.

# 2   Downscaling the ERA40 reanalysis

We have performed a regional downscaling of the ERA40 reanalysis to produce detailed, atmospheric fields using a high-resolution numerical weather prediction model, The High Resolution Limited Area Model (HIRLAM, see Undén *et. al*., 2002) on 10-11 km resolution, hereafter known as HIRLAM10. A version of the WAM wave model on the same grid was then forced with the down-scaled wind fields (hereafter named WAM10). The primary objective has been to provide reliable high-resolution wind and wave fields for Norwegian waters, hence the main focus of this report will be on the quality of the wind and wave parameters produced.

## *2.1   Dynamical downscaling and filtering of the atmospheric fields*

HIRLAM version 6.4.2 is a hydrostatic numerical weather prediction (NWP) model with a semi-implicit semi-Lagrangian two-time level integration scheme for the integration of the model equations. A hybrid coordinate is used for the vertical with pressure levels at the top gradually transitioning to terrain-following coordinates near the surface. A summary of the model equations is given in Appendix A.1.1. Further details on the discretization of the model equations, the handling of non-linear terms, diffusion and boundary relaxation can be found in Chapter 2 of Undén *et. al*. (2002).

The downscaling consisted of a 10km resolution model domain for HIRLAM with ERA40 on the lateral boundaries. The model domain is a rotated spherical grid with the South Pole positioned at 22ºS, 040ºW, see Figure 1. The model domain is resolved by 248x400 grid points with 0.1º horizontal grid resolution (10-11 km).  The vertical is resolved by 40 hybrid levels with variable grid spacing (denser near the surface).
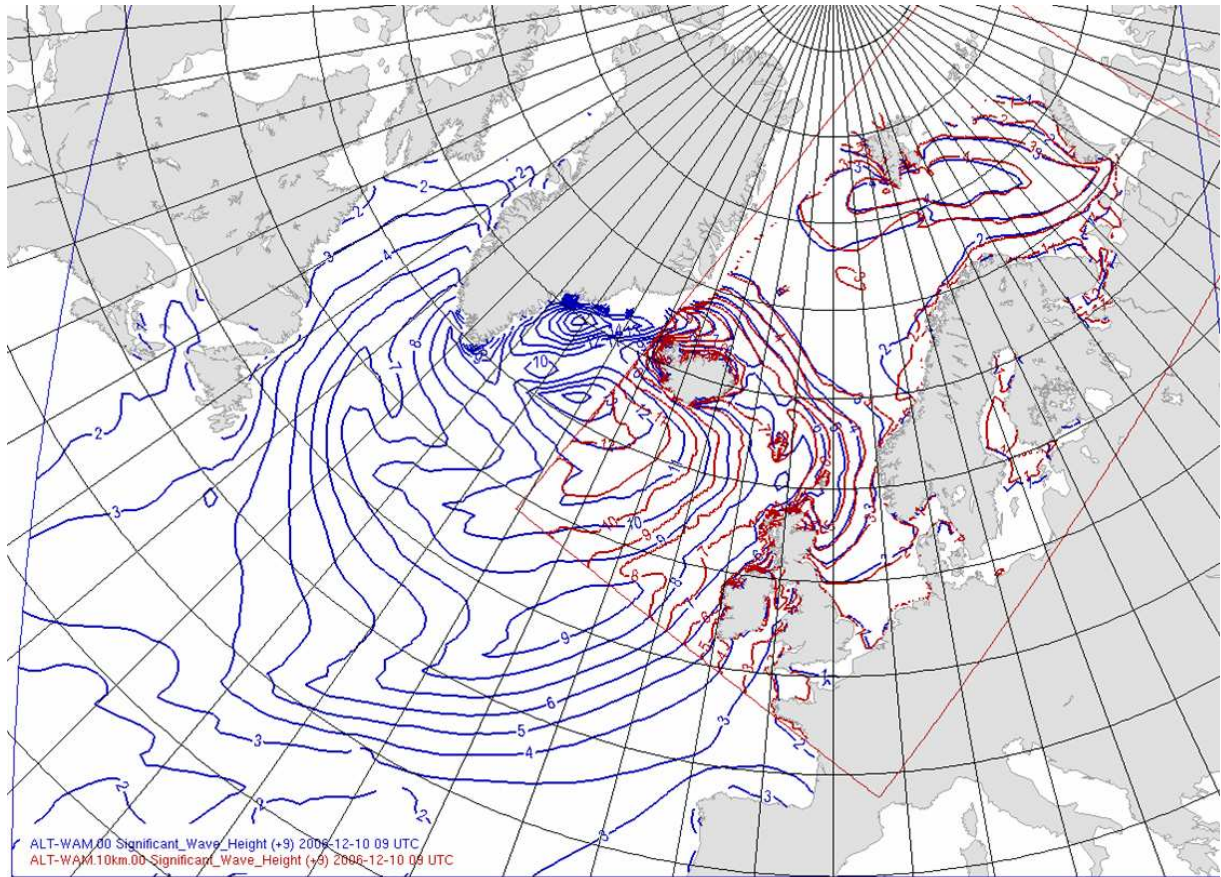
Figure 1. Model domains. HIRLAM10 and WAM10 model domains (identical) are shown in red. The WAM50 model domain is shown in blue. Both domains are rotated spherical projections. A new nesting procedure was developed to allow arbitrary model-domain configurations. The model projection of HIRLAM10/WAM10 has the South Pole positioned at 22ºS, 040ºW. The grid is 248x400 confined by boundaries at 13.25ºS, 26.65ºN, 005.75ºW and 030.45ºE in the rotated spherical projection. The spatial resolution is 0.1º (10-11km).

The model is forced by ERA40 on the boundaries with pressure, temperature, wind velocity, specific humidity and cloud water in all 40 model levels with six-hourly temporal resolution (no higher temporal resolution is available from ERA40). The fields are blended with the last forecast in the beginning of each cycle prior to the forecast integration as described below. Daily fields of sea surface temperature, sea ice fraction and snow depth are also retrieved from ERA40. The ERA40 sea surface temperature fields and sea ice fraction are extrapolated towards the higher resolution coasts in the HIRLAM grid by use of a grid-filling routine.

A sequence of 9-hourly model runs is performed starting from an initialization where ERA40 is blended with the previous 6-h forecast field (the background field) in the interior of the domain. This is done to control the large-scale features of the forecasts (Yang, 2005). The blending is generated by an incremental digital filter initialization (IDFI) scheme (Lynch and Huang, 1994 and Lynch, 1997) with a Dolph window filter, which starts with a 2-hour backward integration to get a filtered model state valid at time -1 hour. The integration is then re-started from -1 hours and integrates 2 hours forward to arrive at the filtered model state at +0 hours. This digital filtering procedure is applied twice; once to the ERA40 fields and once to the background fields. The initialization increment (the difference between the two filtered states) is then added to the background model state to obtain the initialized model state. The parameters which are affected by the incremental digital filter are the pressure and wind velocity, temperature, specific humidity and cloud water in all model levels. The incremental digital filtering initialization is meant to preserve quickly evolving modes in the first-guess (Huang and Yang, 2002). A comparison of IDFI to other filtering techniques can be found in Huang and Yang (2002).

The physical parameterizations in the model comprise processes of radiation, sub-grid scale transports, thermodynamics and surface processes. Physical schemes which are used in the model are the Straco condensation scheme, ISBA surface scheme, TKE-l turbulence scheme and Savijärvi radiation scheme (see Chapter 3 in Undén *et. al*., 2002, for details or Appendix A.1.2 for a short summary).

### 2.1.1  Optimizing the initialization of HIRLAM

A downscaling of the months of February 1978 and January 2000 was performed prior to the production of the hindcast archive to test the performance of the downscaling. We found the lowest root mean square error (RMSE) at +6 hours (see Figure 2 panels c and d). ERA40 shows smaller differences with forecast time. The mean error (ME) is significantly lower better at +6 hours in the February 1978 case, and comparable to the analysis (+0 h) in the January 2000 case. Based on these results we chose to perform the hindcast in sequences of 9-hour integrations every 6 hours (00, 06, 12 and 18 UTC) from blended fields of the previous HIRLAM run at +6 h and ERA40. For consistency we have in the following also evaluated the model performance at +6 hours.

Figure 2 (c) and (d) also confirm that the choice of using the incremental digital filtering initialization results in an improved initialized field for the forecast.



(a)          Mean Error, 197802

(b)          Mean Error, 200001

Red line: HIRLAM,  Blue line: ERA40

Red line: HIRLAM,  Blue line: ERA40

(c)          Root Mean Square Error, 197802

(d)          Root Mean Square Error, 200001

Red line: HIRLAM,  Blue line: ERA40

Red line: HIRLAM,  Blue line: ERA40
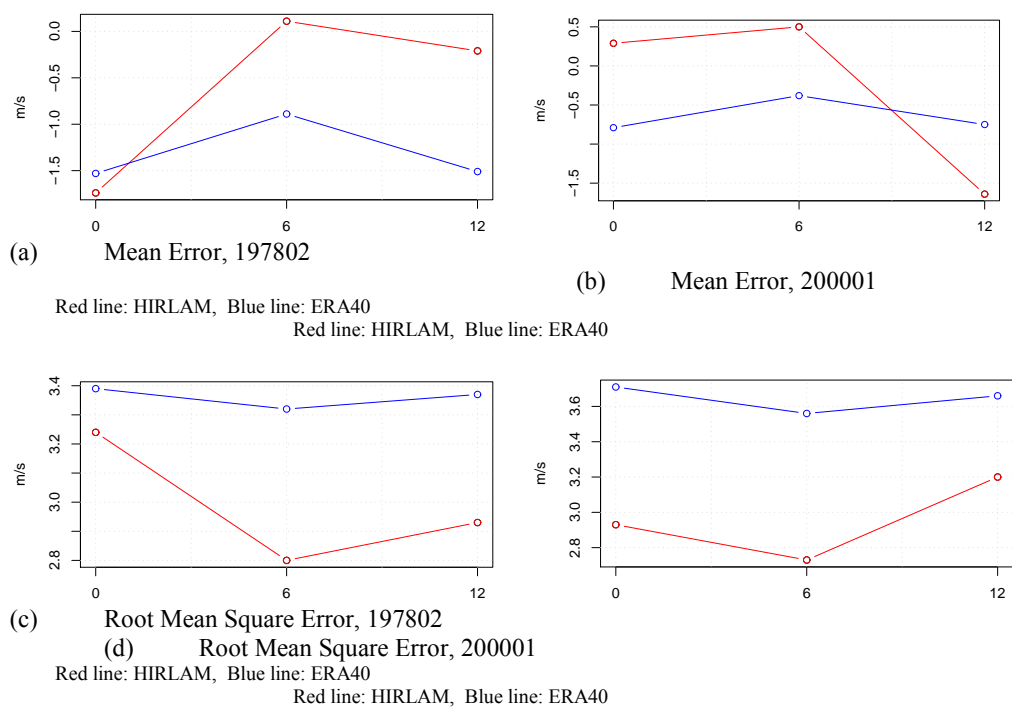
Figure 2. Averaged results at the start time and for the lead times +6 and +12 hours for the months February 1978 and January 2001.

## *2.2  The wave model configuration*

The wave hindcast was generated using a modified version of the WAM Cycle 4 model (WAMDI 1988, Komen *et. al*. 1994, Gunther *et. al*., 1992) set up on the same rotated spherical grid as HIRLAM10. The model is nested inside a 50 km resolution WAM model covering most of the North Atlantic to ensure realistic swell intrusion from the North Atlantic (hereafter referred to as WAM50). The model domains are shown in Figure 1. A new nesting procedure has been developed to allow arbitrary orientation of outer and inner model domains (see Breivik *et. al*.,

2009). The model is set up with twice as many directional bins as ERA40 (15 degrees, 24 bins) and the same 25 frequency bins as ERA40. Ice coverage is updated three times per month.

# 3 Performance of the downscaling

The quality of the atmospheric downscaling has been evaluated in terms of the performance of 10 m wind speed, mean sea level pressure (MSLP) and 2 m temperature (T2m). See Appendix A.1.3 for a list of parameter definitions. The parameters have been compared with observations at 00, 06, 12 and 18 UTC corresponding to the 6 h forecasts of HIRLAM and the analysis of ERA40. Furthermore, two years of QuikSCAT/SeaWinds scatterometer winds have been co-located with HIRLAM10 wind fields providing a domain-wide comparison with satellite observations. Similarly, the performance of the wave model has been compared in terms of significant wave height against *in situ* and satellite altimeter observations.

## 3.1 Atmospheric downscaling

All weather stations having continuous and reliable observations over approximately the whole period (22 stations) have been used to evaluate the performance of HIRLAM and ERA40. These stations are: Jan Mayen, Torsvåg lighthouse, Fruholmen lighthose, Banak, Hopen, Slettnes lighthouse, Kirkenes airport, Vardø, Myken, Bodø, Ørland, Nordøyan lighthouse, Værnes, Gardermoen, Utsira lighthouse, Sola, Lista lighthouse, Oksøy lighthouse, Bjørnøya (1962), Skrova lighthouse (1966), Lindesnes lighthouse (1968) and Svinøy lighthouse (1970). A detailed list of the stations is found in Table A.4.3 of Appendix 1.

| WIND 10 m (m/s) | ME | MAE | RMSE |
|---|---|---|---|
| **HIRLAM** | **0.03** | **1.95** | **2.46** |
| ERA40 | -0.86 | 2.36 | 2.94 |
| MSLP (hPa) | ME | MAE | RMSE |
| **HIRLAM** | **0.15** | **0.77** | **0.99** |
| ERA40 | 0.11 | 0.56 | 0.71 |
| T2M (K) | ME | MAE | RMSE |
| **HIRLAM** | **0.27** | **1.37** | **1.77** |
| ERA40 | -0.34 | 1.34 | 1.68 |

Table 1. Summarized statistics averaged over the whole period.

Table 1 shows that HIRLAM10 has a better overall performance in terms of 10 m wind speed. The mean absolute error (MAE) is 0.41 m/s (17% reduction) lower than ERA40 and the root-mean-square error (RMSE) is 0.5 m/s lower than ERA40. ERA40 is generally underestimating the 10m wind speed with a mean error of -0.86 m/s, while HIRLAM has negligible bias.

ERA40 has a mean error of only 0.11 hPa in MSLP, a mean absolute error of 0.56 hPa and a root mean square of 0.71 hPa. Bromewich et. al. (2007) found that *ERA40 resolves the atmospheric general circulation in the North Atlantic with fidelity* and this is consistent with our findings. HIRLAM follows closely with a good representation of the dominating synoptic scale pressure field, albeit with slightly higher mean and RMS error.

ERA40 is also modelling the 2m temperature (T2m) somewhat better than HIRLAM which has a lower mean error but somewhat larger mean absolute error and also a larger root mean square error. HIRLAM tends to overestimate T2m, while ERA40 is underestimating somewhat. The net overestimation of T2m in HIRLAM is a well known problem and the error is to a large degree caused by the definition of T2m averaged linearly over the different tiles inside a grid square in the coastal zone (see Homleid, 2008). The water tile will influence the T2m value resulting in too high temperatures at coastal stations in the winter time. In the hindcast archive we have stored

T2m on each tile and also the tile fractions and there is a possibility of making a more optimal weighting of the contribution from each tile.

### 3.1.1  Long term (45-year) average surface wind speed

Figure 3 shows a comparison of the mean 10 m wind speed (vector-averaged) over the 45-year period in HIRLAM (Panel a), ERA40 (Panel b) and the vector average of their difference (Panel c). For both HIRLAM and ERA40 the the westerlies south of Iceland away from continental influence are the strongest average winds in the model domain. The is much weaker over the continents where topographical and regional features dominate.

The smallest differences are found over the ocean while the largest differences are found at or near the continents (Panel c). Note from Panel c that there is a mean difference of 0.5 m/s over the ocean, HIRLAM yielding consistently higher winds. As will be seen in the model-observation comparison this is consistent with the bias found between ERA40 and observations from both satellite-borne instruments (scatterometer) and synoptic observations.

HIRLAM exhibits much more fine-scale features in the coastal zone and over the continents than the relatively smooth ERA40 fields.

a) HIRLAM 10m mean wind.

b) ERA40 10m mean wind.

c) The difference between HIRLAM 10m wind speed and ERA40 10m wind speed.
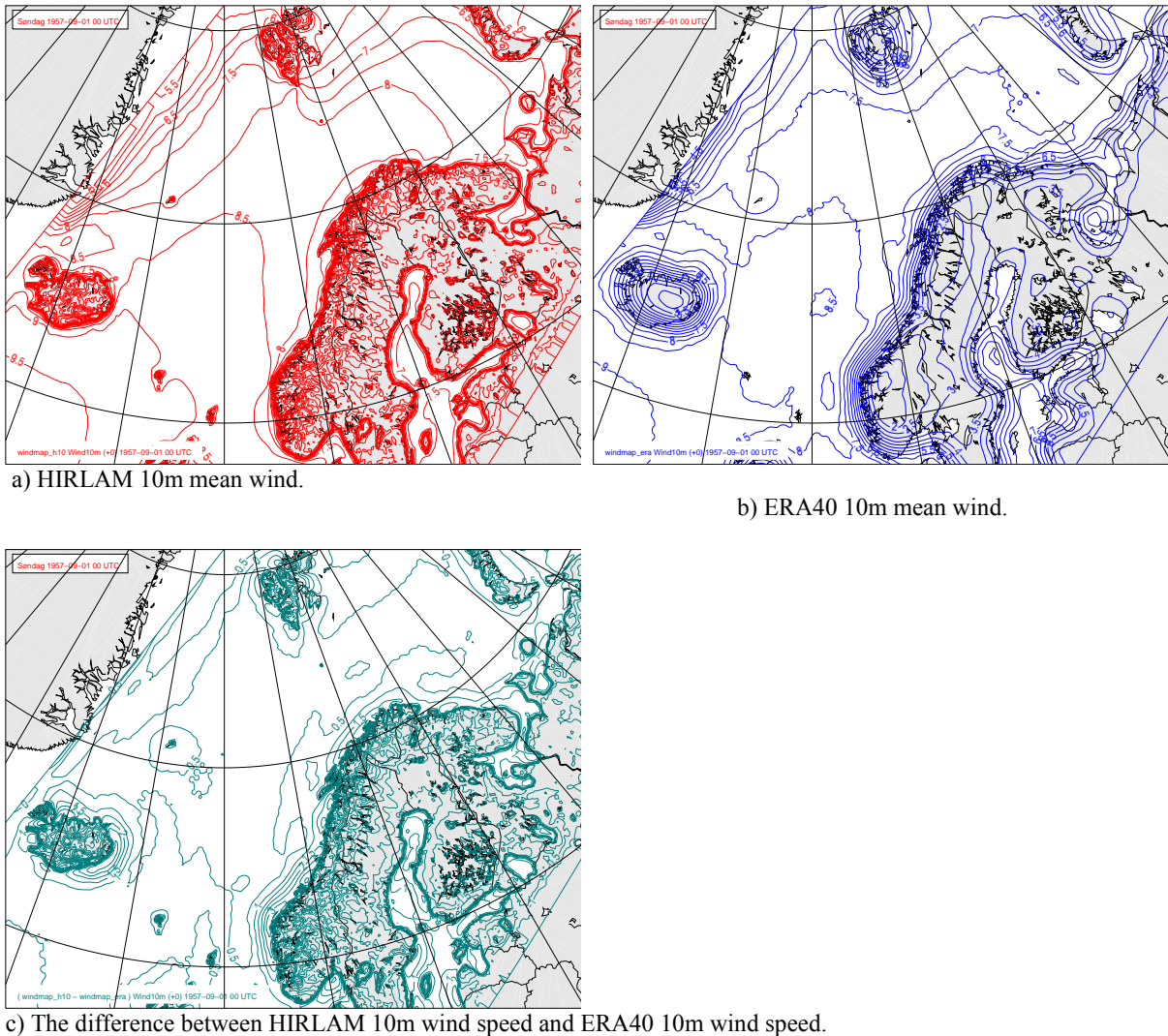
Figure 3.  Mean wind in 10m averaged over the period Sep 1957 to Aug 2002 for HIRLAM (a), ERA40 (b) and the difference between HIRLAM and ERA40 (c).

### 3.1.2 Time series of qualified observation stations

Figures 4-6 show time series of monthly values of ME, MAE and RMSE for 10m wind speed, MSLP and T2m.

Figure 4 (a) shows that HIRLAM has almost zero mean error (ME) in 10 m wind speed. There is no trend over the period. ERA40 underestimates the 10m wind speed (negative ME) while the RMSE and MAE are higher than for HIRLAM. There is a clear annual cycle with the highest errors occurring in the winter in both datasets.  Figure 4 b) shows some typical examples. The time series (December 1975) for Torsvåg lighthouse, Sletnes lighthouse, Bodø, and Ørlandet all illustrate that HIRLAM captures coastal wind conditions much better than ERA40.

Figure 5 (a) shows that ERA40 has negligible mean error in MSLP. ERA40 also shows stepwise improvement during the model period.  After the winter of 1966, the ERA40 MAE dropped to 0.5-0.7 hPa. After the winter of 1978 the MAE was further reduced to 0.4-0.6 hPa. This stepwise improvement is due to the increase in observations ingested by the 3D-Var data assimilation in ERA40 with time (Uppala *et. al.*, 2005, Figure 1). There is more variation in the time series of HIRLAM as can be expected from a higher resolution model. The difference compared with ERA40 is largest during the winter. A substantial contribution to the inferior representation of MSLP by HIRLAM is found in the Northern stations around Svalbard, Jan Mayen and Hopen (see Figure 5 b), but also some stations further south show a winter-time monthly MAE of more than 1 hPa.

Figure 6 (a)  shows that the HIRLAM curve has a significant annual cycle in ME of T2m. The ME is high in the winter and closer to zero or negative in summer. ERA40 does not show this annual variation in has an overall lower ME than HIRLAM, but ERA40 has a MAE and a RMSE comparable with HIRLAM. Figure 6 (b) shows some examples from December 1965, Jan Mayen, Fruholmen, Bodø and Utsira lighthouse. HIRLAM overpredicts T2m at these stations. ERA40 overpredicts T2m at Jan Mayen and underpredicts T2m at the other three stations.

**ME.  Wind 10m.  Reliable stations.  1957.09–2002.08**

Red: H10   Blue: ERA40

**MAE.  Wind 10m.  Reliable stations.  1957.09–2002.08**

Red: H10   Blue: ERA40

**RMSE.  Wind 10m.  Reliable stations.  1957.09–2002.08**

Red: H10   Blue: ERA40
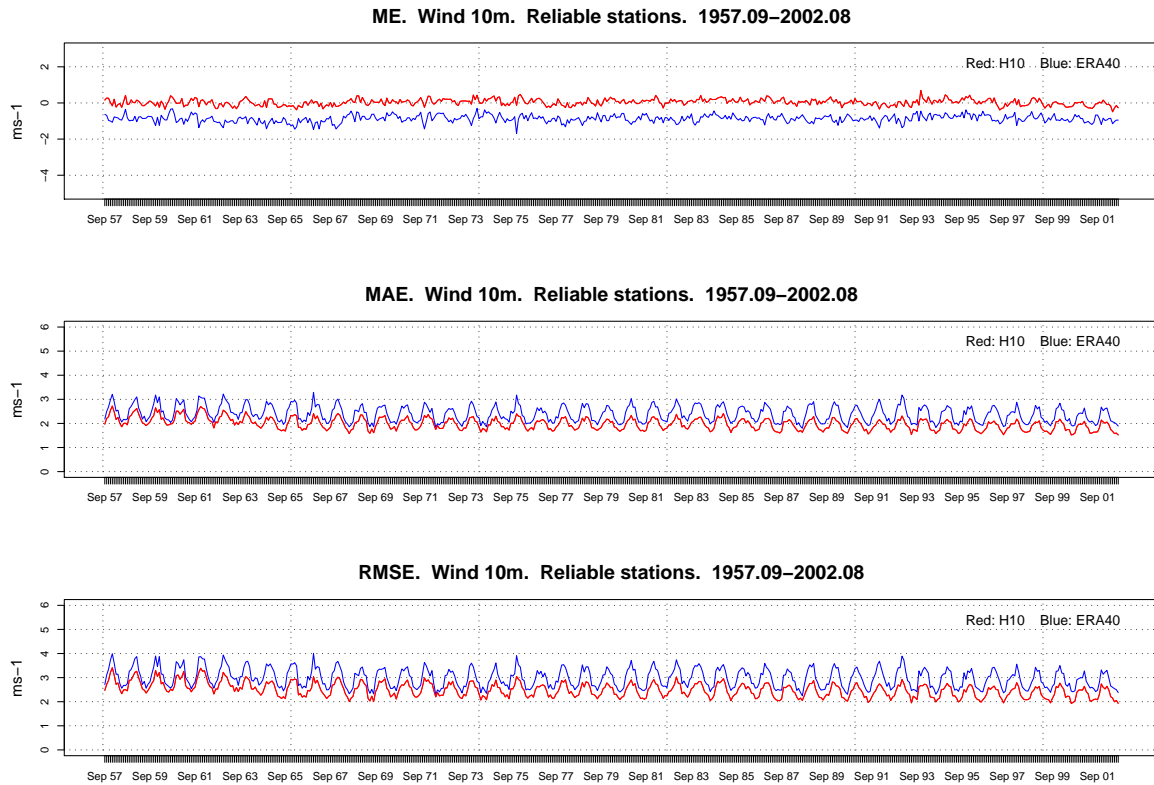
Figure 4a. Time series (1957.09  2002.08) of respectively ME, MAE and RMSE for 10m wind speed. HIRLAM in red, ERA40 blue.
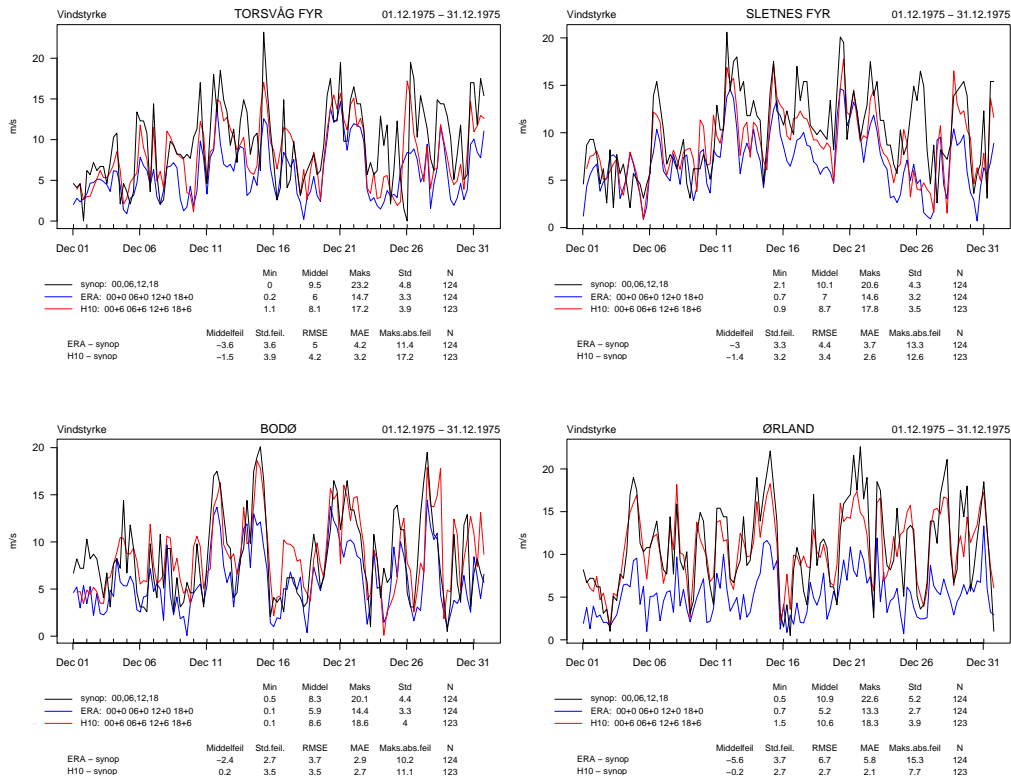
Figure 4b. Some winter examples of 10m wind speed time series, Dec 1975. HIRLAM in red, ERA40 blue and observations in black.

11

**ME. Pressure. Reliable stations. 1957.09–2002.08**



**MAE. Pressure. Reliable stations. 1957.09–2002.08**



**RMSE. Pressure. Reliable stations. 1957.09–2002.08**
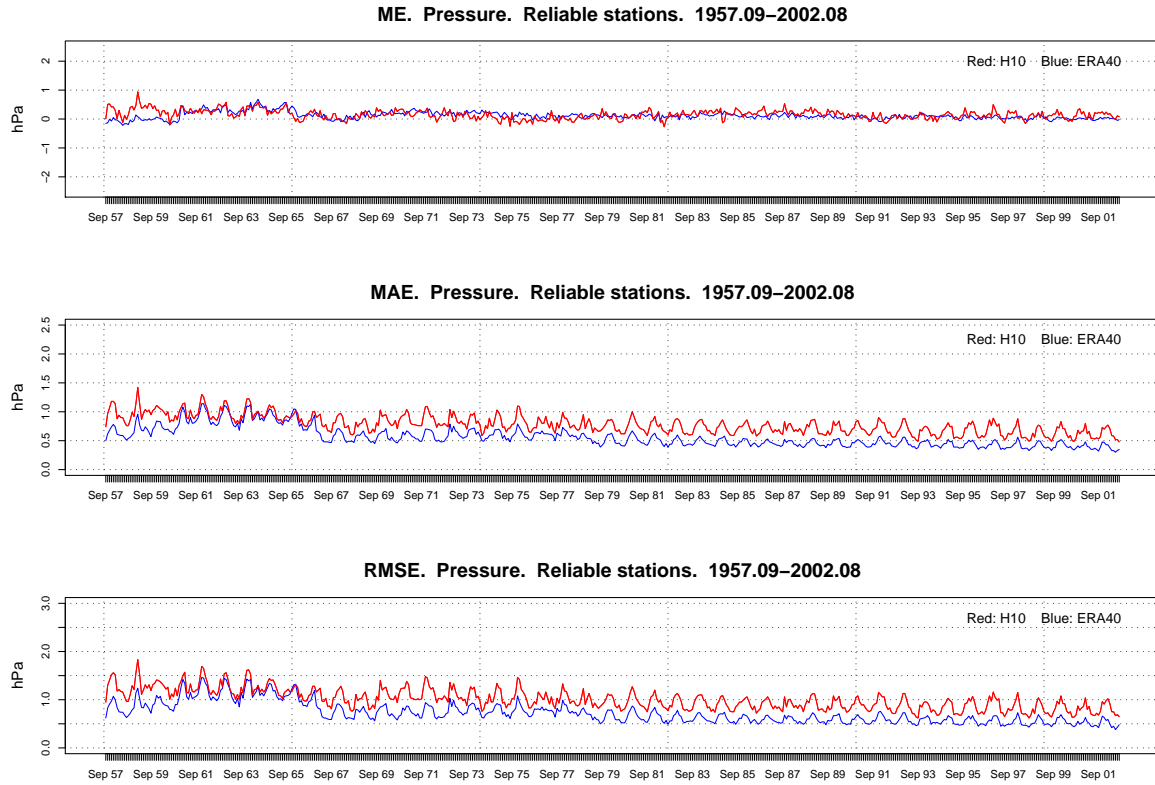


Figure 5a. Time series (1957.09 2002.08) of respectively ME, MAE and RMSE for mean sea level pressure. HIRLAM in red, ERA40 blue.
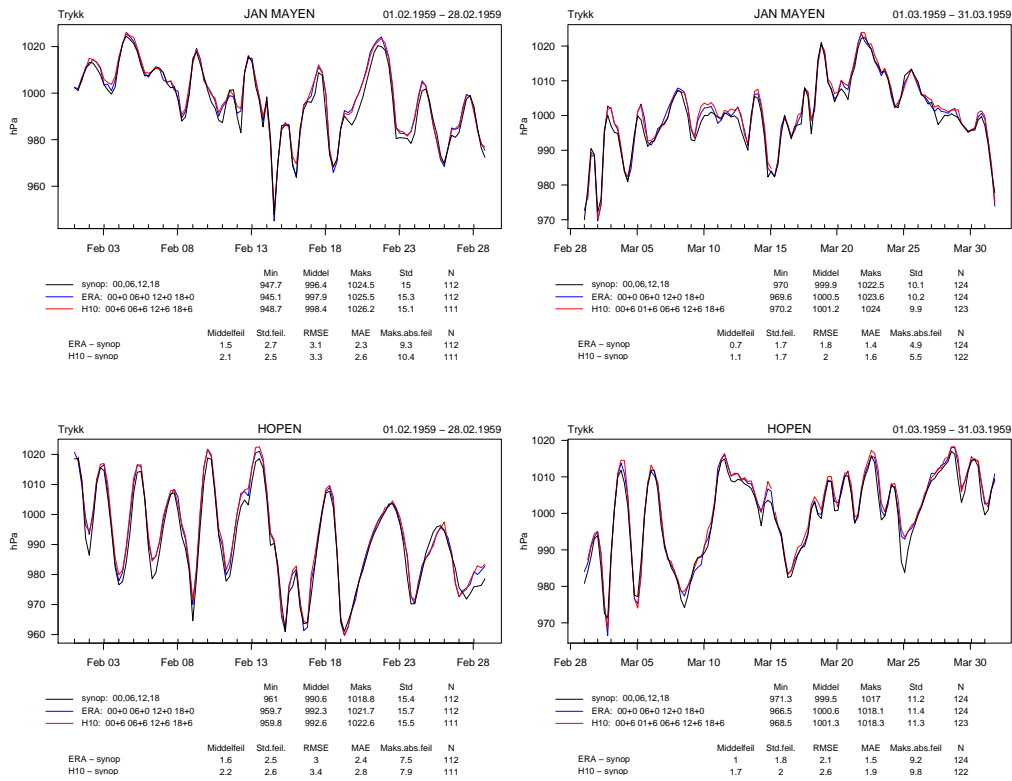


Figure 5b. Some winter examples of the mean sea level pressure time series, Feb-Mar 1959. HIRLAM in red, ERA40 blue and observations in black.

12
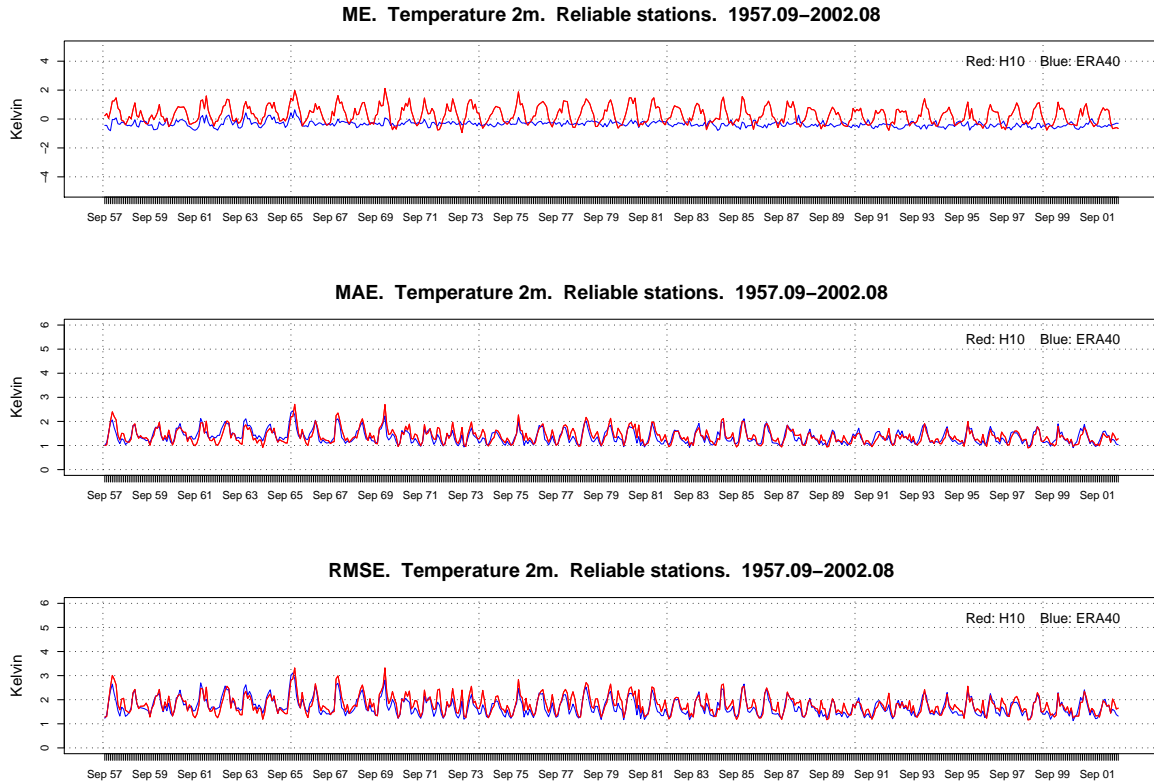
Figure 6a. Time series (1957.09  2002.08) of  respectively ME, MAE and RMSE for 2m temperature. HIRLAM in red, ERA40 blue.
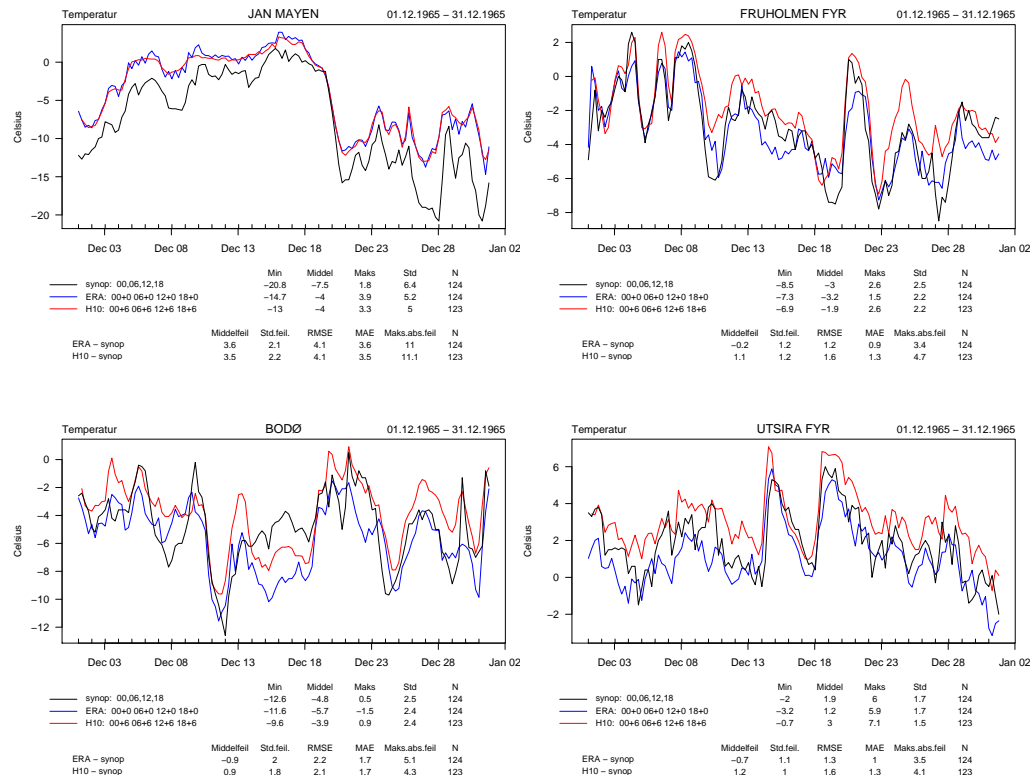


Figure 6b. Some winter examples of time series of 2m temperature, Dec 1965. HIRLAM in red, ERA40 blue and observations in black.

13

### 3.1.3  Wind speed distribution at selected stations

We have looked at the distribution of 10 m wind speed in the datasets of HIRLAM10 and ERA40 compared to the distribution of 10 m wind speed in the observations in observing stations Jan Mayen, Fruholmen lighthouse and Sletnes lighthouse (Figs 7-9).  For HIRLAM10 we show lead time +06 h as this has been found to have the lowest RMS error.

Figure 7 shows that both HIRLAM and ERA40 over-represent the segment from 4-12 m/s for Jan Mayen, wind speeds lower than 4 m/s are under-represented. The quantile *v* quantile (qq) plots indicate that HIRLAM represents the highest winds better than ERA40.

Figure 8 shows that HIRLAM has a distribution curve that fits quite well to the observations for Fruholmen lighthouse. However, both HIRLAM and ERA40 under-represent the highest winds, as is evident from inspection of the quantile distribution. ERA40 over-represents lower wind speed and underpredicts the higher ones. HIRLAM also underpredicts the highest wind speed values, but to a much smaller extent.

Figure 9 shows that HIRLAM has a much better distribution curve than ERA40 for Sletnes lighthouse. Again, the qq-plots show that HIRLAM and ERA40 both underpredict the highest winds, but ERA40 more so than HIRLAM.

Appendix A.4 summarizes the statistical measures for all available stations. Out of 77 stations, HIRLAM has a lower MAE compared to ERA40 for 46 stations and a better correlation compared to ERA40 at 57 stations. HIRLAM has a better 100 percentile (maximum value) than ERA40 in 49 out of 77 stations. However, the difference between the observed T100 and T100 in HIRLAM is usually larger than the difference between ERA40 and HIRLAM.
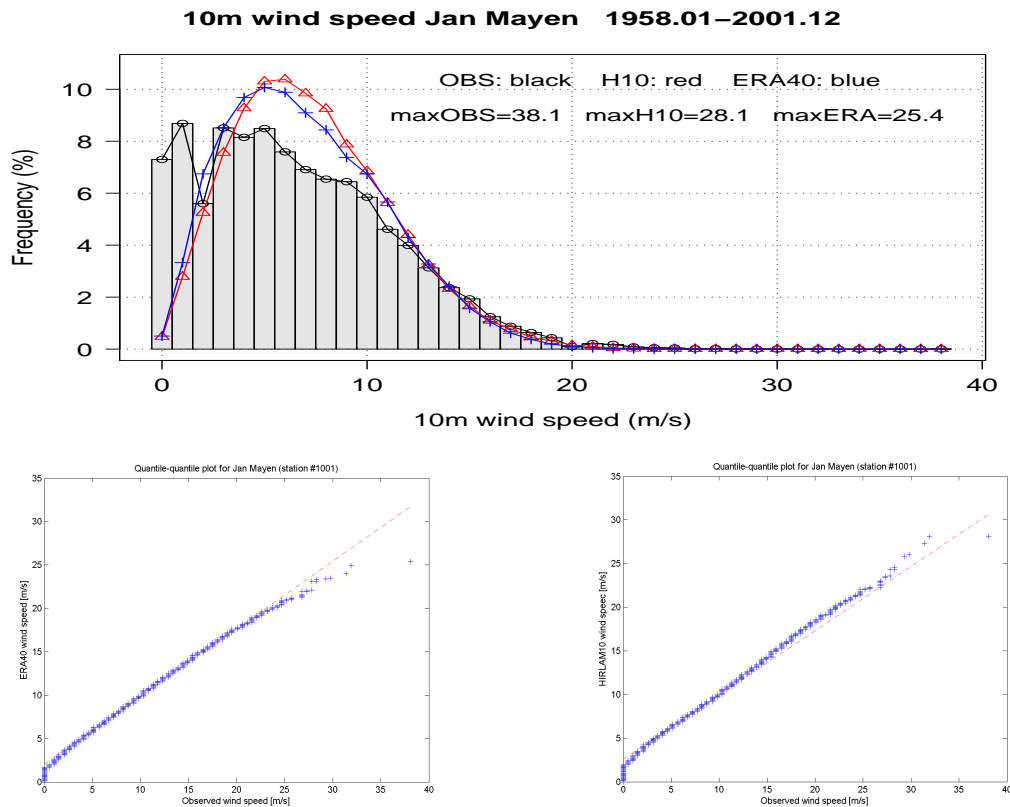


Figure 7. Upper panel: The distribution plot of 10m wind speed for Jan Mayen (HIRLAM in red, ERA40 blue and observations as histogram). Lower left panel: ERA40 qq-plot for Jan Mayen.  Lower right panel: HIRLAM qq-plot for Jan Mayen.

**10m wind speed Fruholmen L.   1958.01−2001.12**
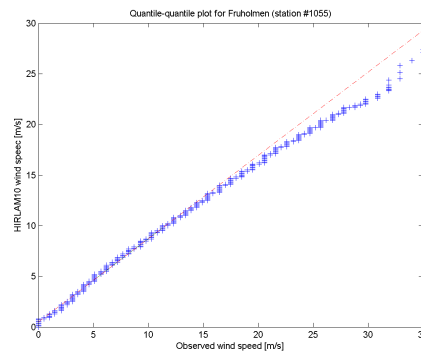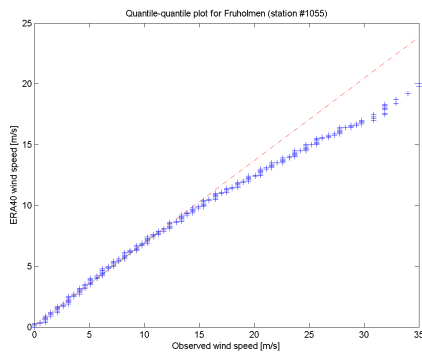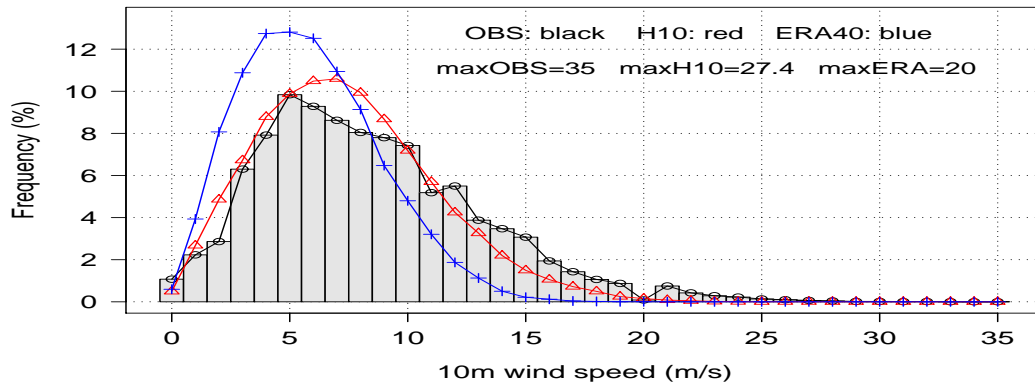


Figure 8. Upper panel: The distribution plot of 10m wind speed for Fruhomlen light house (HIRLAM in red, ERA40 blue and observations as histogram). Lower left panel: ERA40 qqplot for Fruholmen l.h..   Lower right panel: HIRLAM qqplot for Fruholmen l.h..

**10m wind speed Sletnes L.   1958.01−2001.12**
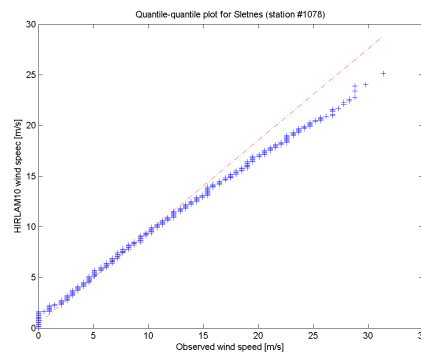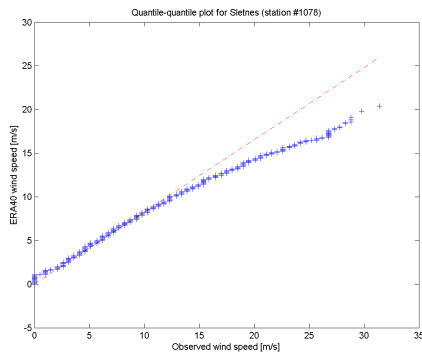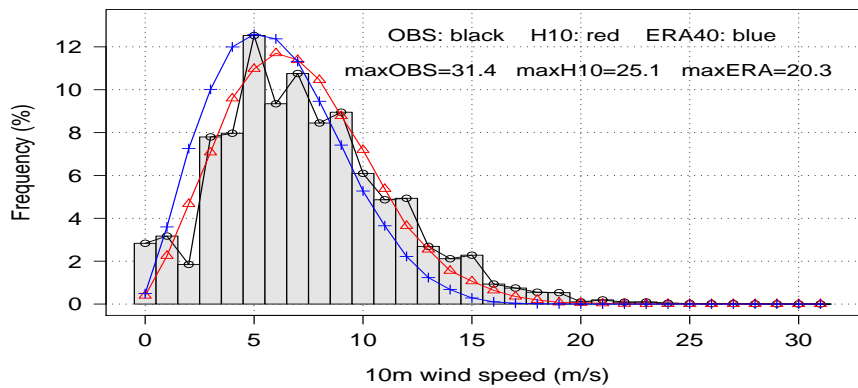


Figure 9. Upper panel: The distribution plot of 10m wind speed for Sletnes light house (HIRLAM in red, ERA40 blue and observations as histogram). Lower left panel: ERA40 qqplot for Sletnes lighthouse. Lower right panel: HIRLAM qq-plot for Sletnes lighthouse.

### 3.1.4 Case studies of three polar lows

Polar lows are difficult to predict due to their relatively small scale, complex model physics and general lack of observations. In this case study we have tried to assess a sample of representative polar lows in the downscaled dataset. We have used the manual registrations done by the Norwegian Meteorological Institute in Tromsø (VNN). The registrations are based on advanced very high-resolution reflecting radar (AVHRR) satellite observations, synoptic observations and visual reports. Extreme values often occur 3 to 9 h later than registered and the real MSLP is assumed to be within +/- 3 hPa of the recorded value.

We have chosen three polar lows where winds exceeded of 23 m/s (45 knots). From the hindcast archive we have hourly wind speed values. From ERA40 we have retrieved wind speed values with 6-hourly intervals.

**Polar low no. 1**

Registered:
Date:                                    1999-12-19
Time:                                    1340 UTC
Position:                         72ºN, 018ºE
Min pressure          989 hPa
Max wind:              23 m/s (NE)

This polar low developed in connection with a synoptic scale low ( the mother low ) centered on the boundary between Finland and Russia in Figure 10 panels (a) and (b), moving northeast. A cold Arctic outbreak (Figure 10 d) results in a strong differential temperature advection and a reversed shear baroclinic zone (Figure 10 c) having wind and thermal wind in opposite direction and weakening the flow with height.

Five hours into the forecast, HIRLAM manages to resolve the beginning of a polar low, and it lasts the remaining 4 hours of the forecast. The scale of the initial polar low is only approximately 30 km. The polar low is not retained in the following forecast and does not develop into a complete polar low having a scale between 100 km and 1000 km (Condron et. al., 2005). Ideally, the polar low would continue developing from one model cycle to another, but the switch to the next cycle does not manage to continue to simulate the development. The HIRLAM forecast is nevertheless a good forecast, resolving the initial state of the polar low with the minimum mean sea level pressure of 992 hPa which is within the observed interval of 989 hPa +/- 3 hPa. The highest wind speed in HIRLAM in connection with the polar low, occurred some hours later, at 21 UTC, and was 17 m/s compared to ERA40 which had a maximum of 14 m/s.

ERA40 does not capture the low pressure centre at all. This is unsurprising as the smallest features represented in a spectral model have a horizontal scale dictated by the spectral truncation limit of the model (Simmons and Gibson, 2000). An accurate representation of the advection of features in a spectral model must be 2-4 times this smallest scale (Pielke, 1991, and Laprise, 1992). It is therefore expected that ERA40 which has a spectral truncation limit of T159 (approximately 125 km) will give an accurate representation only of features larger than 500 km.

Condron et. al. (2005) performed a study of detection of polar mesocyclones in the ERA40 dataset using an automated cyclone detection algorithm. Their work showed that up to 80 % of cyclones larger than 500 km are detected, but the hit rate decreases approximately linearly to ~40% for 250 km and to ~20% for 100 km scale cyclones.
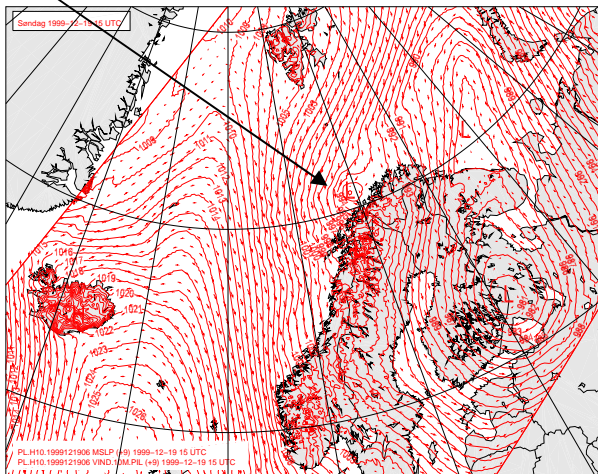
a) MSLP and wind arrows for HIRLAM, 1999121906+09.
1999121912+03
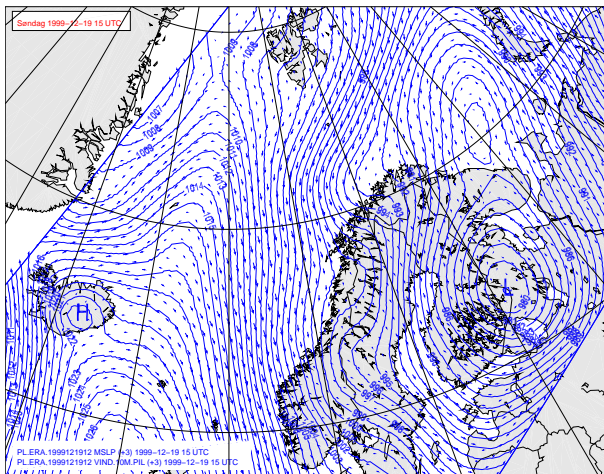


b) MSLP and wind arrows for ERA40, 1999121912+03
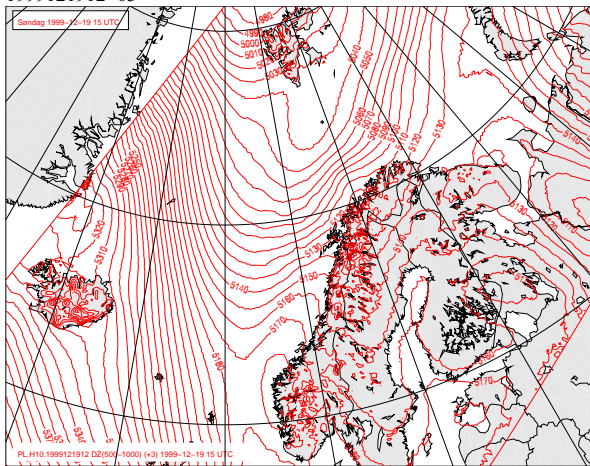




c) DZ 500-1000, HIRLAM, 1999121912+03

d) T2m, HIRLAM, 1999121912+03

e) 10m wind speed, HIRLAM, 1999121912+03

f) 10m wind speed, HIRLAM, 1999121918+05

g) 10m wind speed, ERA40, 1999121912+03
wind speed, ERA40, 19991218+03

h)   10m
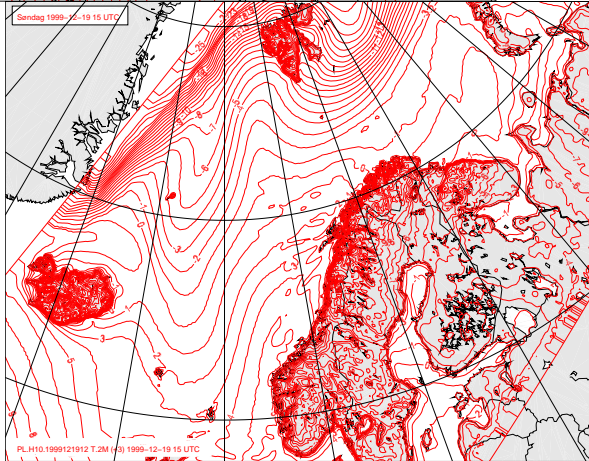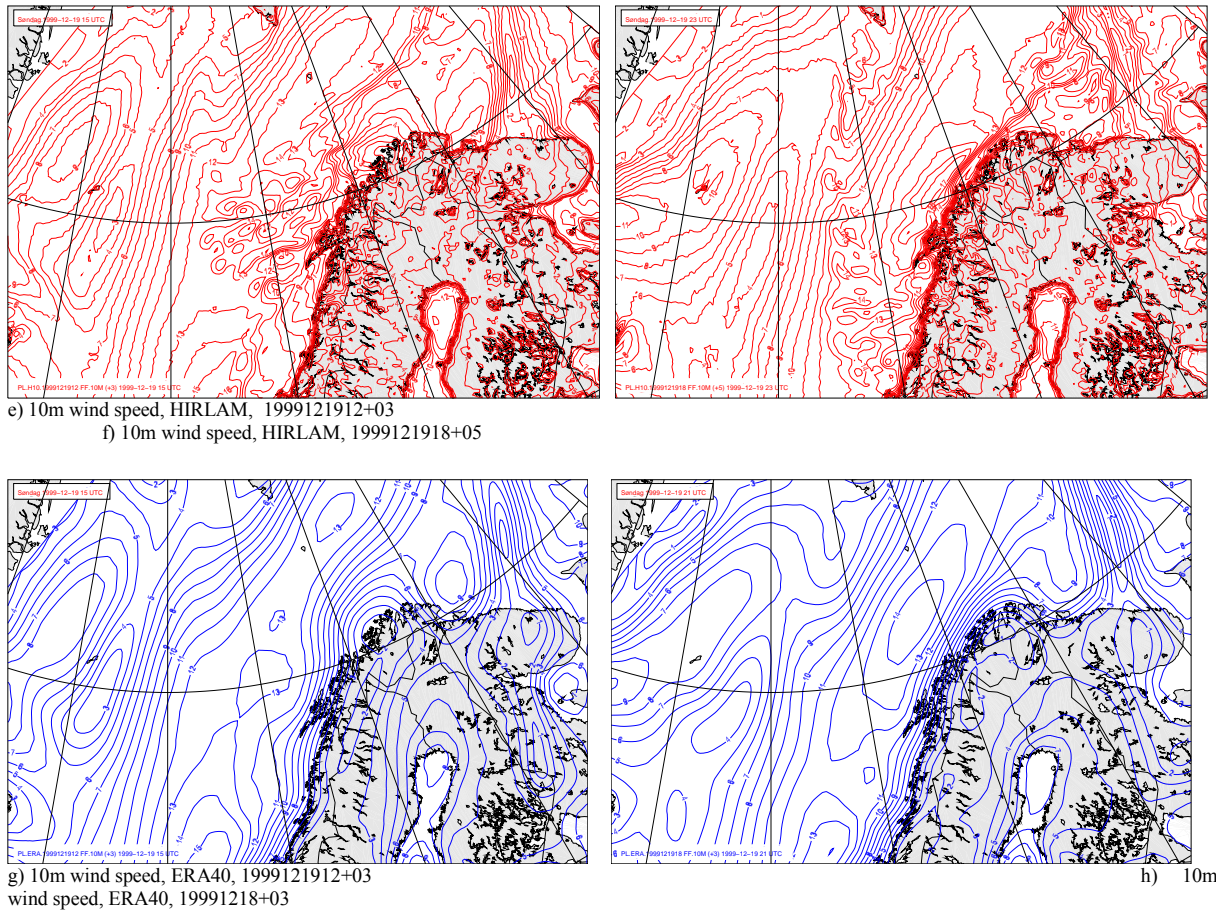
Figure 10. Comparison of  HIRLAM and ERA40 during the evolution of polar low no 1.

## Polar low no. 2

Registered:

| | |
|---|---|
| Date: | 2000-01-31 |
| Time: | 0610 UTC |
| Position: | 65ºN, 004ºE |
| Min pressure | 978 hPa |
| Max wind: | 25.7 m/s (NW) |

The polar low is connected to the outbreak of cold air from northeast over the warmer air further south (Figure 11 c). The mother low is situated off the coast of Finnmark (Figure 11 a, b) and is well presented by both HIRLAM and ERA40. The polar low is captured only by HIRLAM. Though it fails to develop it into a full-fledged polar cyclone a trough is present with a scale of about 25 km with winds slightly above 20 m/s.
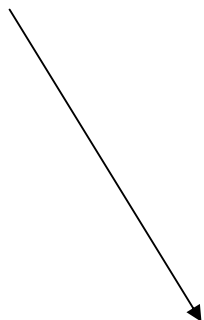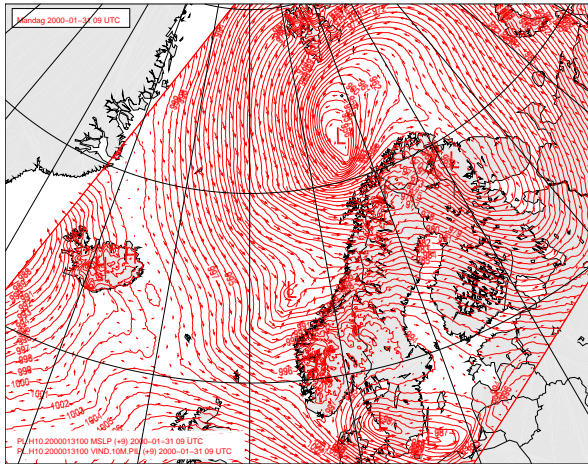
a) MSLP and wind arrows for HIRLAM, 2000013100+09.
2000013106+03
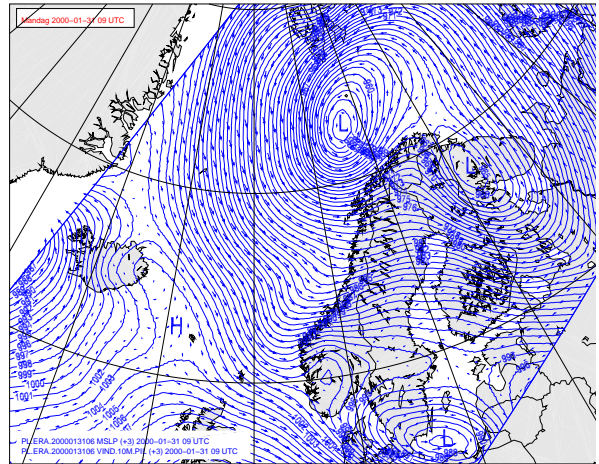


b) MSLP and wind arrows for ERA40,
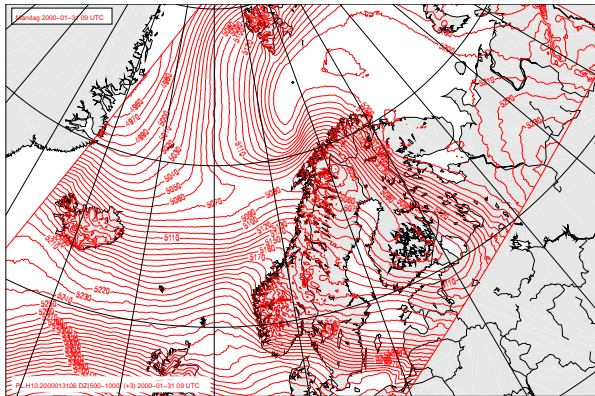


c) D500-1000, HIRLAM, 2000013106+03.
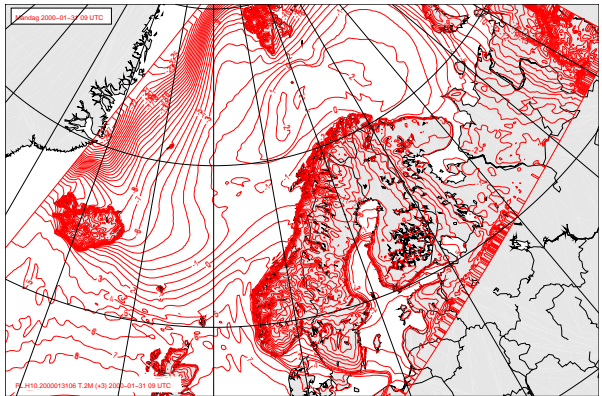


d) T2m, HIRLAM, 2000013106+03
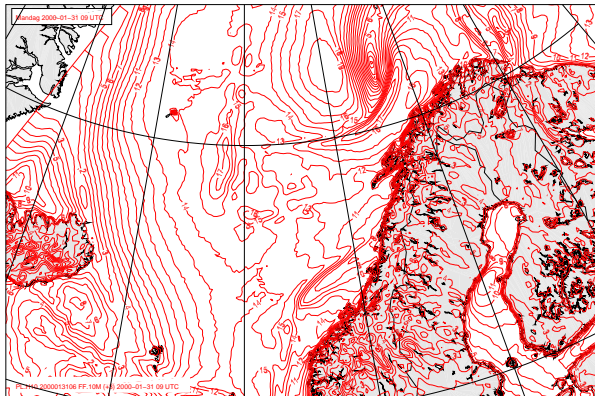


e) 10m wind speed, HIRLAM, 2000013106+09



f) 10m wind speed, HIRLAM, 2000013100+00

g) 10m wind speed, ERA40, 20000013106+03.
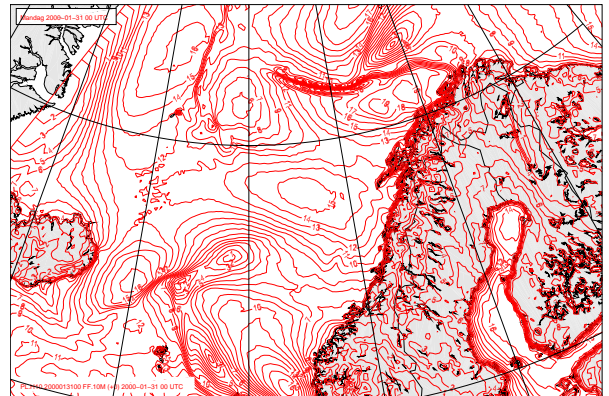
h) 10m wind speed, ERA40, 2000013112+03
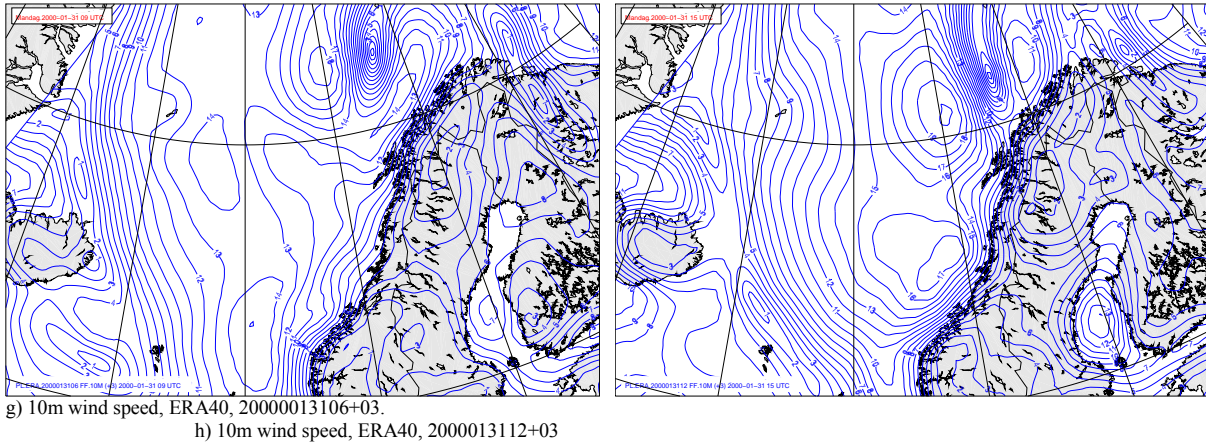
Figure 11. Comparison of  HIRLAM and ERA40 during the evolution of polar low no 2.

**Polar low no. 3**

Registered:
Date:                                                    2001-11-01
Time:                                                    0200 UTC
Position:                                        71ºN, 019ºE
Min pressure          992 hPa,
Max wind:                          25.7 m/s (N)

From Figure 12 we see that there is an outbreak of cold air from the Arctic flowing southwards (panel c). The outbreak is much weaker than in the previous polar low cases and we do not see the same east-west temperature contrast. HIRLAM has a pressure minimum of 998 hPa in the area of the polar low, and ERA40 has a pressure minimum of 1000 hPa in the same region. HIRLAM has a maximum in 10m wind velocity of 15 m/s, whereas ERA40 has maximum of 12 m/s.
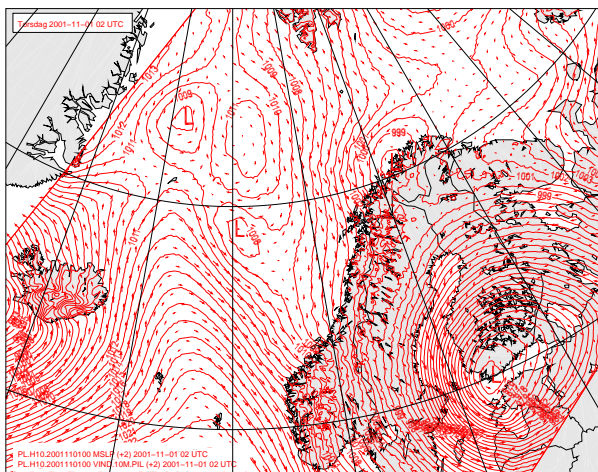


a) MSLP and wind arrows for HIRLAM, 2001110100+02                 b) MSLP and wind arrows for ERA40, 2001110100+03
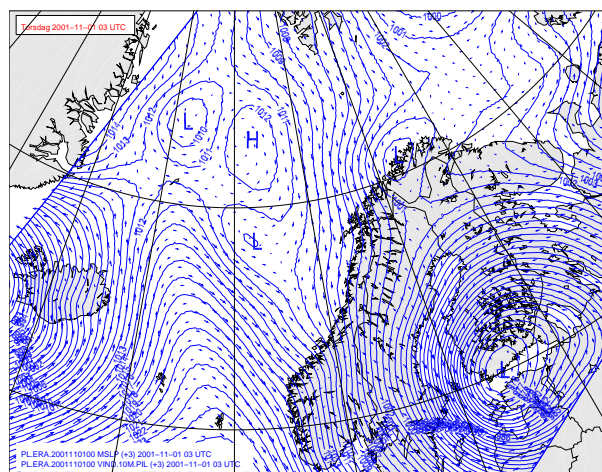
c) DZ500-1000, HIRLAM, 2001110100+03
       d) T2m , HIRLAM, 2001110100+03

e) 10m wind speed, HIRLAM, 2001110100+02.
       f) 10m wind speed, ERA40, 2001110100+03.
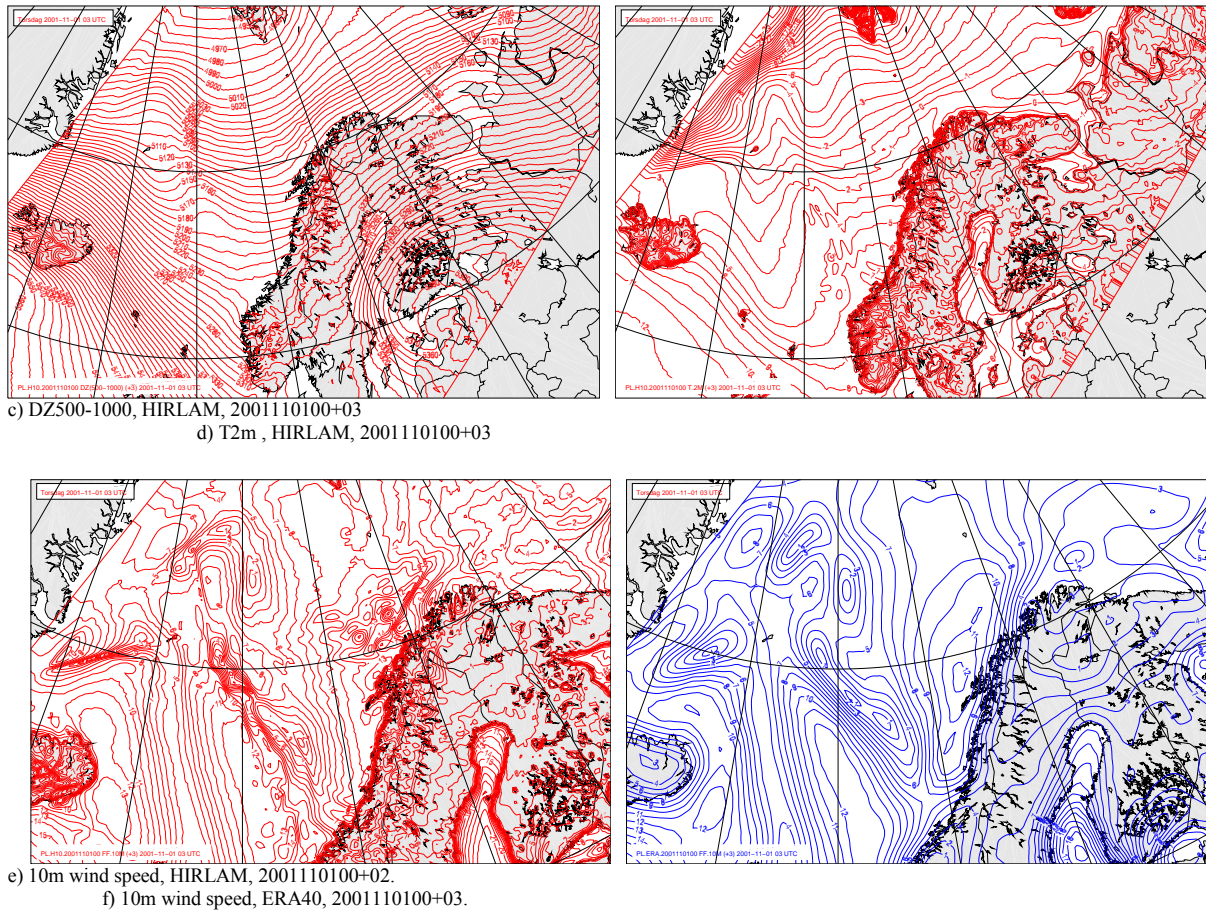
Figure 12. Comparison of  HIRLAM and ERA40 during the evolution of polar low no 3.

### 3.1.5  QuikSCAT/SeaWinds *v* HIRLAM10

The SeaWinds scatterometer onboard the QuikSCAT satellite is a real-aperture microwave radar (Portabella and Stoffelen, 2001). The backscattered signal depends on the wave energy found in surface capillary/gravity waves on the centimetre scale. The 10m wind vector is related to the radar backscatter through an empirical algorithm between the backscatter and the wind speed and direction relative to the antenna viewing angle. The empirical relationship is based on a neutrally stratified atmosphere, which can usually be assumed over the ocean, except in situations of cold air outbreaks. It is well-known that QuikScat winds are biased high for very high wind speeds (above 19 m/s) (see *e.g.* Ebuchi *et. al.*, 2002; Moore *et. al.*, 2008) and when used in assimilation they are reduced overall by 4% while winds above 19 m/s are reduced using the formula $V = v - 0.2(v-19)$, see ECMWF (2002). We have not applied any corrections to QuikScat here.

The errors in wind speed introduced from non-neutral conditions are of limited importance as these conditions are relatively limited in time and coverage over the world ocean (Chelton and Freilich, 2005). Non-neutral conditions at low wind speeds (below 6m/s) may result in 20% error in QuikScat winds (Accadia *et. al.* 2007).

QuikScat is a polar-orbiting satellite and therefore covers the northern regions well (such as the Barents Sea). The number of QuikScat observations per day is 2-7 in our model domain[1].

---

[1]  For more information about QuikScat, see http://winds.jpl.nasa.gov/missions/quikscat/ (http://tr.im/pH4e). The SeaWinds on QuikScat Level 2B product on 25 km swath grid from July 1999 to August 2002 were downloaded from http://podaac.jpl.nasa.gov/.

The co-location and subsequent comparison was performed using a nearest-neighbour selection from the HIRLAM10 grid. Here we show only the results from the winter months December, January and February (DJF), when the differences are largest.

Figures 13 and 14 show the mean 10 m wind speed for the QuikScat data for DJF 1999-2002 and HIRLAM, respectively. The mean difference is shown in Figure 15. The two datasets show generally good agreement, but the influence by the ERA40 boundary values is evident in weaker modelled winds near the boundaries of the model. This is due to ERA40 being generally biased low over the open ocean, as found also in comparison with *in situ* observations in Section 3.1.1.

QuikScat wind speeds are generally higher than HIRLAM resulting in a negative bias (HIRLAM-QuikScat) as expected. However, there are four regions where HIRLAM predicts higher wind in the mean than observed by QuikScat; in the Southern North Sea, North-East of Iceland, in the Greenland Sea and near Bjørnøya. Microwave instruments tend to underestimate the 10 m wind under stable boundary layer conditions (cold sea). This may in part explain the bias in the northern regions and may show that the stability plays a role in the polar regions. The biases may also indicate that there are processes that are not well resolved or included in the HIRLAM integration, but decisively resolving these discrepancies will require a more detailed study.

The RMS difference between QuikScat and HIRLAM shown in Figure 16 reveals that the largest deviations occur south and east of Svalbard in the winter months, most probably in connection with the ice edge. The elevated RMS difference in this region may result from a combination of few observations, poor resolution of the true ice edge in the model integration and ice in the field of view of the scatterometer (erroneous observations may occasionally slip through the ice flag algorithm), *i.e.*, errors are expected to be higher both in the modelled fields and the satellite observations in the marginal ice zone.

Figure 17 shows a scatter diagram and a density plot comparing values of QuikScat wind speed with HIRLAM. Good correlation and low mean error (bias) is found between the two datasets, with the bulk of the observations exhibiting near 1:1 correspondence (very low bias).

Figure 18 shows that the upper quantiles of QuikScat deviate significantly from HIRLAM. This is also clear in the other months of the year when QuikScat can have cases with high wind speed values, while HIRLAM generally has lower wind speed values (not shown here). As we do not see the same pronounced deviation in our comparison with synoptic observations we are led to conclude that QuikScat does not represent high winds reliably. This is also consistent with recent findings for the Mediterranean sea.
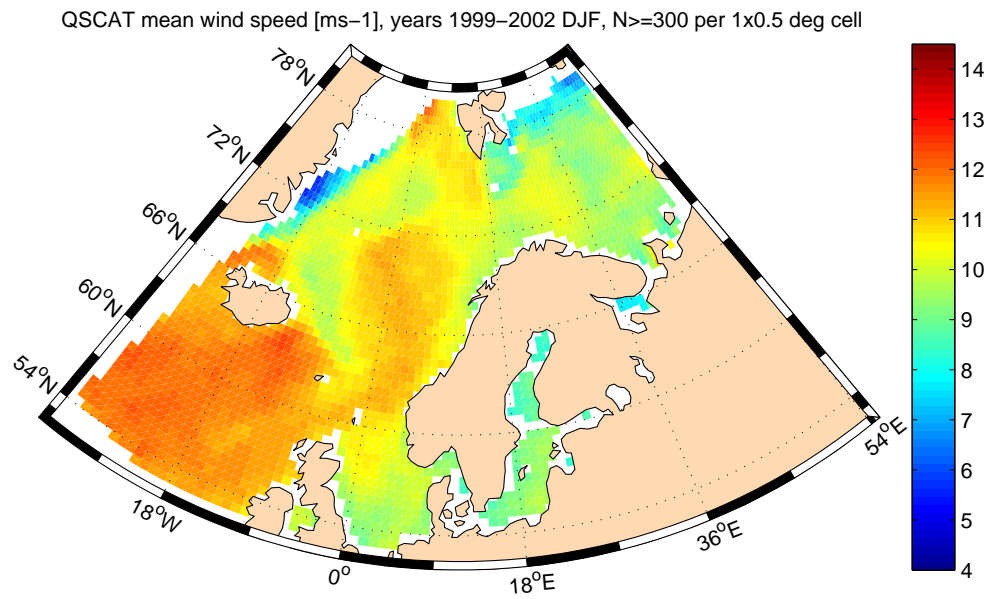
Figure 13. QuickScat mean 10 m wind speed, DJF 1999-2002.
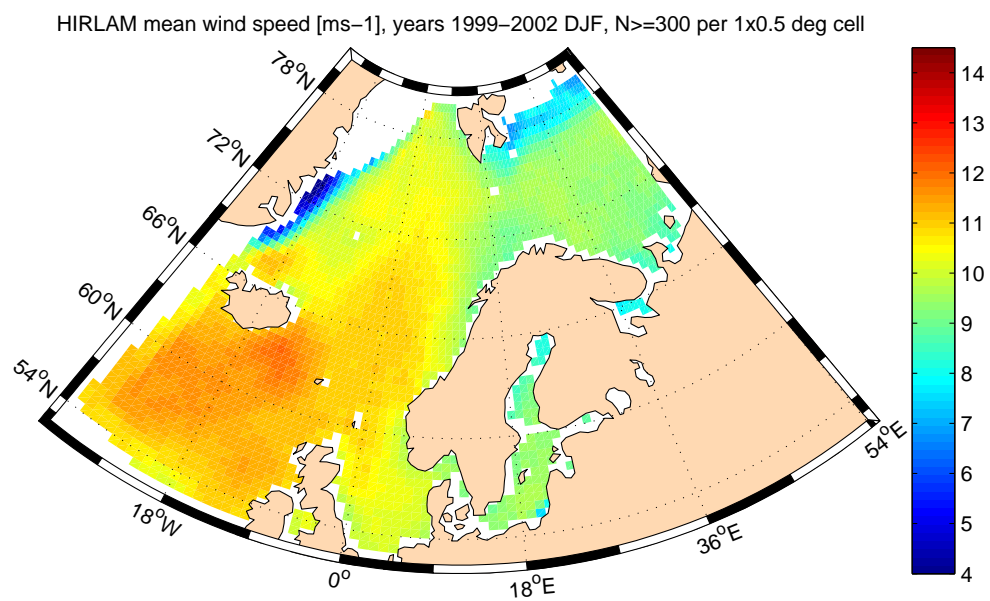


Figure 14. HIRLAM mean 10 m wind speed, DJF 1999-2002.

Mean error HIRLAM – Qscat [ms−1], years 1999–2002 DJF, N>=300 per 1x0.5 deg cell
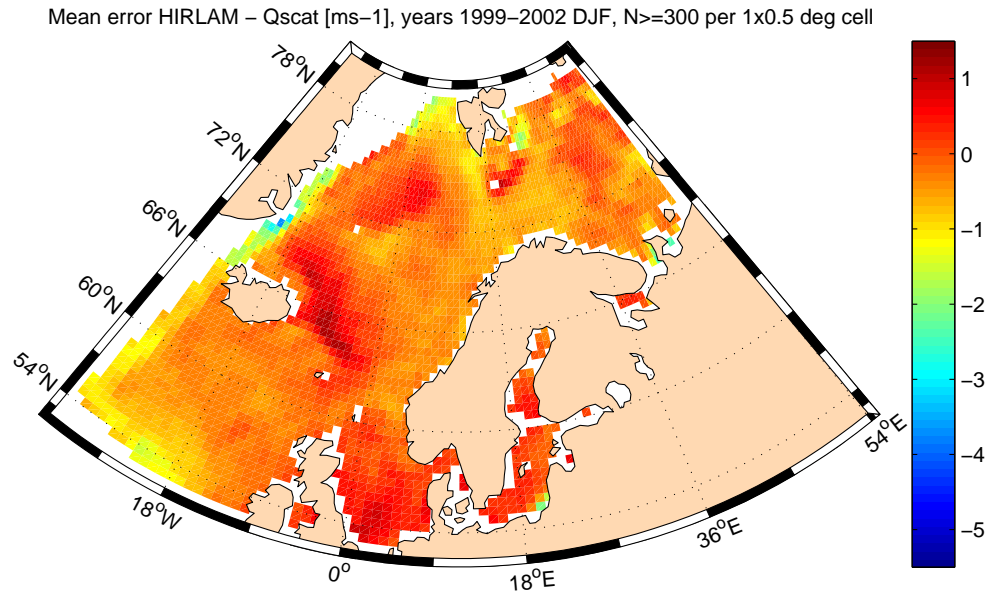
Figure 15. Mean difference, HIRLAM-QuickScat, DJF, 1999-2002.

RMS error HIRLAM – Qscat [ms−1], years 1999–2002 DJF, N>=300 per 1x0.5 deg cell
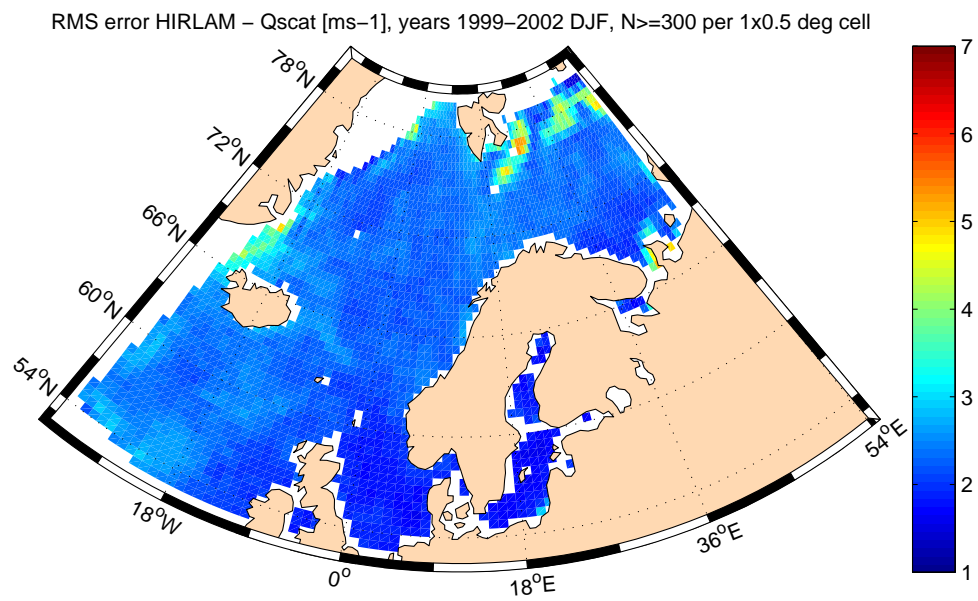
Figure 16. 10 m wind speed RMS difference between HIRLAM and QuikScat, DJF, 1999-2002.
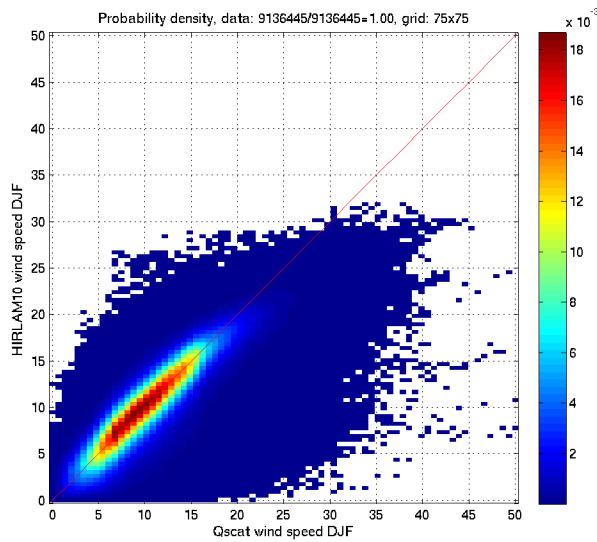
Figure 17. Scatter diagram comparing QuikScat wind speed with HIRLAM wind speed, DJF, 1999-2002.
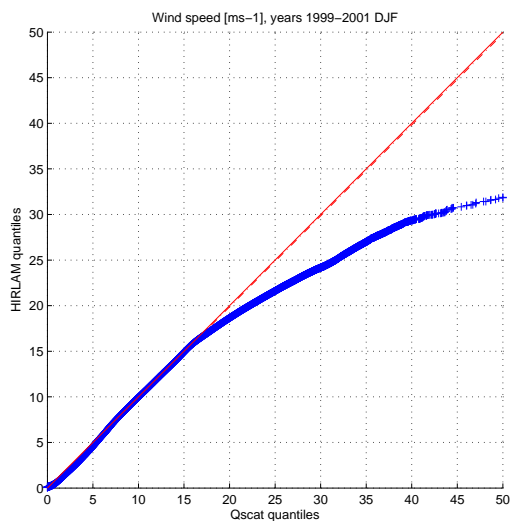


Figure 18. Quantile-quantile comparison of QuikScat and HIRLAM wind speed, DJF, 1999-2002.

## 3.2 Wave hindcast performance

The wave hindcast has been compared both against *in situ* wave observations and satellite altimeter observations.

The general agreement between observations and WAM10 is very good with correlation coefficients ranging from 0.94 to 0.97 for offshore stations (see Table 3). Upper percentile distributions closely follow the observed distribution of significant wave height.

### 3.2.1 A comparison of different wave model configurations

Several model configurations were compared against ERA40 wave fields for two selected periods. Table 2 compares the statistics for six different wave model configurations. These simulations were only performed for selected periods as a preamble to the full 45-year integration to assess the

quality of the high-resolution hindcast archive (Reistad *et. al.*, 2007). WINCH refers to the old hindcast archive described by Reistad and Iden (1998). WAM50 hindcast wind refers to coarse simulations (see WAM50 domain in Figure 1) where winds were derived from digitized pressure fields. WAM50 ERA40 wind refers to simulations on the same domain but with winds from ERA40. ERA40 refers to wave statistics from the ERA40 archive. Finally, WAM10 + ocean model and WAM10 refer to two test configurations, the first with winds from HIRLAM10 with sea surface temperature (SST) and ice cover from an ocean model, the second with winds from HIRLAM10 with SST and ice cover from ERA40. The ocean model had negligible effect on the wave statistics and was subsequently dropped. WAM10 scores very well on correlation, RMS error as well as the upper percentiles of the distribution. The comparison shows that WAM10 scores higher than ERA40 both in terms of RMSE, ME and correlation $H_s$. The scatter index, defined as the RMSE normalized by the mean of the observations (Zambreski, 1989, 1991, Komen *et. al.*, 1994, Ris *et. al.*, 1999), is 0.14 as compared to 0.2 for ERA40.

### 3.2.2 *In situ* observations

Tables 3 and 4 compare the observed and modelled (WAM10 in Table 3 and ERA40 in Table 4) significant wave height at six stations from Ekofisk at 56.5ºN, 003.2ºE in the middle North Sea to Ami at 71.5ºN, 019.0ºE off the coast of Northern Norway over the whole observational period. Note that the WAM10 integration extends to December 2008 while ERA40 ends in August 2002. Of these, Ekofisk is the longest and most reliable time series, starting in 1980. The WAM10 statistics for Ekofisk (Table 3) appear nearly stationary throughout the model period with very high correlation (0.96) and low RMS error (0.35 m). WAM10 appears to overestimate the mean annual wave height only very slightly (4 cm), but the upper percentile (P99) is overestimated by 0.2 to 0.7 m (average of 0.3 m). ERA40 (Table 4) correlates very well with the observed time series in all six stations, with correlations only slightly weaker than WAM10. However, the mean wave height is consistently underestimated, ranging from 10 to 35 cm. Furthermore, the RMSE is higher than for WAM10. The disagreement with observed values becomes increasingly worse for the higher percentiles. ERA40 is underestimating P99 by 0.6 to 1.3 m (Draugen).

Figure 20 shows annual mean values of model wave heights and measured wave heights and annual RMSE and MAE for Ekofisk (1980-2008), Gullfaks (1990-2008) and Draugen (1995-2008). The statistics for these three stations is almost stationary. At Ekofisk and Draugen there is a small tendency to overestimate the significant wave height during the last years (after the ERA40 period), while that tendency is not seen at Gullfaks. RMSE and MAE are nearly constant through the years with measurements for all three stations.

We have furthermore evaluated WAM10 and ERA40 against a collection of *in-situ* wave measurements covering the North-East Atlantic Ocean, see Figure 21. The data set is a collection of buoy and platform measurements covering the period August 1991 – August 2002 which partially overlaps with the data found in Figure 19. However, the data have been subjected to a more rigorous quality control by removing outliers in monthly time series as well as through visual inspection as explained in Saetra and Bidlot (2004). The individual time series vary in length from half a year to slightly more than nine years. All observations are four-hourly means (±2 h) centred on synoptic times, *i.e*. 00, 06, 12 and 18 UTC. While most platforms are permanently fixed to one location, some buoys are subjected to movement. Here we have only used data within an area of +/- 0.2° of the median latitude and +/- 0.4° of the median longitude of the individual time series. So, data originating from areas with slightly different wave climatology are coarsely filtered out, meaning the time series contain some gaps. This may also be a result of missing data or filtered spike values.

Figure 22 compares observed and modelled $H_s$ from WAM10 and ERA40, respectively, as well as a comparison of the two model integrations. Besides a slightly higher correlation, 0.95 *v* 0.93,

WAM10 is very nearly unbiased while ERA40 clearly underestimates $H_s$. It should be mentioned that the ERA40 reanalysis is run with a deep-water model and does not account for bottom topography, unlike the WAM10. This will certainly influence the performance of the hindcast in coastal areas where bottom friction becomes important, highlighting the advantage of a high-resolution regional hindcast integration over ERA40. Table 4 summarizes the verification of WAM10 and ERA40 compared to the available observations.

Figure 23 compares observed and modelled 95- and 99-percentiles from ERA40 and WAM10. Also for the tail of the distribution does WAM10 perform better than ERA40 with higher correlation and smaller bias. Overall, WAM10 is biased a little high, with mean absolute bias 8% compared to observations, while ERA40 is biased low with mean absolute bias 10% for the 95-percentile. One interpretation of the regression analysis is that the WAM10 is slightly high in areas with a weaker wave climate, while ERA 40 is low in areas with higher wave climate.

### 3.2.3  Co-located altimeter observations

WAM10 significant wave height is also compared with the significant wave height as estimated from satellite altimeter data. A co-location of data from the three altimeters onboard ERS-2, Topex and Geosat Follow-On (GFO) for the years 2000-2001 was performed using a nearest-neighbour selection from the WAM10 gridded fields. The temporal resolution of the gridded fields is 3 hours, hence the maximum time difference between satellite observations and modelled significant wave height is 1.5 hours and the maximum spatial separation is approximately 7 km. The overall agreement is very good, as can be seen from Figures 24-26 and Table 5 with correlations against individual satellite altimeters in the range of 0.94-0.96 with very low bias.
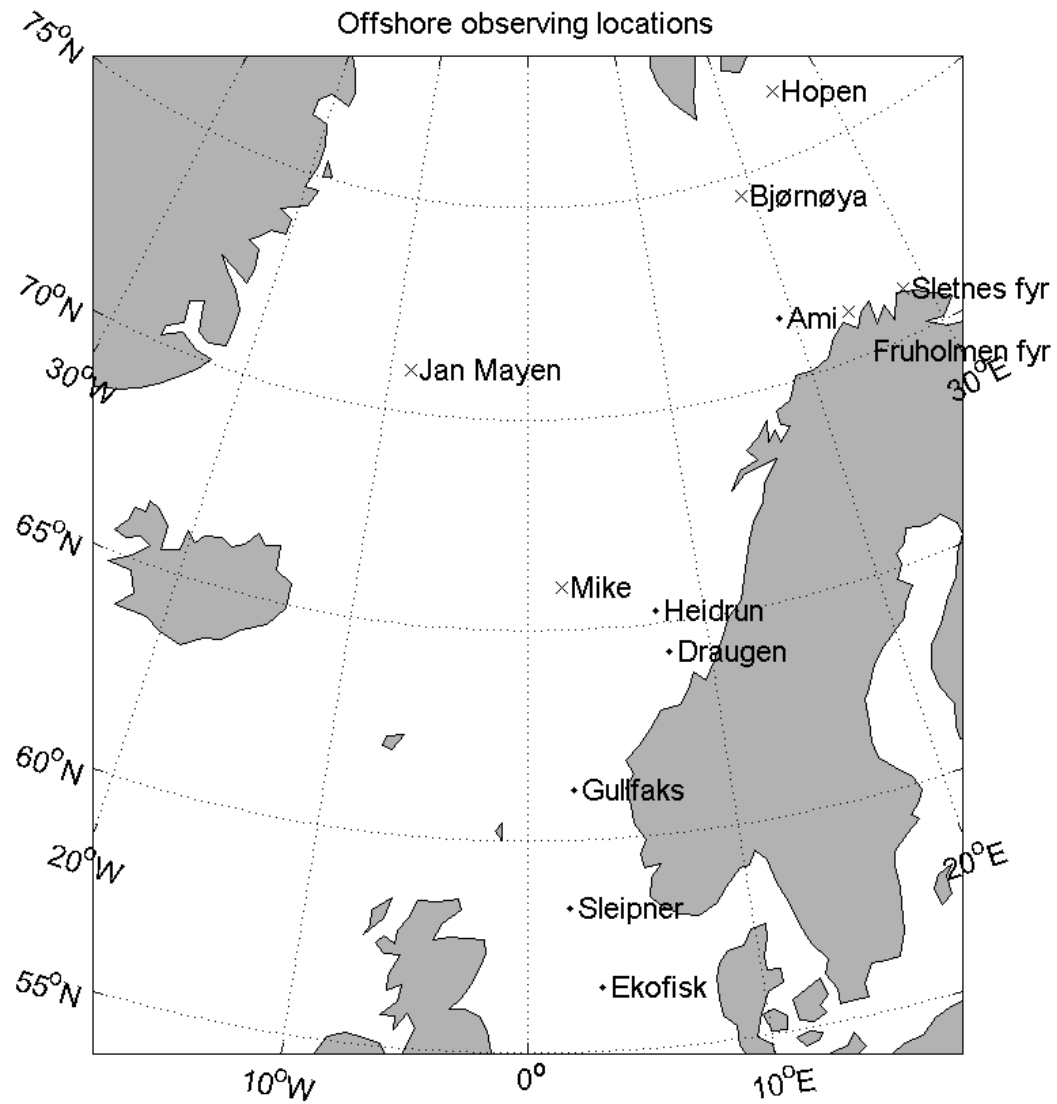
Figure 19: Offshore locations with wave and wind observations (crosses indicate locations where only wind measurements are available). The observations presented are taken from Ekofisk, Sleipner, Gullfaks, Draugen, Heidrun, and Ami. Weather ship M (66°N, 002°E) is marked as Mike . The measurements cover the period 1980-2008.

| Draugen January 2000 | | | | | | | | | |
|---|---|---|---|---|---|---|---|---|---|
| Significant wave height | Mean | St.d | RMSE | SI | Corr | P90 | P95 | P99 | Max. |
| Obs | 4.95 | 1.95 | - | - | - | 7.8 | 8.4 | 9.6 | 10.0 |
| WINCH | 5.34 | 1.71 | 1.05 | 0.21 | 0.86 | 7.8 | 8.1 | 10.3 | 10.8 |
| WAM50 hindcast wind | 5.16 | 2.16 | 1.08 | 0.22 | 0.87 | 8.0 | 9.1 | 12.0 | 13.5 |
| WAM50 ERA40 wind | 4.46 | 1.61 | 0.86 | 0.17 | 0.94 | 6.8 | 7.2 | 8.8 | 9.1 |
| ERA40 | 4.23 | 1.48 | 1.02 | 0.20 | 0.94 | 6.4 | 6.9 | 7.6 | 8.0 |
| WAM10 +ocean model | 4.80 | 2.02 | 0.72 | 0.15 | 0.94 | 7.8 | 8.9 | 9.8 | 10.1 |
| WAM10 | 4.77 | 2.01 | 0.71 | 0.14 | 0.94 | 7.7 | 8.8 | 9.7 | 10.1 |

Table 2. Statistics of significant wave height at station Draugen for six different wave model configurations, January 2000.

| Ekofisk 1980-2008 | | | | | | | | | |
|---|---|---|---|---|---|---|---|---|---|
| Significant Wave height | N | Mean | St.dev. | Mean abs. difference | RMS difference | Corr. coefficient | P90 | P95 | P99 |
| Obs. | 78226 | 2.04 | 1.25 | - | - | - | 3.7 | 4.5 | 6.1 |
| WAM10 | 78226 | 2.08 | 1.31 | 0.25 | 0.35 | 0.96 | 3.9 | 4.7 | 6.3 |
| **Sleipner 1995-2008** | | | | | | | | | |
| Obs. (MIROS) | 33600 | 2.30 | 1.40 | - | - | - | 4.2 | 5.0 | 6.6 |
| WAM10 | 33600 | 2.50 | 1.41 | 0.42 | 0.57 | 0.93 | 4.5 | 5.3 | 6.9 |
| **Gullfaks 1990-2008** | | | | | | | | | |
| Obs. (MIROS) | 44901 | 2.72 | 1.54 | - | - | - | 4.9 | 5.7 | 7.4 |
| WAM10 | 44901 | 2.78 | 1.58 | 0.35 | 0.50 | 0.95 | 5.0 | 5.9 | 7.7 |
| **Draugen 1995-2008** | | | | | | | | | |
| Obs. (MIROS) | 36668 | 2.62 | 1.65 | - | - | - | 4.9 | 5.9 | 7.8 |
| WAM10 | 36668 | 2.68 | 1.62 | 0.40 | 0.56 | 0.94 | 4.9 | 5.9 | 8.1 |
| **Heidrun 1996-2008** | | | | | | | | | |
| Obs. (MIROS) | 33519 | 2.62 | 1.52 | - | - | - | 4.7 | 5.6 | 7.4 |
| WAM10 | 33519 | 2.75 | 1.63 | 0.47 | 0.64 | 0.92 | 4.9 | 6.0 | 8.1 |
| **Ami 1993-1998** | | | | | | | | | |
| Obs | 7462 | 2.41 | 1.45 | - | - | - | 4.3 | 5.3 | 7.5 |
| WAM10 | 7462 | 2.42 | 1.49 | 0.36 | 0.52 | 0.94 | 4.3 | 5.4 | 8.0 |

Table 3. Significant wave height observed *v* WAM10 at Ekofisk, Sleipner, Gullfaks, Draugen, Heidrun and Ami.

| Ekofisk 1980-2002 | | | | | | | | | |
|---|---|---|---|---|---|---|---|---|---|
| Significant Wave height | N | Mean | St.dev. | Mean abs. difference | RMS difference | Corr. coefficient | P90 | P95 | P99 |
| Obs. | 29044 | 2.08 | 1.29 | - | - | - | 3.8 | 4.5 | 6.3 |
| ERA40 | 29044 | 1.88 | 1.11 | 0.36 | 0.56 | 0.91 | 3.4 | 4.1 | 5.5 |

| | | | | | | | | | |
|---|---|---|---|---|---|---|---|---|---|
| **Sleipner 1995-2002** | | | | | | | | | |
| Obs. (MIROS) | 8889 | 2.29 | 1.38 | - | - | - | 4.2 | 4.9 | 6.4 |
| ERA40 | 8889 | 2.19 | 1.16 | 0.45 | 0.62 | 0.90 | 3.8 | 4.5 | 5.8 |
| **Gullfaks 1990-2002** | | | | | | | | | |
| Obs. (MIROS) | 15230 | 2.69 | 1.55 | - | - | - | 4.9 | 5.7 | 7.4 |
| ERA40 | 15230 | 2.60 | 1.35 | 0.46 | 0.65 | 0.91 | 4.5 | 5.3 | 6.8 |
| **Draugen 1995-2002** | | | | | | | | | |
| Obs. (MIROS) | 8043 | 2.62 | 1.67 | - | - | - | 5.0 | 6.0 | 7.9 |
| ERA40 | 8043 | 2.35 | 1.27 | 0.50 | 0.70 | 0.94 | 4.1 | 4.9 | 6.6 |
| **Heidrun 1996-2002** | | | | | | | | | |
| Obs. (MIROS) | 8043 | 2.67 | 1.48 | - | - | - | 4.7 | 5.5 | 7.5 |
| ERA40 | 8043 | 2.43 | 1.30 | 0.45 | 0.62 | 0.92 | 4.2 | 5.1 | 6.7 |
| **Ami 1993-1998** | | | | | | | | | |
| Obs | 3730 | 2.41 | 1.45 | - | - | - | 4.3 | 5.3 | 7.4 |
| ERA40 | 3730 | 2.07 | 1.17 | 0.44 | 0.65 | 0.93 | 3.5 | 4.3 | 6.6 |

Table 4: Significant wave height observed *v* ERA40 at Ekofisk, Sleipner, Gullfaks, Draugen, Heidrun and Ami.



(a) Ekofisk

31
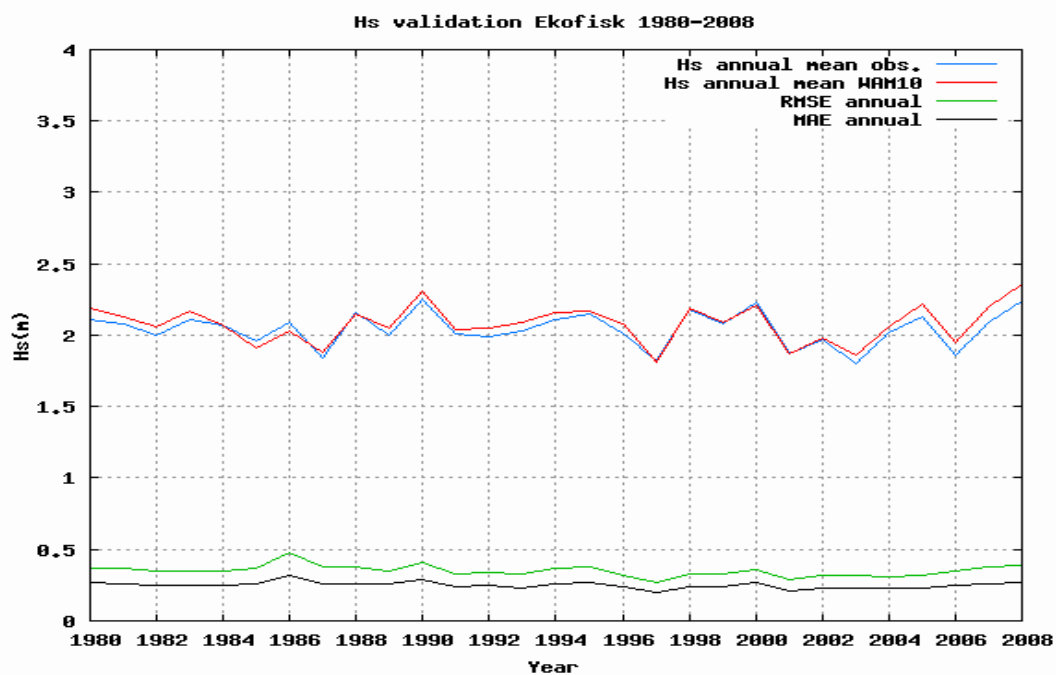
(b) Gullfaks
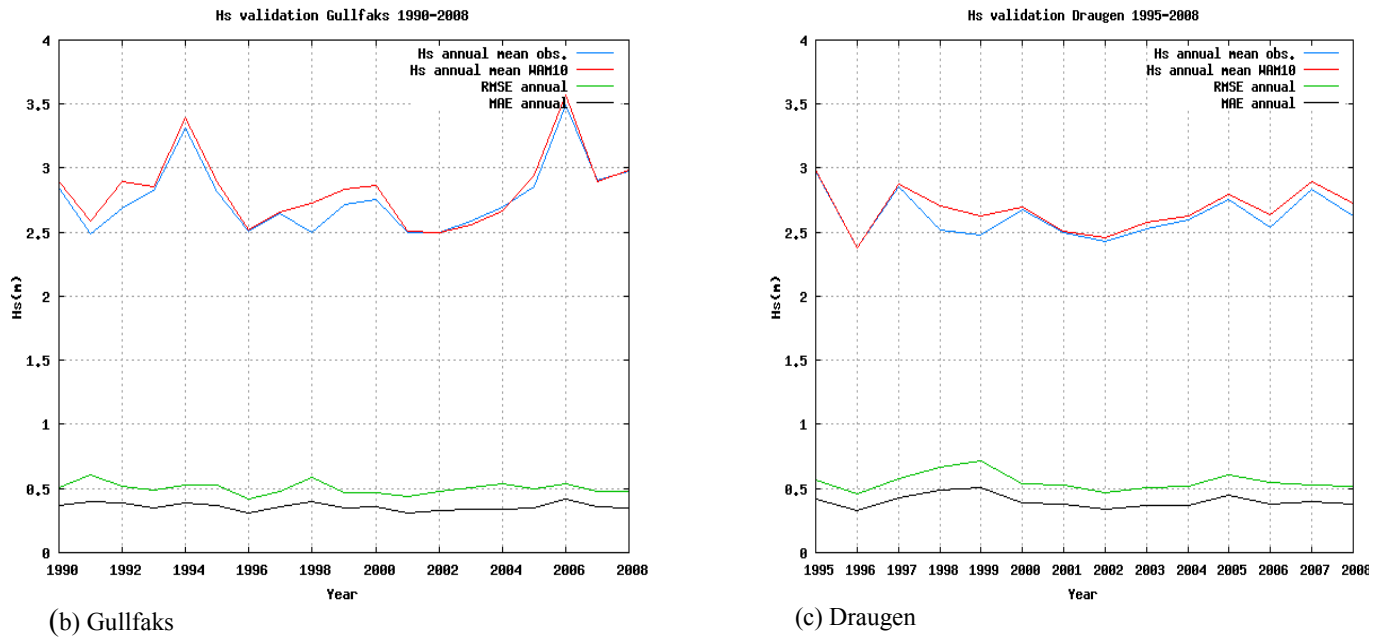


(c) Draugen

Figure 20: Comparison of modelled and observed $H_s$ at (a) Ekofisk 1980-2008, (b) Gullfaks 1990-2008, (c) Draugen 1995-2008. Blue line is the observed annual mean $H_s$, red is modelled annual mean $H_s$, green is annual RMSE and black is annual MAE.
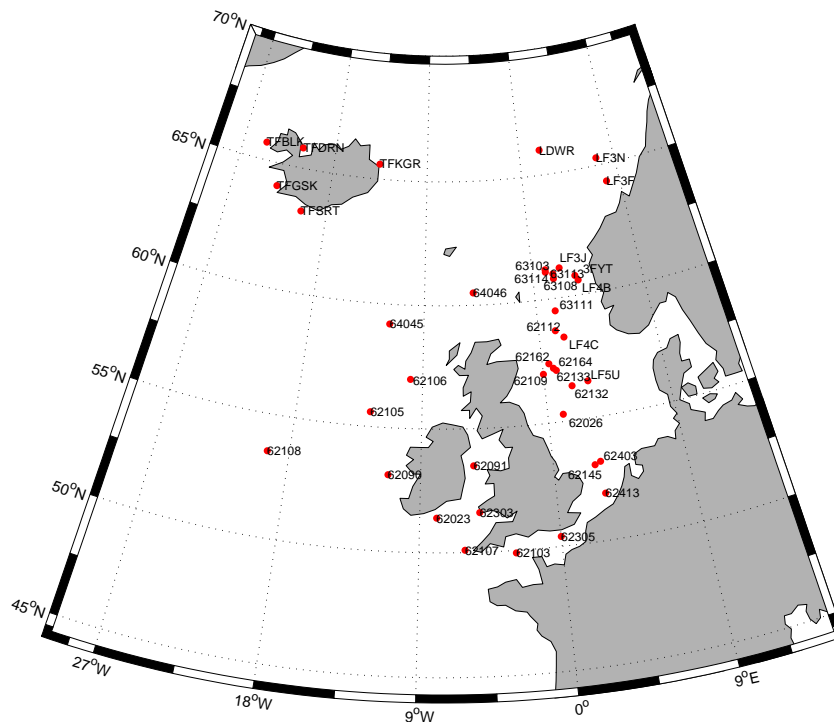


Figure 21: *In-situ* measurements covering the North-East Atlantic Ocean averaged over four hours on the synoptic times (00, 06, 12 and 18 UTC) have been quality-controlled and prepared by ECMWF (Saetra and Bidlot, 2004). The measurements cover the period 1991-2002.
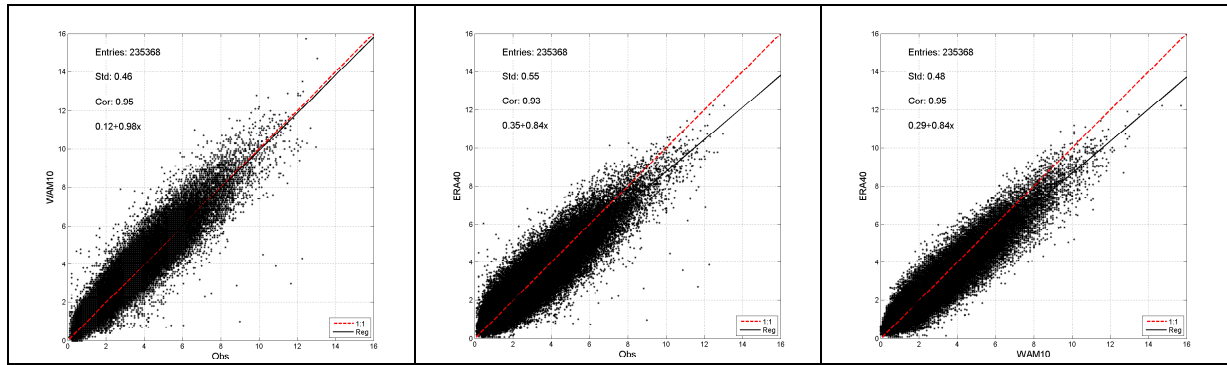
Figure 22: Scatter diagrams of significant wave height. Left: observation *v*. WAM10. Middle: Observation *v*. ERA40. Right: WAM10 *v* ERA40.

| Location | Position | $n_t$ | $r$ | | | $y = ax + b$ | | | | | | Nth-Percentile | | | | | |
| | | | Buoy WAM10 | Buoy ERA40 | WAM10 ERA40 | Buoy WAM10 | | Buoy ERA40 | | WAM10 ERA40 | | Buoy | | WAM10 | | ERA40 | |
| | | | | | | $a$ | $b$ | $a$ | $b$ | $a$ | $b$ | 95th | 99th | 95th | 99th | 95th | 99th |
|---|---|---|---|---|---|---|---|---|---|---|---|---|---|---|---|---|---|
| 3FYT | 60.80N 3.40E | 8156 | 0,93 | 0,86 | 0,93 | 1,12 | -0,04 | 0,83 | 0,46 | 0,75 | 0,46 | 4,9 | 6,2 | 5,7 | 7,4 | 4,9 | 6,2 |
| 62023 | 51.40N 7.90W | 3672 | 0,97 | 0,94 | 0,93 | 0,98 | -0,06 | 0,98 | 0,45 | 0,96 | 0,57 | 4,5 | 6 | 4,5 | 5,7 | 5,1 | 6,5 |
| 62026 | 55.40N 1.20E | 5313 | 0,96 | 0,94 | 0,96 | 1,04 | -0,16 | 0,87 | 0,05 | 0,81 | 0,21 | 3,7 | 4,9 | 3,9 | 5 | 3,4 | 4,4 |
| 62090 | 53.10N 11.20E | 1937 | 0,97 | 0,97 | 0,98 | 1,16 | -0,06 | 1,05 | 0,17 | 0,88 | 0,28 | 5,2 | 6,8 | 6,1 | 8 | 5,7 | 7,7 |
| 62091 | 53.50N 5.40W | 1925 | 0,95 | 0,87 | 0,88 | 1,28 | -0,33 | 0,94 | 0,1 | 0,71 | 0,37 | 2,5 | 3,2 | 3,1 | 4 | 2,8 | 3,8 |
| 62103 | 49.90N 2.90W | 13526 | 0,93 | 0,91 | 0,92 | 1,06 | 0,16 | 1,06 | 0,39 | 0,93 | 0,34 | 3,5 | 4,6 | 4 | 5,4 | 4,3 | 5,7 |
| 62105 | 55.50N 13.00W | 5903 | 0,97 | 0,97 | 0,98 | 0,97 | -0,07 | 0,86 | 0,19 | 0,87 | 0,32 | 6,7 | 8,9 | 6,5 | 8,6 | 6,1 | 8,1 |
| 62106 | 57.00N 9.90W | 9389 | 0,97 | 0,97 | 0,98 | 1,01 | -0,12 | 0,87 | 0,17 | 0,85 | 0,33 | 6,5 | 8,4 | 6,5 | 8,7 | 5,9 | 7,9 |
| 62107 | 50.10N 6.10W | 8779 | 0,95 | 0,95 | 0,97 | 0,93 | 0,2 | 0,99 | 0,29 | 1,02 | 0,16 | 4,9 | 6,3 | 4,9 | 6,2 | 5,3 | 6,8 |
| 62108 | 53.50N 19.50W | 6410 | 0,97 | 0,97 | 0,98 | 0,87 | 0 | 0,86 | 0,15 | 0,96 | 0,22 | 6,9 | 9,4 | 6,2 | 8,4 | 6,2 | 8,4 |
| 62109 | 57.00N 0.00E | 9770 | 0,96 | 0,95 | 0,97 | 1,06 | -0,19 | 0,89 | 0,03 | 0,83 | 0,21 | 4,1 | 5,3 | 4,3 | 5,6 | 3,8 | 5 |
| 62112 | 58.70N 1.30E | 10216 | 0,94 | 0,92 | 0,97 | 1,03 | 0,12 | 0,84 | 0,32 | 0,8 | 0,25 | 4,5 | 6,3 | 5,1 | 6,8 | 4,3 | 5,9 |
| 62132 | 56.50N 2.09E | 6719 | 0,96 | 0,94 | 0,97 | 1 | 0,04 | 0,83 | 0,24 | 0,81 | 0,24 | 4,2 | 5,5 | 4,4 | 5,7 | 3,9 | 5,1 |
| 62133 | 57.20N 1.00E | 5953 | 0,96 | 0,95 | 0,97 | 1,09 | 0,08 | 0,9 | 0,27 | 0,81 | 0,23 | 4 | 5,2 | 4,6 | 5,8 | 4 | 5,1 |
| 62145 | 53.10N 2.80E | 4394 | 0,95 | 0,92 | 0,94 | 1,04 | 0 | 0,91 | 0,14 | 0,85 | 0,18 | 3 | 4 | 3,3 | 4,3 | 3,1 | 4,1 |
| 62162 | 57.40N 0.50E | 5989 | 0,97 | 0,95 | 0,97 | 1,05 | 0,01 | 0,86 | 0,22 | 0,81 | 0,24 | 4,3 | 5,5 | 4,6 | 5,8 | 4 | 5,1 |
| 62164 | 57.20N 0.80E | 1309 | 0,96 | 0,95 | 0,97 | 1,08 | 0,03 | 0,87 | 0,22 | 0,79 | 0,22 | 3,6 | 5 | 4 | 5,4 | 3,4 | 4,5 |
| 62303 | 51.60N 5.10W | 6114 | 0,96 | 0,89 | 0,92 | 1,05 | -0,1 | 0,61 | 0,11 | 0,58 | 0,17 | 4,1 | 5,3 | 4,3 | 5,7 | 2,8 | 3,7 |
| 62305 | 50.40N 0.00E | 11813 | 0,93 | 0,82 | 0,82 | 1,2 | 0,19 | 0,96 | 0,59 | 0,75 | 0,51 | 2,5 | 3,6 | 3,3 | 4,5 | 3,3 | 4,5 |
| 62403 | 53.20N 3.20E | 5509 | 0,95 | 0,91 | 0,93 | 1,09 | 0,01 | 0,97 | 0,14 | 0,87 | 0,17 | 3,1 | 4,1 | 3,6 | 4,8 | 3,4 | 4,5 |
| 62413 | 51.90N 3.20E | 5521 | 0,95 | 0,89 | 0,91 | 1,13 | -0,13 | 0,95 | 0,13 | 0,82 | 0,26 | 2,9 | 3,8 | 3,3 | 4,5 | 3,1 | 4,1 |
| 63103 | 61.10N 1.10E | 9347 | 0,97 | 0,95 | 0,96 | 0,97 | 0,08 | 0,87 | 0,36 | 0,87 | 0,34 | 5,8 | 7,5 | 5,9 | 7,5 | 5,6 | 7,2 |
| 63108 | 60.80N 1.70E | 7434 | 0,95 | 0,92 | 0,94 | 1,03 | 0,05 | 0,91 | 0,39 | 0,86 | 0,4 | 5,2 | 6,8 | 5,6 | 7,3 | 5,3 | 7,1 |
| 63111 | 59.50N 1.50E | 10538 | 0,94 | 0,92 | 0,96 | 1 | 0,15 | 0,85 | 0,38 | 0,84 | 0,29 | 5,1 | 6,7 | 5,4 | 7,2 | 4,9 | 6,6 |
| 63113 | 61.00N 1.70E | 2239 | 0,96 | 0,93 | 0,95 | 1,03 | 0,01 | 0,91 | 0,28 | 0,86 | 0,31 | 4,7 | 6,3 | 4,9 | 6,6 | 4,7 | 6 |
| 63114 | 61.10N 1.10E | 1350 | 0,97 | 0,96 | 0,97 | 0,94 | 0,09 | 0,81 | 0,28 | 0,84 | 0,24 | 5,8 | 8,1 | 5,6 | 7,8 | 5,1 | 6,6 |
| 64045 | 59.00N 11.50W | 10982 | 0,97 | 0,97 | 0,98 | 1 | -0,16 | 0,85 | 0,2 | 0,83 | 0,4 | 6,6 | 8,8 | 6,7 | 8,9 | 6 | 7,8 |
| 64046 | 60.50N 5.00W | 2715 | 0,96 | 0,97 | 0,98 | 0,98 | 0,03 | 0,81 | 0,34 | 0,8 | 0,39 | 6,7 | 8,5 | 6,7 | 8,5 | 5,8 | 7,1 |
| LDWR | 66.14N 1.80E | 7791 | 0,95 | 0,95 | 0,97 | 1,04 | 0,17 | 0,87 | 0,37 | 0,81 | 0,3 | 5,5 | 7,4 | 6,1 | 8,1 | 5,3 | 6,9 |
| LF3F | 64.30N 7.80E | 6152 | 0,94 | 0,94 | 0,96 | 0,96 | 0,19 | 0,76 | 0,36 | 0,76 | 0,29 | 6 | 8 | 6,2 | 8,5 | 5,1 | 6,9 |
| LF3J | 61.20N 2.30E | 10168 | 0,96 | 0,93 | 0,96 | 1 | 0,12 | 0,83 | 0,43 | 0,83 | 0,35 | 5,9 | 7,6 | 6,1 | 8 | 5,5 | 7,2 |
| LF3N | 65.30N 7.30E | 6074 | 0,92 | 0,92 | 0,97 | 1,07 | -0,1 | 0,84 | 0,19 | 0,76 | 0,33 | 5,2 | 7 | 5,9 | 7,8 | 4,8 | 6,4 |
| LF4B | 60.60N 3.70E | 3207 | 0,92 | 0,85 | 0,91 | 1 | 0,27 | 0,76 | 0,63 | 0,75 | 0,47 | 5,4 | 6,8 | 5,9 | 7,6 | 5 | 6,4 |
| LF4C | 58.40N 1.90E | 6924 | 0,92 | 0,89 | 0,97 | 0,94 | 0,3 | 0,75 | 0,49 | 0,8 | 0,24 | 5 | 6,5 | 5,3 | 6,8 | 4,6 | 5,7 |
| LF5U | 56.50N 3.20E | 9619 | 0,96 | 0,94 | 0,97 | 1,01 | 0,02 | 0,83 | 0,21 | 0,82 | 0,21 | 4,5 | 6,2 | 4,7 | 6,5 | 4,1 | 5,7 |
| TFBLK | 65.70N 24.80W | 527 | 0,93 | 0,91 | 0,92 | 0,91 | 0,01 | 0,71 | 0,4 | 0,74 | 0,46 | 4,4 | 5,1 | 4 | 5,2 | 3,6 | 4,4 |
| TFDRN | 65.80N 21.20W | 493 | 0,95 | 0,87 | 0,87 | 0,9 | 0,12 | 0,49 | 0,15 | 0,52 | 0,11 | 3,5 | 6,2 | 3,3 | 5,4 | 2 | 3,5 |
| TFGSK | 64.10N 22.90W | 463 | 0,95 | 0,93 | 0,92 | 0,87 | 0,15 | 0,78 | 0,49 | 0,85 | 0,44 | 3,9 | 5,5 | 3,6 | 5,2 | 3,6 | 5,2 |
| TFKGR | 65.60N 13.60W | 454 | 0,93 | 0,9 | 0,86 | 0,99 | -0,01 | 0,83 | 0,54 | 0,75 | 0,69 | 3,4 | 5,1 | 3,4 | 5,4 | 3,3 | 4,7 |
| TFSRT | 63.30N 20.30W | 574 | 0,95 | 0,93 | 0,91 | 0,92 | 0,12 | 0,77 | 0,49 | 0,78 | 0,52 | 4,2 | 5,6 | 4 | 5,2 | 3,9 | 5,3 |

Table 4: Verification results of the WAM10 and ERA40 compared to *in-situ* measurements, buoys and platforms. Location is represented by the buoy/observation number. *nt* is the total number of available data. *r* is the correlation coefficient. *y* gives the regression line. The N-th percentile is the 95- and 99-percentile of all available data.
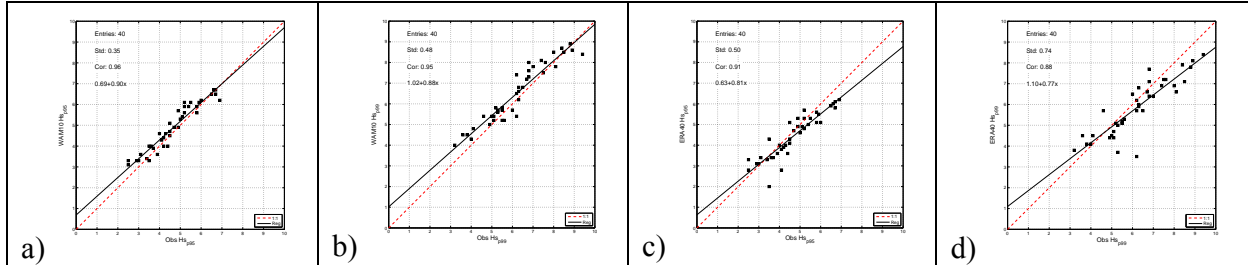


Figure 23: Model performance of the 95 and 99 percentiles of significant wave height compared to observations. WAM10: (a) 95% and (b) 99%. ERA40: (c) 95% and (d) 99%.

| | $N$ | $a$ | $b$ | *corr* |
|---|---|---|---|---|
| ERS-2 | 1.142.018 | 0.96 | 0.16 | 0.94 |
| TOPEX | 745.466 | 0.95 | 0.07 | 0.96 |
| GFO | 1.129.881 | 0.97 | 0.18 | 0.95 |

Table 5: Statistics between significant wave height from altimeters (ERS2, TOPEX and GFO) and WAM 10km model data for the years 2000 and 2001. Here $N$ is the number of co-located observations, and $a$ and $b$ are regression coefficients. Correlation is denoted *corr*.
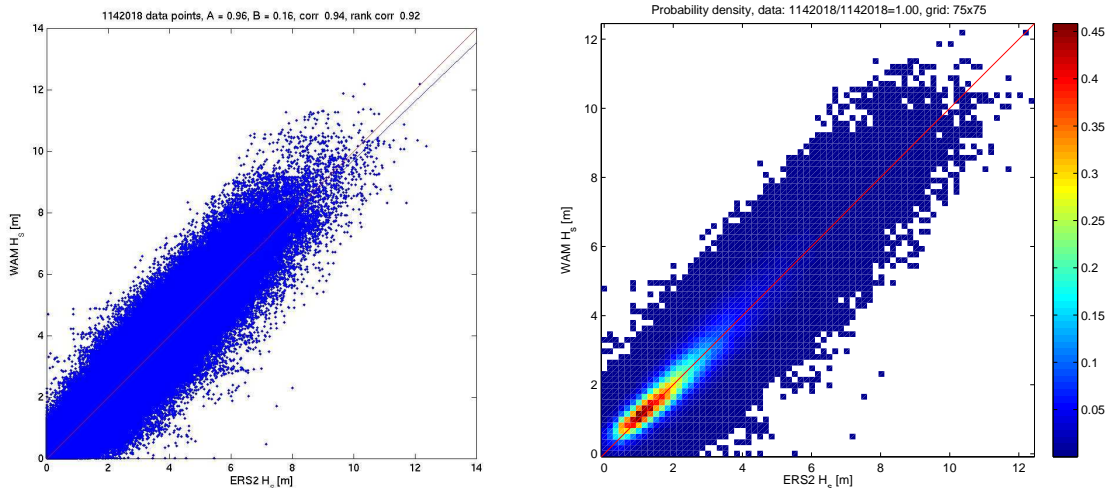


Figure 24: Comparison between WAM10 significant wave height (WAM $H_s$) and co-located altimeter wave heights from ERS-2, years 2000-2001. Statistics are given in Table 4.
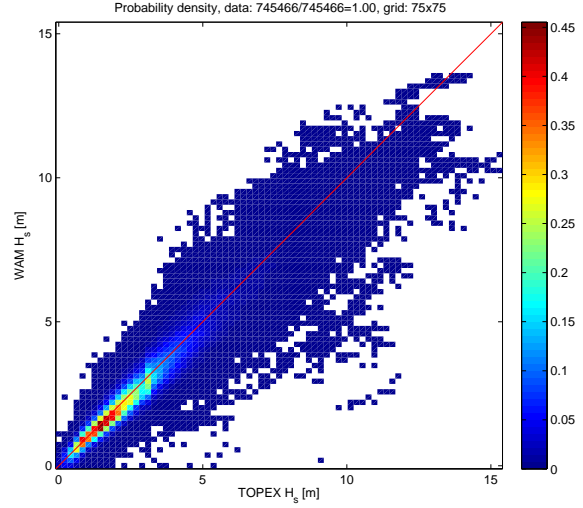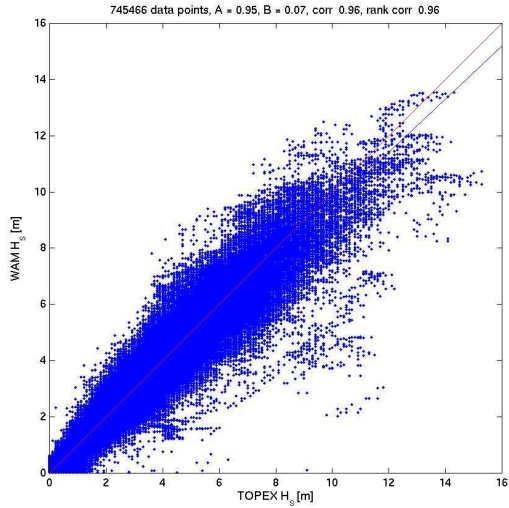
Figure 25: As Figure 24, for TOPEX.
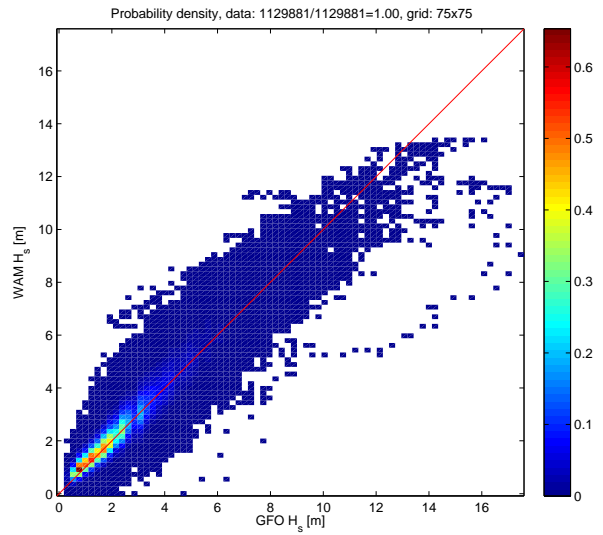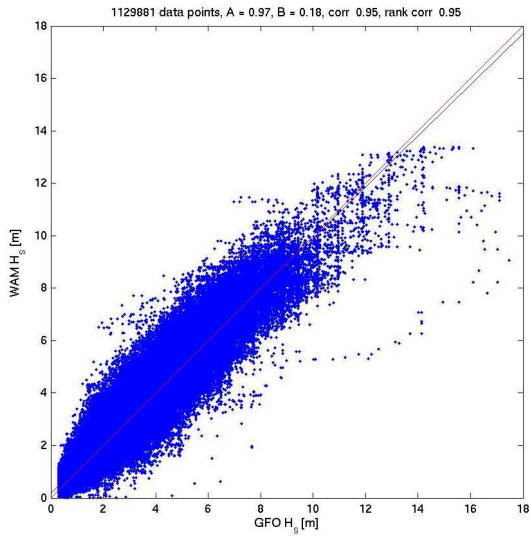


Figure 26: As Figure 24, for Geosat Follow-on (GFO).

## 3.3 Trend analysis of the significant wave height

Ocean wave variability is one aspect influencing activities at sea and at its boundaries, *e.g.* offshore industries, shipping and coastal development. Any significant positive trends in the wave field need to be accounted for in future constructions to better withstand the climate to come.

While the main focus on storm variability in the North Atlantic has been made on atmospheric changes, there are also a few studies on ocean wave variability. Kushnir *et al.* (1997) combined a shorter 10-year (1980-1989) wave hindcast with a longer 24-year (1962-86) period of sea level pressure (SLP) to obtain a statistical hindcast of the monthly mean $H_s$. In their study they found a positive trend in the mean $H_s$ at several locations within the Northeast Atlantic and related this to a systematic increase in the North Atlantic Oscillation index (NAO) over the same period.

Günther *et al.* (1998) based their analysis on a hindcast covering a 40-year period (1955-94). Using a third generation wave model forced by wind fields obtained from the U.S. Navy Fleet Numerical Meteorology and Oceanography Centre and the Norwegian Meteorological Institute, they found significant changes in the wave field in the north-eastern part of the Atlantic. The annual trend in the 99-percentile $H_s$ was found to increase with about 3 cm/yr for certain locations just north of the North Sea, while the max $H_s$ ranged between 5-10 cm/yr. This was concluded to be partly related to the NAO-index, but also explained by some artificially worsening of the storm climate in areas of poor model coverage.

Wang and Swail (2001) looked at trends in the 90 and 99-percentiles $H_s$ for the North Atlantic and the North Pacific. They used a 40-year hindcast (1958-1997) based on wind fields obtained from the NCEP/NCAR reanalysis, forcing a second generation wavemodel, ODGP2. In their analysis only trends in the winter months of January-March were found statistically significant. For the North Atlantic the trend in the 99-percentile $H_s$ was found to peak around 7 cm/yr. Wang and Swail (2002) performed a similar study to Wang and Swail (2001) using a third generation wave model, forced by winds from a kinematic reanalysis of the NCEP/NCAR fields. Once again, only trends obtained in the winter months (January-March) were found statistically significant, with a maximum increase in the 90-percentile $H_s$ around 6 cm/yr and the 99-percentile $H_s$ peaking around 8.5 cm/yr in the North Atlantic.

The linear trend is defined as *Y(t) = a + bt + e*, where *a* and *b* are the regression parameters determined by least-squares and *e* represents the residuals. If the parent distribution of the data is non-Gaussian, the slope parameter *b* is subject to large errors and should rather be based on a nonparametric method. In the following analysis we use the estimator of *b* proposed by Sen (1968), which is based on Kendall s rank correlation, see Kendall (1955),

$$b = \text{median}(\frac{X_j - X_i}{j - i}) \quad \forall \, i < j,$$

where *X* represents data of some time series at times *j* and *i*. Like Wang and Swail (2001, 2002) we utilize the Mann-Kendall test, also known as the Kendall s tau ($\tau$) test (Mann, 1945; Kendall 1955) to assess the significance of the trend. Here, the null hypothesis of randomness $H_0$ states that the data $(X_1, X_2, \quad , X_n)$ are a sample of independent and identically distributed random variables. The statistic *S* of Kendall s $\tau$ is given by

$$S = \sum_{i=1}^{n-1} \sum_{j=i+1}^{n} \text{sgn}(X_j - X_i),$$

where *n* is the length of the data set, and

$$\text{sgn}(\theta) = \begin{cases} 1, & \theta > 0 \\ 0, & \theta = 0 \\ -1, & \theta < 0. \end{cases}$$

With $n \geq 8$, the statistics $S$ is approximately normally distributed with the variance represented by

$$V_S^2 = n(n-1)(2n+5)/18.$$

The standardized test statistic $Z$ is obtained with

$$Z = \begin{cases} \dfrac{S-1}{V_S}, & S > 0 \\ 0, & S = 0 \\ \dfrac{S+1}{V_S}, & S < 0. \end{cases}$$

A two-sided test for trend may be performed with a chosen critical value of $Z$. The 5% significance level is set at $Z=1.96$. So, if the $Z$ statistic exceeds 1.96 there is a 5% likelihood of performing a type 1 error, i.e. stating that $H_0$ is false when it is actually true, or similarly, stating there is a trend when there really is none.

An important issue to consider when using the Mann-Kendall test is the sensitivity of the test to positive autocorrelation (serial correlation) in the time series. This is well documented by von Storch and Navarra (1995) and Kulkarni and von Storch (1995). They used 1000 trend free Monte Carlo simulations to prove that with a lag-1 autocorrelation >0.1 the rejection rate of $H_0$ is about the nominal rate of 5%, however, with a lag-1 autocorrelation of 0.3 the rejection rate is as high as 15%. In order to deal with this problem we follow the proposed procedure of Yue (2002):

- If there exists a trend ($b$), we assume it to be linear and a function of time ($t$). We then de-trend the original time series $X_t$ by

$$X_t' = X_t - bt$$

- We calculate the lag-1 serial correlation of the ranks of the de-trended time series, $RX_t$, based $t$ on the Salas *et al*. (1980) for $k=1$.

$$r_k = \dfrac{\dfrac{1}{n-1}\sum_{t=1}^{n-k}[RX_t' - E(RX_t')][RX_{t+k}' - E(RX_t')]}{\dfrac{1}{n}\sum_{t=1}^{n}[RX_t' - E(RX_t')]^2},$$

$$E(RX_t') = \dfrac{1}{n}\sum_{t=1}^{n} RX_t'$$

and remove the first order autoregressive process AR(1) from the de-trended time series $X_t$, which is a pre-whitening procedure. The new residual time series

$$Y_t' = X_t' - r_1 X_{t-1}'$$

is a trend-free pre-whitened (TFPW) times series, which also should be independent.

- We then blend the residual $Y_t$ with the trend $bt$

$$Y_t = Y_t' + bt_t$$

and are left with a time series that preserves the true trend, but which no longer exhibits autocorrelation.

- Perform the Mann-Kendall test.

In the following analysis we only focus on the winter season, December to February (DJF). All $H_s$ data from the period 1957-2002 have been gathered into individual histograms of bin size 0.1m per year. Besides land, grid points influenced by winter ice have also been censored. Based on the histograms we get a total of 45 entries of mean Hs, 90-percentile $H_s$, 99-percentiles $H_s$ and max $H_s$.

Figure 27 summarizes the findings of the trend analysis for the period 1957-2002. Here, the slope parameter $b$, colour-coded blue to red, represents the seasonal changes of the mean $H_s$, 90-percentile $H_s$, 99-percentile $H_s$ and max $H_s$, respectively, for the winter months (DJF). Notice that the colour scaling is different in the four plots. As stated above, some areas in the north have been removed due to the presence of sea ice. Only trends marked by the black hatching have been found statistical significant, at the 5% level, based on the Mann-Kendall test.

(a)  (b)



(c)  (d)
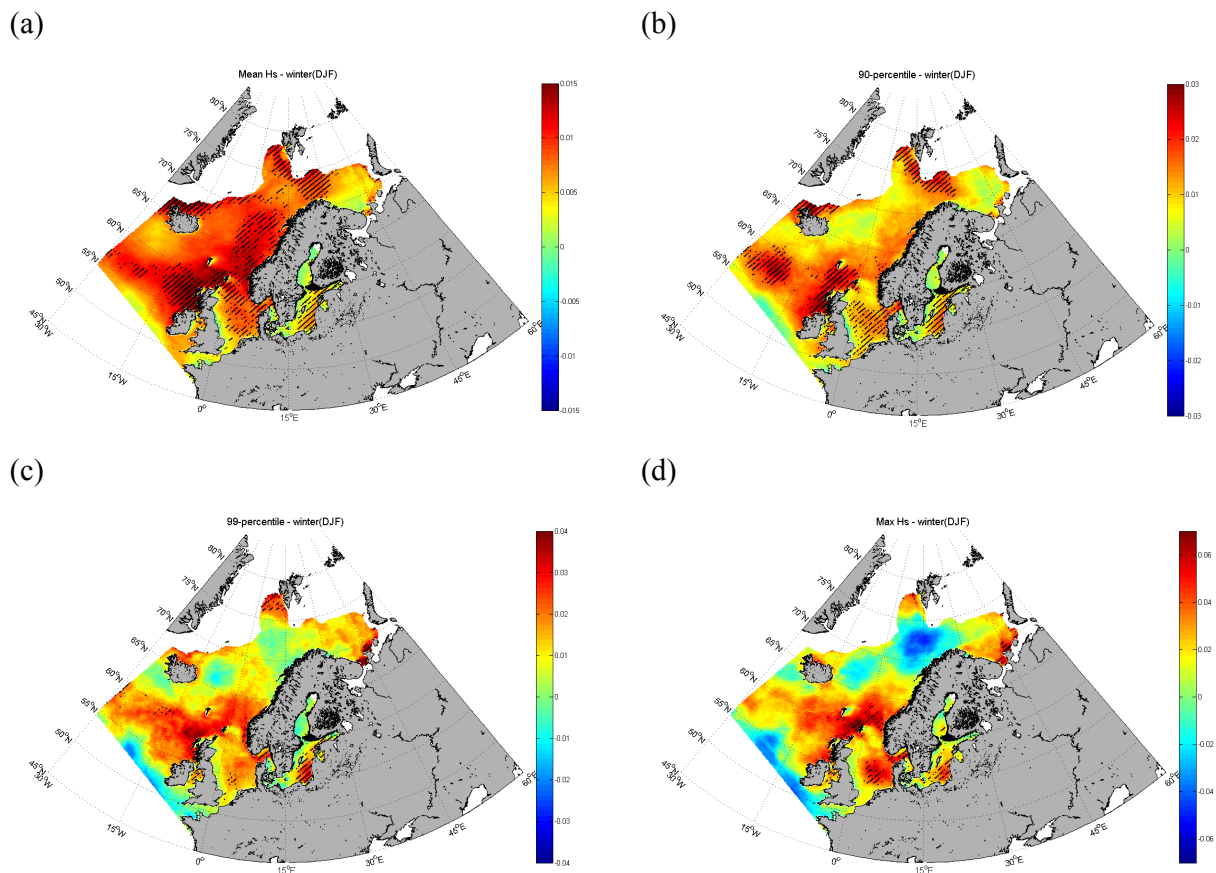
Figure 27. Changes (m/yr) in the (a) mean $H_s$, (b) 90-percentile Hs, (c) 99-percentile $H_s$ and (d) max $H_s$ for the winter season December-February for the period 1957-2002. Areas colour coded

red represent positive trends, while blue areas represent negative trends. Note that the scaling used in the four different plots is different. The black hatching indicates areas where the trend is statistically significant at the 5% level.

Changes to the mean $H_s$ is as expected moderate compared to the three other statistical parameters, however, the result is significant over a wider area. More or less without exception the trend is positive for the whole model domain, with some smaller areas showing no change. The trend is peaking around 1.5 cm/yr west of Scotland, while the southern North Sea sees a change of 0.8-1 cm/yr. The biggest trend within Norwegian waters is found near the westernmost tip of Stad, of about 1.4 cm/yr. For the Norwegian Sea, the changes are gradually decreasing going north. For the 90-percentile $H_s$ the total area of significance is smaller compared to the trend of mean $H_s$. However, we see a larger area of significant trend south of Iceland, while the trends in the Norwegian Sea no longer are statistical significant. Once again the trend is peaking west of Scotland, at about 3 cm/yr.

The significance of the 99-percentile $H_s$ trend is almost nonexistent, with a very few exceptions, *e.g.* in the eastern Baltic Sea. It is also worth noticing that there is a growing area of no trend in the northern Norwegian Sea and east of Iceland, while the maximum change has moved slightly Northwest relative to Scotland, peaking around 4 cm/yr.

The area of significant trend in max $H_s$ is covering a slightly larger area than the 99-percentile $H_s$. There is also an area of negative trend, about -4.5 cm/yr in the northern Norwegian Sea. The largest positive trend is situated north of Scotland, near the Faroe Islands, peaking around 7.5 cm/yr.

## 4   Extension of the hindcast archive, Sep 2002 to Dec 2008

The ERA40-period lasts until August 2002. The hindcast archive has been extended to cover also the period September 2002 to the end of  2008 with ECMWF operational analyses as initial and boundary conditions for the HIRLAM integration. In contrast to ERA40, which was produced with consistency in mind by running the same model version with the same data assimilation scheme over the whole period using only a subset of the available observations, ECMWF-analyses are continually upgraded and improved. The ECMWF analyses are produced using model cycles Cy25r1 T511L60 (operational in April 2002) up to Cy32r3 T799L91 (operational in September 2008) of the integrated forecast system (IFS) with approximately 15 cycles in between. The horizontal resolution of T511 corresponds to approximately 40 km and T799 corresponds to approximately 25 km. The change from T511L60 to T799L91 was done on 1 February 2006. Since we are now downscaling data with a horizontal resolution of 25-40 km, we no longer expect the same gain in accuracy in the representation of the wind field as from the downscaling of the ERA40 period[2].

---

[2]   Other changes in the ECMWF-operational system are documented on the site: http://www.ecmwf.int/products/data/operational_system/evolution/

| WIND10M (m/s) | ME | MAE | RMSE |
|---|---|---|---|
| HIRLAM | -0.01 | 1.53 | 1.95 |
| ECMWF ANA | -0.32 | 1.69 | 2.12 |
| MSLP (hPa) | ME | MAE | RMSE |
| HIRLAM | 0.03 | 0.40 | 0.55 |
| ECMWF ANA | 0.03 | 0.31 | 0.43 |
| T2M (K) | ME | MAE | RMSE |
| HIRLAM | 0.16 | 1.00 | 1.31 |
| ECMWF ANA | -0.02 | 0.81 | 1.00 |

Table 6. Summarized statistics averaged over the whole period.

Table 6 shows an improvement in all parameters compared with the period 1957-2002 found in Table 1. The trend in performance of 10m wind speed seen between the ERA40 and HIRLAM is also seen between the ECMWF-analyses and HIRLAM, although the difference is much smaller. HIRLAM still yields somewhat better wind speed scores, while MSLP and T2m are slightly better represented in the ECMWF analyses.

The trend in underestimating the 10m wind speed in ERA40 has been reduced from a total ME of -0.86 to -0.32 in the ECMWF analyses. The MAE is reduced from 2.36 to 1.69. A similar improvement is seen in the HIRLAM wind speed score. HIRLAM shows a mean error of -0.01 compared to 0.03 with ERA40, and an MAE of 1.53 compared to 1.95 with ERA40.

**Time series**
Time series of ME and RMSE for 10m wind, MSLP and T2m are shown in detail for the different types of stations in Appendix 2. Figures A2.1.1-A2.1.3 show results from 22 qualified stations. Figure A2.1.1 shows that ECMWF analyses underestimate the 10m wind speed slightly until February 2006. The change from 40 km to 25 km horizontal resolution in the ECMWF analyses essentially eliminates this difference. Figure A2.1.2 shows that the ME of MSLP for HIRLAM and the ECMWF-analyses are now almost identical, while the ECMWF-analyses have a somewhat lower RMSE. Figure A2.1.3 shows that the ME of T2m for the ECMWF analyses is approximately zero during the whole period, while HIRLAM follows a cycle with overestimation during autumn, winter and early spring and an underestimation during summer.

Figures A2.2.1-A2.2.3 are based on a comparison of 77 stations (all stations available during the ERA40 period). Figure A2.2.1 shows as A2.1.1 an underestimation of wind speed in the ECMWF analyses that vanishes February 2006. The RMSE in MSLP in A2.2.2 shows a high peak February 2005 in both the ECMWF analyses and for HIRLAM, probably due to a drop in MSLP observed at Polarfront 26 February, that the models did not capture.

Figure A2.2.3 does also show a peak in RMSE February 2005. This is probably due to very low T2m values at the stations Røros, Drevsjø and Trysil, the low temperatures were not well represented by the models.

Figures A2.3.1 A2.3.3 show time series for coastal stations. The time series of ME for 10m wind speed show a small difference between the ECMWF analyses and HIRLAM, the difference becomes even smaller during the period. Regarding MSLP, there is almost zero ME in both the ECMWF analyses and in HIRLAM (Figure A2.3.2). Figure A2.3.3 shows the trend in the HIRLAM T2m with too high temperatures in winter and too low in summer. This trend is however clearly reduced compared to the trend in the ERA40 period.

Figures A2.4.1-A2.4.3 show timeseries for the Svalbard region. The overestimation of the wind that was seen in the ERA40 period in this region, does not exist in neither the ECMWF analyses nor in HIRLAM (Figure A2.4.1). There are small differences between the ECMWF analyses and HIRLAM, but HIRLAM has some lower ME and RMSE. Regarding MSLP, Figure A2.4.2 shows quite low ME and RMSE, but with some peaks in the RMSE, indicating that there has been some decisive cases not caught in the models. Figure A2.4.3 shows ME and RMSE for T2m that are continuously reduced for the ECMWF analyses during the period. HIRLAM has a higher RMSE and is underestimating T2m at this stations.

Figure A2.5.1 showing ME and RMSE for 10m wind at Draugen, Heidrun and Norne, displays high ME and RMSE in 2007. This is due to relatively high differences between the wind speed values in the models and  wind speed values observed at Heidrun. The observations at Draugen and Norne are few in the period. The high RMSE of MSLP are mainly due to differences between MSLP at Draugen and in the ECMWF analyses and in HIRLAM. Figure A2.5.3 shows that HIRLAM has somewhat too high T2m also here over sea in winter although the overestimation is less compared to stations at the coast.

Figure A2.6.1-A2.6.3 shows timeseries for stations in the North Sea. The ECMWF analyses show slightly less ME and RMSE for 10m wind speed compared to HIRLAM. Figure A2.6.2 shows almost equal ME and RMSE of MSLP for the ECMWF analyses and HIRLAM, while Figure A2.6.3 shows some more variation in ME and RMSE for T2m in HIRLAM compared to ECMWF analyses, but without the too warm winter temperatures in HIRLAM.

**Statistical measures by station**
Statistical measures of 10m wind speed for a selection of stations are given in Tables A2.1 and A2.2. The selection of stations is based on qualified stations as described in Section 3.1 and some additional offshore stations. Table A2.1 shows that the ECMWF analyses have highest COR at more stations compared to HIRLAM. However, HIRLAM has the lowest ME and RMSE in most stations. Table A2.2 shows that HIRLAM has 20 of 25 possible 100  percentile-values closest to the observed value.

**Quantile-quantile comparison**
Figure A2.8 shows the quantile-quantile distribution (qq-plot) of 10m wind speed for the stations Jan Mayen, Fruholmen, Norne, Draugen, Ekofisk and Sleipner.

For Jan Mayen, the qq-plot shows quite good agreement between the quantiles of the ECMWF analyses and HIRLAM compared to the the quantiles in the observations although both tend to over-represent the lowest values. The ECMWF analyses under-represent the highest observed quantiles, whereas HIRLAM performs better for these highest quantiles.

The station Fruholmen does not show the same good agreement between the ECMWF analyses and HIRLAM compared to the observations. Both datasets have a significant underrepresentation of the observed quantiles from 10 m/s and above. HIRLAM is though performing better than the ECMWF analyses.

For the stations Norne, Draugen, Ekofisk and Sleipner, the quantiles for the ECMWF analyses and HIRLAM are in very good agreement with the quantiles of the observations. The ECMWF analyses has a tendency to give too low values for the highest observed quantiles while HIRLAM in some cases has too high values for the highest observed quantiles (for example at Norne and Ekofisk).

## 4.1 Discussion and conclusion

We find that in general the new atmospheric downscaling and wave hindcast yields significantly improved wind and sea state statistics compared with ERA40. In particular, the negative wind speed bias of ERA40 is not present in the HIRLAM10 downscaling. Likewise, the significant wave height of the WAM10 hindcast is also less biased. The upper tail of the distribution of both wind and significant wave height correspond better with the observed distributions. The improvement in the wave height statistics in the open ocean is mainly due to the superior wind fields (almost unbiased) of HIRLAM, but in the coastal zone the high-resolution topography obviously further improves on ERA40 by allowing a much more accurate representation of coastal features and sheltering by islands.

The downscaling of ERA40 using HIRLAM with 10-11 km horizontal resolution shows a significant improvement in the skill of 10m wind speed. Wind-field improvement is particularly pronounced at coastal stations, but small-scale features in the open ocean such as polar lows are also better resolved. However, though the polar lows are better resolved than in ERA40, we are still not modelling the full evolution of such small-scale cyclones. It is likely that this is in part due to the strict constraints placed upon the evolution of the atmosphere through the use of a digital filter and short (9 h) prognostic runs. This does not allow the model enough freedom to properly develop the polar lows. An alternative approach might be to use a spectral nudging technique similar to what Zahn *et. al.* (2008) did with a limited area model of 0.44º resolution. This method is however still in its infancy and requires substantial tuning to strike the right balance between fine-scale freedom and large-scale constraint. In particular we maintain that for a high-resolution reanalysis/hindcast study the overall precision of the atmospheric field must have higher priority, if necessary at the expense of the exact reproduction of polar lows. Around Svalbard the performance of both datasets is lower than in the rest of the area. HIRLAM shows however somewhat lower winter-time MAE and RMSE than ERA40, but both HIRLAM and ERA40 overestimate 10m wind speed in this area without properly capturing the extreme events. This is probably due to imprecisions in the representation of the ice cover.

Regarding MSLP there are small differences between the performance of this parameter in the two datasets. Both datasets represent the large scale MSLP well, but HIRLAM exhibits somewhat higher RMSE values. In single cases, for example in connection with polar lows, HIRLAM is generally performing better than ERA40, which does not resolve these small scale features. It is well known that T2m is biased towards the sea surface temperature in the coastal zone in HIRLAM, resulting in a clear seasonal cycle with too high temperatures in winter time and too low temperatures during summer. The error is considerably worse during the winter. In the summer, the errors are small and comparable with the errors in ERA40 or in some cases even smaller than ERA40. It is likely that by splitting the coastal grid points using a more detailed land-sea mask it would be possible to improve the HIRLAM T2m field comparable or even better than ERA40 (Homleid, 2008). However, it is unlikely that this will improve the wind field of the coastal zone significantly.

The significant wave height of WAM10 has been compared against two sets of buoy measurements as well as altimeter wave height estimates. Both *in situ* and satellite observations are found to correspond closely to the modelled wave field. The ERA40 wave field is found to be biased low both for the mean and for the upper percentiles. However, the lower wave heights are generally overestimated by ERA40 while higher waves are underestimated, as is evident from Figure 22. On average, ERA40 seems to underestimate the upper percentiles of the significant wave height by approximately 10% while WAM10 overestimates somewhat the higher

percentiles. The WAM10 regression slope is very nearly 1:1 both compared to *in situ* observations (Figure 22) and altimeter data (Figures 24-26)

We find a positive trend in the mean $H_s$ for the winter season over the period 1957-2002 in the North-East Atlantic. This result is statistically significant for certain regions and ranges from 0.5-1.5 cm/yr. Our results are in line with the earlier work of Günther *et al* (1998) and moderate compared to the findings of Wang and Swail (2001, 2002). A positive trend is also found in the higher part of the Hs distribution, *i.e.* the 90/99-percentile $H_s$ and the max $H_s$. These changes are most pronounced in the Southern North Sea, the Western Norwegian Sea and West and North-West of Scotland. However, any conclusions must be drawn with caution as only a few areas offer a significant result at the 5% level. It should also be stressed that we rely on ERA-40 as boundary values for our downscaled atmospheric integration. We are therefore not free of the effect of a growing amount of assimilated observations in ERA-40, particularly evident in the increasing number of satellite measurements over the period (see Uppala *et al.*, 2005). This feature may have influenced the trend analysis.

# References

Accadia, C., S. Zecchetto, A. Lavagnini and A. Speranza, 2007. Comparison of 10m wind forecasts from a regional area model and QuikScat scatterometer wind observations over the Mediterranean Sea. *Mon. Wea. Rev*, **135**, 1945-1960

Avissar, R., and R. A. Pielke, 1989. A parameterization of heterogeneous land surfaces for atmospheric numerical models and its impact on regional meteorology. *Mon. Wea. Rev.*, **117**, 2113-2136

Bjørge, D., J.E. Haugen, M. Homleid, O. Vignes, and V. Ødegaard, 2003. *Updating the HIRLAM numerical weather prediction system at met.no 2000-2002*. Norwegian Meteorological Institute, Research Report No.145.

Breivik, Ø, Y Gusdal, B R Furevik, O J Aarnes and M Reistad, 2009. Nearshore wave forecasting and hindcasting by dynamical and statistical downscaling, *J Marine Sys*, **78,** 235-243, doi:10.1016/j.jmarsys.2009.01.025

Bromwich, D. H., R. L. Fogt, K .I. Hodges and J. E. Walsh, 2007. A tropospheric assessment of the ERA-40, NCEP and JRA-25 global reanalyses in the polar regions, *J. Geophys. Res*, **112**

Caires S and A Sterl, 2005. 100-year return value estimates for ocean wind speed and significant wave height from the ERA-40 data. *J Climate* **18**, 1032 1048

Chelton, D. B., and M. H. Freilich, 2005. Scatterometer-based assessment of 10 m wind analysis from the operational ECMWF and NCEP numerical weather prediction models, *Mon. Wea. Rev.*, **133**, 409-429

Condron A., G.R. Bigg and I. A. Renfrew, 2005. Polar Mesoscale Cyclones in the Northeast Atlantic: Comparing Climatologies from ERA-40 and Satellite Imagery, *Mon. Wea. Rev.*, **134**, 1518-1533.

Cox, AT and Greenwood, JA and Cardone, VJ and Swail, VR, 1995. An interactive objective kinematic analysis, *Proc. Fourth Int. Workshop on Wave Hindcasting and Forecasting*, 109-118

Cox, A. T., and V. R. Swail, 2001. A global wave hindcast over the period 1958 1997: Validation and climate assessment, *J. Geophys. Res.*, **106**(C2), 2313 2329

Cuaxart J., P. Bougeault, and J.L. Redelsberger, 2000. A turbulence scheme allowing for mesoscale and large-eddy simulations. *Quart. J. Roy. Met. Soc.*, **126**, 1-30.

Ebuchi, N., H.C. Graber, and M.J. Caruso, 2002. Evaluation of Wind Vectors Observed by QuikSCAT/SeaWinds Using Ocean Buoy Data. *J. Atmos. Oceanic Technol.*, **19**, 2049 2062.

Eide, L.I, M.Reistad, J.Guddal, 1985: *A database of computed wind and wave parameters for the North Sea , The Norwegian Sea and the Barents Sea for every 6 hours for the years 1955-1981* (In Norwegian). Norwegian Meteorological Institute, project report.

ECMWF, 2002. *IFS Documentation, CY25R1 Operational implementation 9 April 2002*, Available online at  http://www.ecmwf.int/research/ifsdocs/CY25r1/index.html or http://tinyurl.com/ygb7fu4  (Accessed 10 November 2009).

Furevik, B. R., L. A. Breivik and F. Tveter, 2008. *QuikScat validation report*, Norwegian Meteorological Institute report no. 3

Günther, H., S.Hasselmann and P.A.E.M.Janssen, 1992. *The WAM model cycle 4*. Technical Report, Deutsches KlimaRechenZentrum, Hamburg, Germany

Günther, H., Rosenthal, W., Stawarz, M., Carretero, JC, Gomez, M., Lozano, I., Serrano, O. and Reistad, M, 1998. The wave climate of the Northeast Atlantic over the period 1955-1994 : The WASA wave hindcast, *The Global Atmosphere and Ocean System*, **6**(2),  121-163

Gibson, JK, P. Kållberg, S. Uppala, 1996. The ECMWF re-analysis (ERA) project, *ECMWF newsletter*, **73**, 7-17

Gibson, JK, P. Kållberg, S. Uppala, A. Hernandez, A. Nomura and E. Serrano, 1997. *ERA-15 description*, ECMWF Reanalysis Project Report Series, **1**, 72 pp

Haug, O. and J. Guddal, 1981. *Hindcasting the Wind and Wave Climate of Norwegian Waters*. Norwegian Meteorological Institute, project report.

Homleid, M., 2008. *Modified weighting of HIRLAM 2 meter temperature forecasts*. Norwegian Meteorological Institute report no. 14.

Huang X-Y, and X. Yang, 2002. *A new implementation of digital filtering initialization schemes for HIRLAM*. DMI Technical Report.

Källén, E., 1996. HIRLAM documentation manual. System 2.5. Technical report, HIRLAM, 178pp. Available from SMHI, S-60176, Norrköping, Sweden.

Kalnay, E., M Kanamitsu, R Kistler, W Collins, D Deaven, L Gandin, M Iredell, S Saha, G White, J Woollen *et. al.*, 1996. The NCEP/NCAR 40-year reanalysis project, *Bulletin of the American Meteorological Society*,   **77**(3), 437-471

Komen, G.J., L. Cavaleri, M. Donelan, K. Hasselmann, S. Hasselmann, and P.A.E.M. Janssen, 1994. *Dynamics and Modelling of Ocean Waves*. Cambridge University Press, Cambridge.

Kendall, M. G., 1955. *Rank Correlation Methods*. Griffin: London.

Kulkarni, A. and von Storch, H., 1995. Monte Carlo experiments on the effect of serial correlation on the Mann Kendall test of trend. *Meteorologische Zeitschrift* 4(2): 82 85.
Mann, H. B., 1945: Nonparametric tests against trend. *Econometrica* 13: 245 259.

Kushnir, Y., Cardone, V. J., Greenwood, J. G. and Cane, M. A., 1997. The recent increase in North Atlantic wave heights. *Journal of Climate,* **10,** 2107 2113.

Laprise, R., 1992. The resolution of global spectral models, *Bull. Amer. Meteor. Soc.*, **73**, 1453-1454.

Lynch, P., McGrath, R. and McDonald, A., 1999. *Digital filter initialization for HIRLAM*, HIRLAM Tech. Rep. 42, 22 pp. Available from Met Eireann, Glasnevin Hill, Dublin 9, Ireland.

Lynch, P., 1997. The Dolph-Chebyshev Window: A Simple Optimal Filter, *Mon. Wea. Rev.*, **125**, 655-660.

Moore GW, Pickart KRS, Renfrew IA, 2008. Buoy observations from the windiest place in the world ocean, Cape Farewell, Greenland, *Geophysical Research Letters*; **35**, DOI: 10.1029/2008GL034845.

Noilhan, J. and S. Planton, 1989. A simple parameterization of land surface processes for meteorological models. *Mon. Wea. Rev.*, **117**, 536-549.

Onogi, K., H Koide, M Sakamoto, S Kobayashi, J Tsutsui, H Hatsushika, T Matsumoto, N Yamazaki, H Kamahori, K Takahashi, *et. al.*, 2005. JRA-25: Japanese 25-year re-analysis project-progress and status, *Quarterly Journal of the Royal Meteorological Society*, **131**

Paulson, C. A., 1970. The Mathematical Representation of Wind Speed and Temperature Profiles in the Unstable Atmospheric Surface Layer, *J. Appl. Meteor*, **9**(6), 857-861

Pielke, R.A., 1991. Recommended specific definition of resolution . *Bull. Amer. Meteor. Soc.*, **72**, 1914

Portabella, M., and A. Stoffelen, 2001. Rain Detection and Quality Control of SeaWinds. *J. Atmos. Oceanic Technol.*, **18**, 1171 1183

Reistad, M. and K. Iden, 1998. *Updating, correction and evaluation of a hindcast data base of air pressure, wind and waves for the North Sea, the Norwegian Sea and the Barents sea*. Norwegian Meteorological Institute Research report No. 9

Reistad, M, Ø Breivik and H Haakenstad, 2007. A High-Resolution Hindcast Study for the North Sea, the Norwegian Sea and the Barents Sea, *in Proceedings of the 10th International Workshop on Wave Hindcasting and Forecasting and Coastal Hazard Symposium*, 13pp

Ris, R.C, L. H. Holthuijsen, and N. Booij, 1999. A third-generation wave model for coastal regions, 2. Verification, *J. Geophys. Res,* **104**(C4), 7667 7681

Salas, J. D., Delleur, J. W., Yevjevich, V., Wallis, W. L., 1980. *Applied Modelling of Hydrologic time series*. Water Resource Publications: Littelton, CO, USA.

Sass B. H., L. Rontu and P. Räisänen, 1994. HIRLAM-2 Radiation Scheme: Documentation and Tests. Technical Reprot 16, The HIRLAM-3 Project, SMHI, S-60176 Norrköping, Sweden.

Saetra, O. and Bidlot, J. R., 2004: On the potential benefit of using probabilistic forecast for waves and marine winds based on the ECMWF ensemble prediction system. *Wea. Forecasting* **19**, pp. 673-689.


Savijäervi H.,1990. Fast radiation parameterization schemes for mesoscale and short-range forecast models. *J. Appl. Meteor.*, 29, pages 437-447.

Sen, P. K., 1968. Estimates of the regression coefficient based on Kendall s tau. *Journal of the American Statistical Association* **63**, 1379 1389.

Simmons, A.,J., and J.K. Gibson, Eds., 2000. The ERA-40 Project Plan, ERA-40 Project Report Series 1, 63 pages

Sterl, A., G. J. Komen, and P. D. Cotton, 1998. Fifteen years of global wave hindcasts using winds from the European Centre for Medium-Range Weather Forecasts reanalysis: Validating the reanalyzed winds and assessing the wave climate, *J. Geophys. Res.*, **103**(C3), 5477 5492.

von Storch, H. and Navarra, 1995. *Analysis of Climate Variability   Applications of Statistical Techniques*. Springer-Verlag, 334 pp.

Sundquist, H., 1993. Inclusion of Ice Phase of Hydrometeors in Cloud Parameterization  for Mesoscale and Largescale Models. Contr. Atm. Phys., 66, pages 137-147.

Swail, V.R., and A.T. Cox, 2000. On the Use of NCEP  NCAR Reanalysis Surface Marine Wind Fields for a Long-Term North Atlantic Wave Hindcast. *J. Atmos. Oceanic Technol.*, **17**, 532  545.

Undén, P., Rontu, L., Järvinen, H., Lynch, P., Calvo, J., Cats, G., Cuaxart, J., Eerola, K., Fortelius, C., Garcia-Moya, J.A., Jones, C., Lenderlink, G., McDonald, A., McGrath, R., Navascues, B., Nielsen, N.W., Ødegaard, V., Rodriguez,E., Rummukainen, M., Rööm, R., Sattler, K., Sass, B.H., Savijärvi, H., Schreur, B.W., Sigg, R., The, H. and Tijm,A., 2002. *HIRLAM-5 Scientific Documentation, HIRLAM-5 Project.* Available from SMHI, S-601767 Norrköping, Sweden.

Uppala, S.M., Kållberg, P.W., Simmons, A.J., Andrae, U., da Costa Bechtold, V., Fiorino, M., Gibson, J.K., Haseler, J., Hernandez, A., Kelly, G.A., Li, X., Onogi, K., Saarinen, S., Sokka, N., Allan, R.P., Andersson, E., Arpe, K., Balmaseda, M.A., Beljaars, A.C.M., van de Berg, L., Bidlot, J., Bormann, N., Caires, S., Chevallier, F., Dethof, A., Dragosavac, M., Fisher, M., Fuentes, M., Hagemann, S., Hólm, E., Hoskins, B.J., Isaksen, L., Janssen, P.A.E.M., Jenne, R., McNally, A.P., Mahfouf, J.-F., Morcrette, J.-J., Rayner, N.A., Saunders, R.W., Simon, P., Sterl, A., Trenberth, K.E., Untch, A., Vasiljevic, D., Viterbo, P., and Woollen, J., 2005. *The ERA-40 re-analysis. Quart. J. R. Meteorol. Soc.*, **131**, 2961-3012.

The WAM-Development and Implementation Group (WAMDI), 1988.
S. Hasselmann, K. Hasselmann, E. Bauer, L. Bertotti, C. V. Cardone, J. A. Ewing, J. A. Greenwood, A. Guillaume, P. A. E. M. Janssen, G. J. Komen, P. Lionello, M. Reistad, and L. Zambresky: *The WAM Model - a third generation ocean wave prediction model. J. Phys. Oceanogr.*, **18** (12), 1775-1810.

The WASA group, 1998. Changing waves and storms in the Northeast Atlantic? *Bull Am Meteorol Soc* **79**, 741  760

Wang, X.L., and V.R. Swail, 2001. Changes of Extreme Wave Heights in Northern Hemisphere Oceans and Related Atmospheric Circulation Regimes. *J. Climate*, **14**, 2204  2221

Wang, X.L., and V.R. Swail, 2002. Trends of Atlantic Wave Extremes as Simulated in a 40-Yr Wave Hindcast Using Kinematically Reanalyzed Wind Fields. *J. Climate*, **15**, 1020  1035

Weisse, R  and H Günther, 2007. Wave climate and long-term changes for the Southern North Sea obtained from a high-resolution hindcast 1958  2002, *Ocean Dynamics*, **57**(3), 162-171

WMO, 1998: *Guide to wave analysis and forecasting*, World Meteorological Organization, Report No. 702

Wyser K., L. Rontu and H. Savijäervi, 1999. Introducing the effective radius into a fast radiation scheme of a mesoscale model. *Contr. Atm. Phys.* **72**, 205-218.

Yang, X., 2005. Background blending using an incremental spatial filter, *Hirlam Newsletter*, **49**, 3-11

Yue, S., Pilon, P., Phinney, B. and Cavadias, G., 2002. The influence of autocorrelation on the ability to detect trend in hydrological series. *Hydrological processes,* **16**, 1807-1829.

Zahn, M. H von Storch, and S Bakan, 2008. Climate mode simulation of North Atlantic polar lows in a limited area model, *Tellus* A, **60**(4), 620-631

Zambreski, L., 1989: A verification study of the global WAM model, *Tech. Rep. 63*, ECMWF

Zambreski, L., 1991: An evaluation of two WAM hindcasts for LEWEX, in *Directional Ocean Wave Spectra*, edited by R. C. Beal, 167  172

**Appendix 1**

**A.1.    Theory**

**A.1.1.  Numerical schemes and physical parameterizations in HIRLAM**

A Semi-Lagrangian scheme is used in the discretization of the equations (Undén *et. al.*, 2002) while a hybrid sigma-pressure coordinate is used as vertical coordinate

The surface scheme is called   Mosaic of tiles  of Avissar and Pielke (1989).          The surface is classified into five types, or tiles, which evolve independently and couple directly to the atmosphere of the model.  The five tiles defined within each grid square are: sea/lake water, ice, bare land, forests and agricultural terrain/low vegetation.

For the land surface types, the scheme ISBA (Noilhan and Planton, 1989) is used. Soil temperature and soil water content are treated with force-restore models. The soil is divided in two layers; one surface layer with a depth of 1 cm and a total layer extending down to a depth of about 1 m.

The turbulence scheme is based on prognostic turbulent kinetic energy combined with a diagnostic length scale and is built on the CBR-scheme (Cuxart *et. al*., 2000).

The condensation scheme used is called STRACO (Soft TRAnsition Condensation scheme). The scheme    parameterizes large scale and convective condensation with special emphasis in achieving gradual transitions between the condensation types. Cloud water is a prognostic variable. Convection is based on Kuo while large scale condensation and precipitation procedures are built on microphysics from Sundquist, 1993.

The radiation scheme provides the surface net radiative fluxes plus the temperature tendency of air resulting from terrestrial and solar radiation. The Savijärvi scheme is described in Sass *et. al*. (1994) and in Wyser *et. al*. (1999).

### A.1.2. Diagnostic calculation of near surface parameters

Below the lowest model level most variables are held constant except for geopotential, temperature, winds and the vertical pressure coordinate velocity. Mean sea level pressure is calculated assuming a dry hydrostatic atmosphere with a constant lapse rate of 6.5 K/km with modifications for very warm or very high temperatures. 10m wind velocity ($u$ and $v$) and temperature ($T$) in a stably stratified surface layer is obtained from the formula (1), which is a modified form of the log-linear, integrated Businger profiles:

$$u(z) = (u_*/k)\ln\left(\frac{z}{z_0}\right) + u_n\left(1 - \exp\left(-b_m\ k^{-1} u_* u_n^{-1} z L^{-1}\right)\right)$$

$$v(z) = (v_*/k)\ln\left(\frac{z}{z_0}\right) + v_n\left(1 - \exp\left(-b_m\ k^{-1} v_* v_n^{-1} z L^{-1}\right)\right)$$

$$(1)$$

$$T(z) = T_S + (\theta_*/k)\ln\left(\frac{z}{z_0}\right) + \Delta\theta_n\left(1 - \exp\left(-b_h\ k^{-1}\theta_*\theta_n^{-1} z L^{-1}\right)\right)$$

where
$k$ is the index for numbering model levels,
$n$ is the lowest model level and
$b_m = 1/\text{Ri}_{cr} \sim 4$, while
Ri is the Richardson number,
$z$ is the height above surface and
$z_0$ is the roughness length.
$L$ is the Monin-Obukhov stability length
$\Delta\theta_n = \theta_n - \theta_s$

In the case of an unstably stratified surface layer, the near the 10m wind velocity is obtained from:

$$u(z) = (u_*/k) \cdot \left\{\ \ln\left(\frac{z}{z_0}\right) - \left(\ln\frac{1+x^2}{2} + 2\ln\frac{1+x}{2} - 2\tan^{-1}x + \frac{\pi}{2}\right)\ \right\}$$

$$v(z) = (v_*/k) \cdot \left\{\ \ln\left(\frac{z}{z_0}\right) - \left(\ln\frac{1+x^2}{2} + 2\ln\frac{1+x}{2} - 2\cdot\tan^{-1}x + \frac{\pi}{2}\right)\ \right\}$$

$$(2)$$

$$T(z) \cong T_S + c_\theta\ \frac{\theta_*}{k}\ \left\{\ln\frac{z}{z_0} - 2\cdot\ln\frac{1+y}{2}\ \right\}$$

where
$x = (1-15\ (z/L))^{1/4}$,
$y = (1-9(z/L))^{1/2}$,
$c_\theta = c_q = 1$.

For more details, see Källèn (1996) and Paulson (1970).

Wind velocity in 10m level and temperature in 2m level are defined on each tile in a grid square. The 10m wind velocity and 2m temperature used in the validation of the model results are averaged values on the 5 tiles. The fields have been weighted linearly with respect to the fractions of each tile.

## A.2. Verification measures

Mean Error (ME) $\quad = \quad \dfrac{1}{n}\sum_{i=1}^{n}(f_i - o_i)$

Mean Absolute Error (MAE) $\quad = \quad \dfrac{1}{n}\sum_{i=1}^{n}|f_i - o_i|$

Root Mean Square Error (RMSE) $\quad = \quad \left(\dfrac{1}{n}\sum_{i=1}^{n}(f_i - o_i)^2\right)^{1/2}$

Standard Deviation of Error (SDE) $\quad = \quad \left(\dfrac{1}{n}\sum_{i=1}^{n}(f_i - o_i - ME)^2\right)^{1/2}$

Correlation (COR) $\quad = \quad \dfrac{\dfrac{1}{n}\sum_{i=1}^{n}\left(f_i - \bar{f}\right)\left(o_i - \bar{o}\right)}{SD(f)\,SD(o)}$

where $\;\bar{f} = \dfrac{1}{n}\sum_{i=1}^{n} f_i\,$, and $\bar{o} = \dfrac{1}{n}\sum_{i=1}^{n} o_i$

SD($f$) = $\quad \left(\dfrac{1}{n}\sum_{i=1}^{n}(f_i - \bar{f})^2\right)^{1/2}$

SD($o$) = $\quad \left(\dfrac{1}{n}\sum_{i=1}^{n}(o_i - \bar{o})^2\right)^{1/2}$

are the means and the standard deviation to the forecasts and observations.

Percentiles:
T100: The max value in the dataset.
T99: The specific value where 1 % of all the values in the dataset are above this limit.
T95: The specific value where 5 % of all the values in the dataset are above this limit.
T90: The specific value where 10 % of all the values in the dataset are above this limit.

## A.3 Stations by region

Appendix A.3 shows time series of monthly values of ME, MAE and RMSE for 10m wind speed, MSLP and T2m. The time series are divided into different categories depending on the geographical positions of the stations used in the validation.

Figures A.3.1.1 to A.3.1.3 show results from validation including all weather stations available, counting 77 stations, of which not all have observations over the whole period (see table A.4.3). Figures A.3.1.1 - A.3.1.3 reflect the results in the Figures 4a - 6a where only the most reliable stations were taken into account, but with a smaller difference between HIRLAM and ERA40. Regarding MSLP (Figure A.3.1.2) the lines of ERA40 and HIRLAM are varying more in the last part of the period and it turned out that Tryvasshøgda has several erroneous observations of MSLP disturbing the results (fore example MSLP of 700 hPa on 27 June 1995). Figure A.3.1.3 shows a clear reduction in the ME of T2m in HIRLAM compared to Figure 6 (a) and a less significant yearly cycle, as expected because of the introduction of more land stations in the evaluation.

Figures A.3.2.1 to A.3.2.3 show results from validation with only coastal stations (counting 29 stations, of which not all have observations over the whole period). The time series of 10m wind in coastal stations show larger differences between HIRLAM and ERA40, with HIRLAM performing best. Figure A.3.2.3 also shows that the errors in HIRLAM T2m is to a large extent a coastal problem.

Figures A.3.3.1 to A.3.3.3 show results from validation with only stations nearby Svalbard (counting 6 stations, of which only 2 stations have observations from the beginning of the period). The figures show worse results for this area both for 10m wind speed, MSLP and T2m compared to the other areas. This area is often influenced by small scale and intense weather phenomena which are difficult to predict. The few number of observation stations does also limit the conclusions of the results. However, what we see is that 10m wind speed in HIRLAM has a somewhat lower MAE and RMSE in winter time compared to the 10m wind speed in ERA40. In summer time there is no clear difference. Both HIRLAM and ERA40 overpredict the 10m wind speed. ERA40 shows better results than HIRLAM for MSLP and the trend is the same as seen in the previous results, but the error is small in both models. The over-prediction of winter-time T2m is exacerbated this area by the increased temperature contrast between land and sea. Both HIRLAM and ERA40 overpredict T2m in winter in this area but the overprediction is larger in HIRLAM than in ERA40.

Figures A.3.4.1 to A.3.4.3 show results from validation including stations in the Norwegian sea; Draugen, Heidrun and Norne (Oct 1993 Dec 2001), of which only Draugen has observations for the whole period. Since the results are based on so few stations, it is not possible to say anything sure about the results, but the figures do show that HIRLAM calculate 10m wind speed better than ERA40 during almost the whole period. MSLP is somewhat better for ERA40, while T2m shows good results in both ERA40 and HIRLAM.

Figures A.3.5.1 A.3.5.3 show results from validation including stations in the North Sea (Ekofisk, Frigg, Sleipner and Gullfaks). The figures show high values of MAE and RMSE for 10m wind speed and also for MSLP in the beginning of the period both in HIRLAM and in ERA40, but only Frigg was operational the 2 first years in the time series. The following 8 years are based on results from 2 stations (Frigg and Ekofisk). The results are therefore not reliable. The time series show however a gradual improvement of ME, MAE, and RMSE in the 10m wind speed with time. An improvement can also be seen in MSLP.

**ME. Wind 10m. All stations. 1957.09–2002.08**

Red: H10    Blue: ERA40

**MAE. Wind 10m. All stations. 1957.09–2002.08**

Red: H10    Blue: ERA40

**RMSE. Wind 10m. All stations. 1957.09–2002.08**

Red: H10    Blue: ERA40
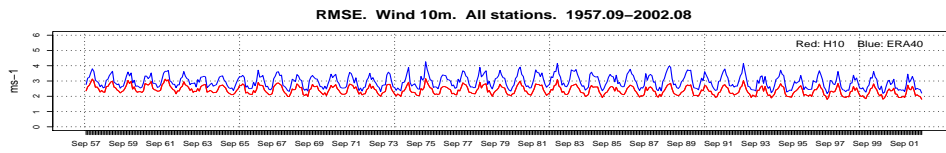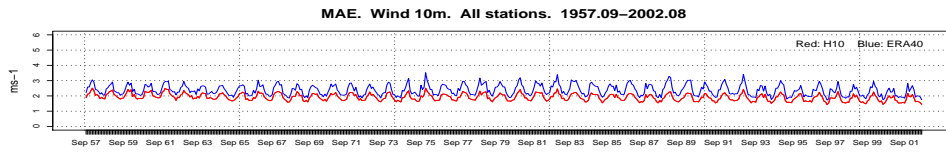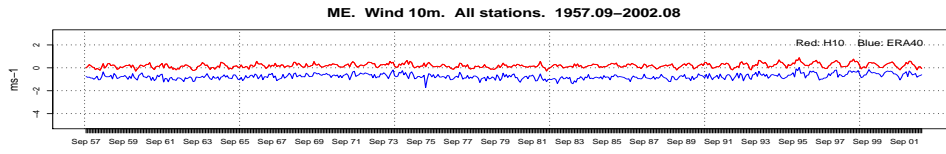
A.3.1.1. Time series (1957.09  2002.08) of  respectively ME, MAE and RMSE for 10m wind (77 stations).

**ME. Pressure. All stations. 1957.09–2002.08**

Red: H10    Blue: ERA40

**MAE. Pressure. All stations. 1957.09–2002.08**

Red: H10    Blue: ERA40

**RMSE. Pressure. All stations. 1957.09–2002.08**

Red: H10    Blue: ERA40
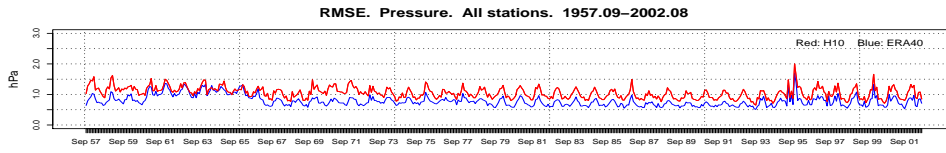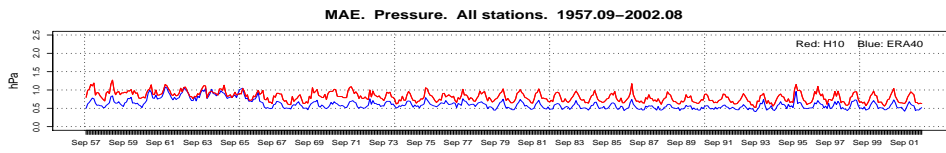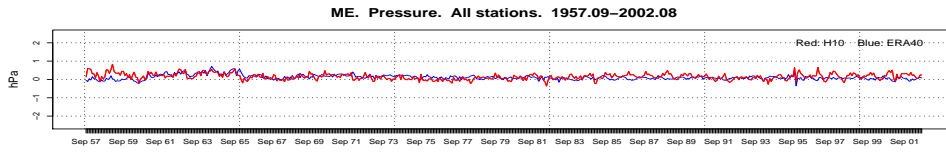
A.3.1.2. Time series (1957.09 2002.08) of respectively ME, MAE and RMSE for MSLP (77 stations).



ME. Temperature 2m. All stations. 1957.09–2002.08



MAE. Temperature 2m. All stations. 1957.09–2002.08



RMSE. Temperature 2m. All stations. 1957.09–2002.08
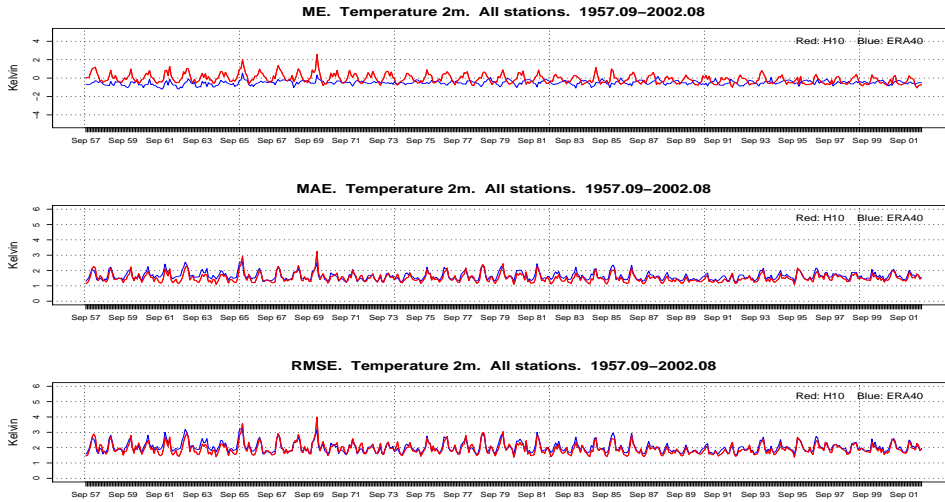
A.3.1.3. Time series (1957.09 2002.08) of respectively ME, MAE and RMSE for T2m (77 stations).



ME. Wind 10m. Coastal stations. 1957.09–2002.08



MAE. Wind 10m. Coastal stations. 1957.09–2002.08



RMSE. Wind 10m. Coastal stations. 1957.09–2002.08
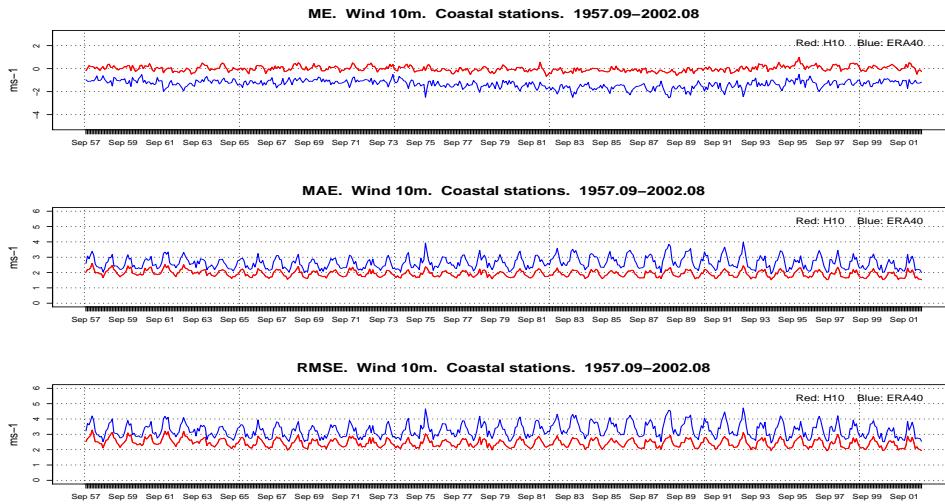
A.3.2.1. Time series (1957.09 2002.08) of respectively ME, MAE and RMSE for 10m wind (coastal stations).



ME. Pressure. Coastal stations. 1957.09–2002.08



MAE. Pressure. Coastal stations. 1957.09–2002.08



RMSE. Pressure. Coastal stations. 1957.09–2002.08
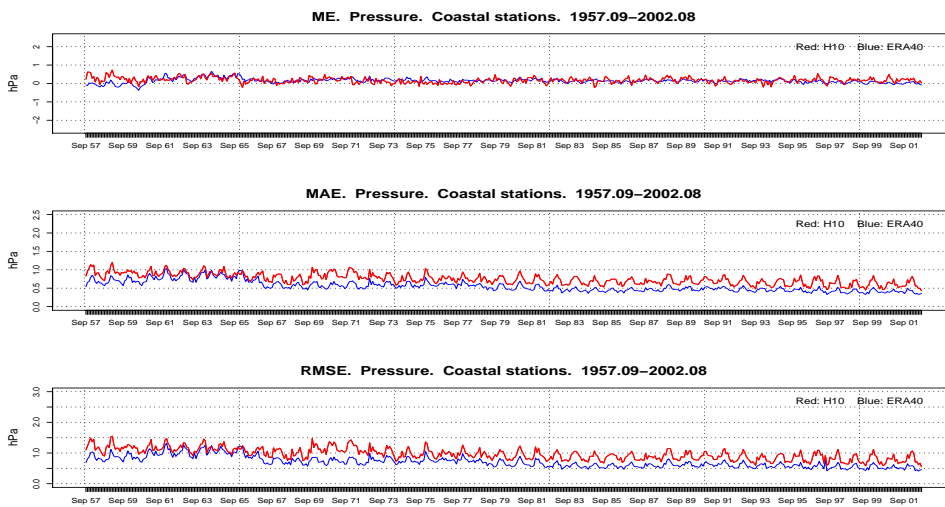
A.3.2.2. Time series (1957.09 2002.08) of respectively ME, MAE and RMSE for MSLP (coastal stations).
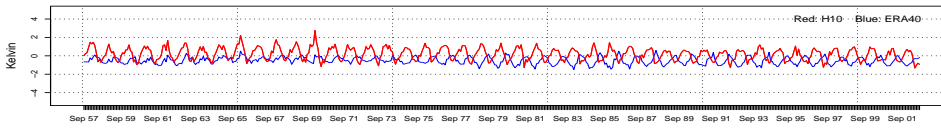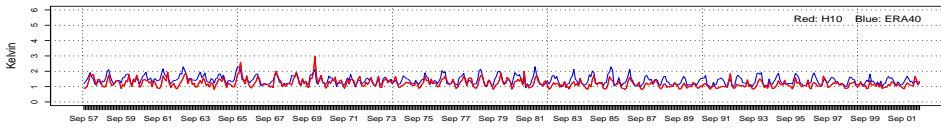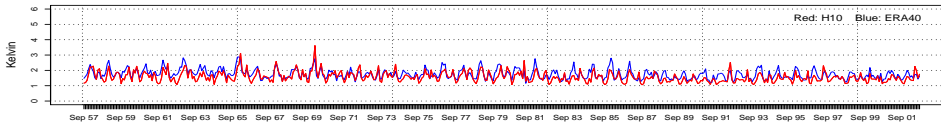
A.3.2.3. Time series (1957.09 2002.08) of respectively ME, MAE and RMSE for T2m (coastal stations).
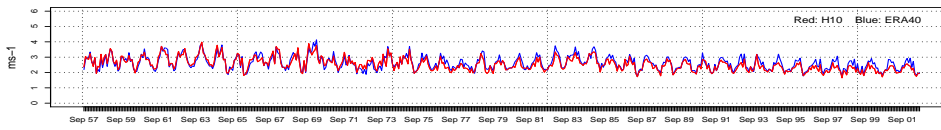


A.3.3.1. Time series (1957.09 2002.08) of respectively ME, MAE and RMSE for 10m wind (Svalbard).



A.3.3.2. Time series (1957.09 2002.08) of respectively ME, MAE and RMSE for MSLP (Svalbard).

**ME. Temperature 2m. Svalbard. 1957.09–2002.08**
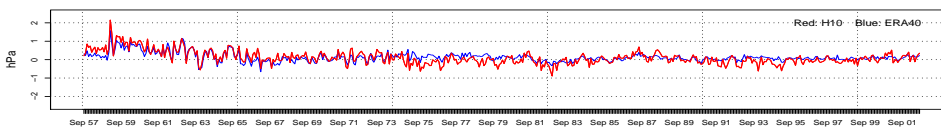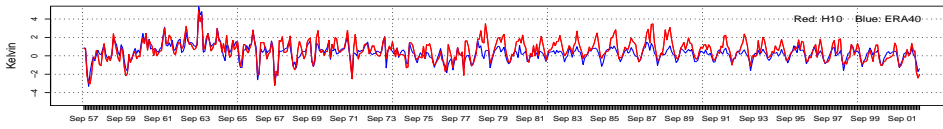
**MAE. Temperature 2m. Svalbard. 1957.09–2002.08**
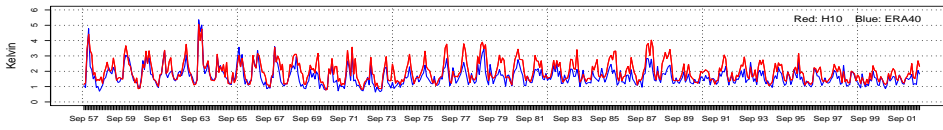
**RMSE. Temperature 2m. Svalbard. 1957.09–2002.08**
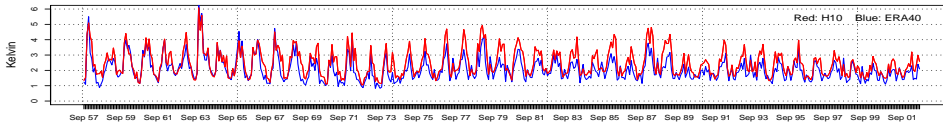
A.3.3.3. Time series (1957.09  2002.08) of  respectively ME, MAE and RMSE for T2m (Svalbard).



**ME. Wind 10m. Draugen, Heidrun and Norne. 1993.10–2002.08**
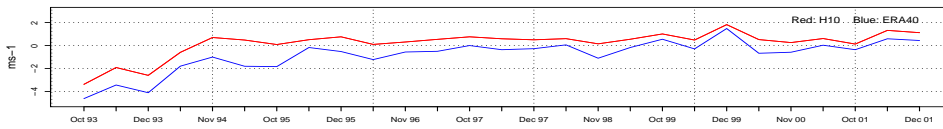
**MAE. Wind 10m. Draugen, Heidrun and Norne. 1993.10–2002.08**
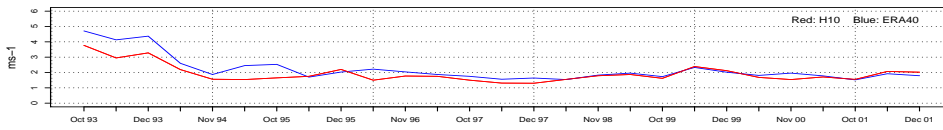
**RMSE. Wind 10m. Draugen, Heidrun and Norne. 1993.10–2002.08**
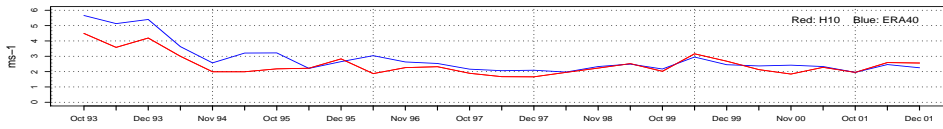
A.3.4.1.  Time series (1993.10  2002.08) of respectively ME, MAE and RMSE for 10m wind.
(Stations: Draugen, Heidrun and Norne)



**ME. Pressure. Draugen, Heidrun and Norne. 1993.10–2002.08**
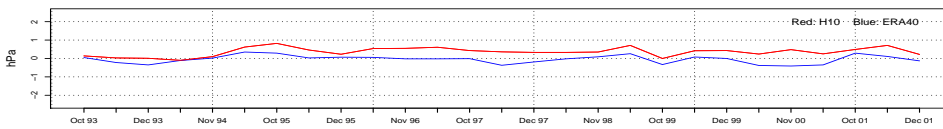
**MAE. Pressure. Draugen, Heidrun and Norne. 1993.10–2002.08**
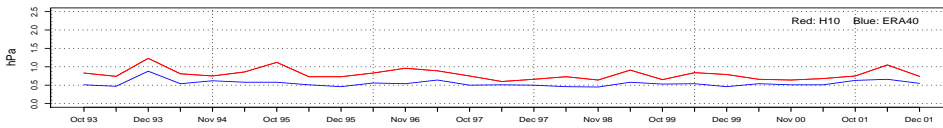
**RMSE. Pressure. Draugen, Heidrun and Norne. 1993.10–2002.08**
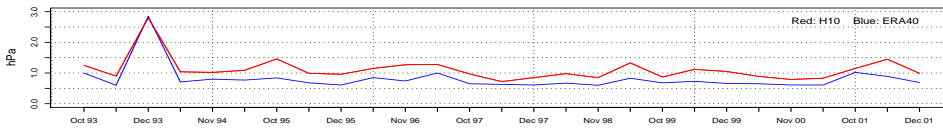
A.3.4.2.  Time series (1993.10  2002.08) of respectively ME, MAE and RMSE for MSLP.
(Stations: Draugen, Heidrun and Norne)

56

**ME. Temperature 2m. Draugen, Heidrun and Norne. 1993.10–2002.08**
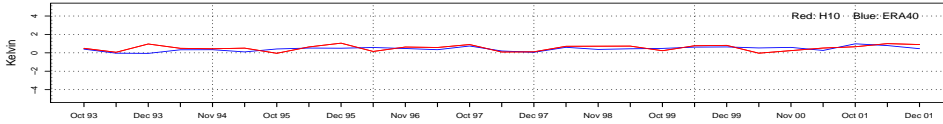
**MAE. Temperature 2m. Draugen, Heidrun and Norne. 1993.10–2002.08**
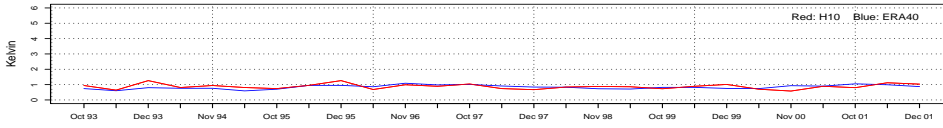
**RMSE. Temperature 2m. Draugen, Heidrun and Norne. 1993.10–2002.08**
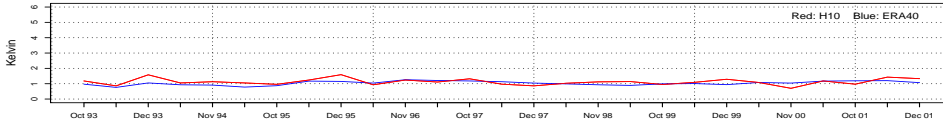
A.3.4.3. Time series (1993.10  2002.08) of respectively ME, MAE and RMSE for T2m.
(Stations: Draugen, Heidrun and Norne)

**ME. Wind 10m. North Sea. 1978.03–2002.08**
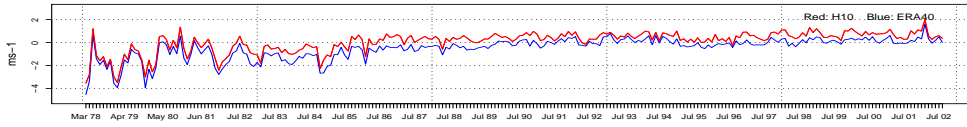
**MAE. Wind 10m. North Sea. 1978.03–2002.08**
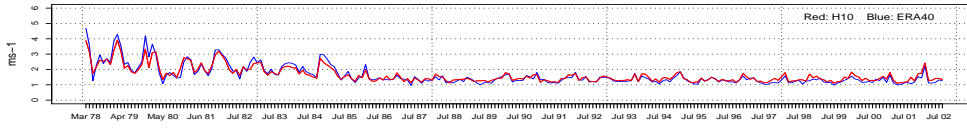
**RMSE. Wind 10m. North Sea. 1978.03–2002.08**
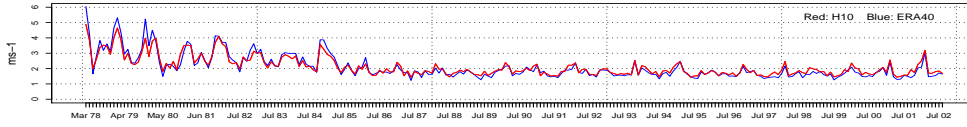
A.3.5.1. Time series (1978.03  2002.08) of respectively ME, MAE and RMSE for 10m wind speed.
(Stations in the North Sea)

**ME. Pressure. North Sea. 1978.03–2002.08**
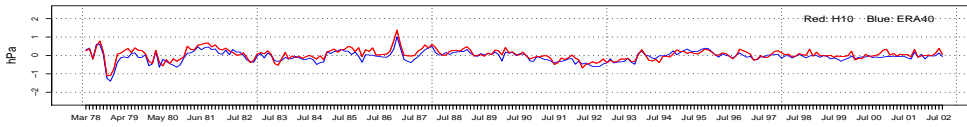
**MAE. Pressure. North Sea. 1978.03–2002.08**
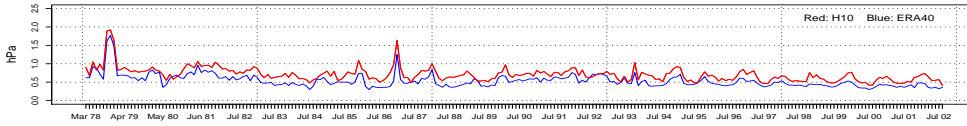
**RMSE. Pressure. North Sea. 1978.03–2002.08**
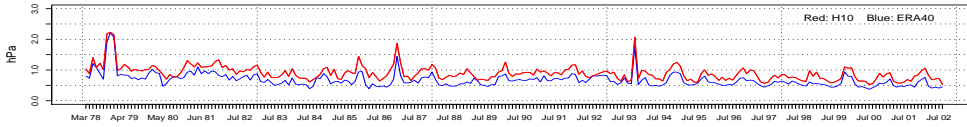
A.3.5.2. Time series (1978.03  2002.08) of respectively ME, MAE and RMSE for MSLP.
(Stations in the North Sea.)
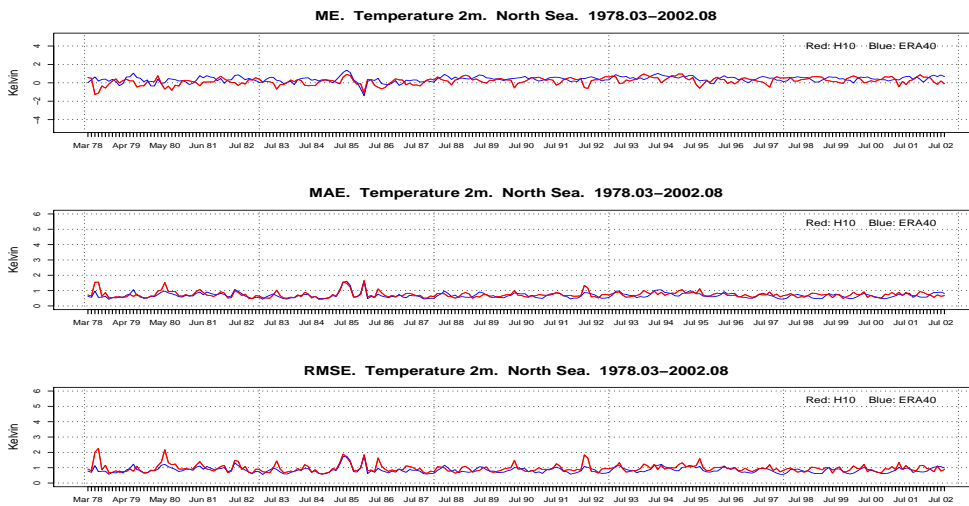
A.3.5.3. Time series (1978.03  2002.08) of respectively ME, MAE and RMSE for T2m.
(Stations in the North Sea.)

## A.4. Wind statistics, all stations

Table A.4.1 shows ME, MAE, RMSE, STDE and COR for each station.

Table A.4.2 shows the percentiles T100, T99, T95 and T90 for the observations, HIRLAM and ERA40. The observations should be used with some caution, although a quality check has been performed. Some stations show clearly unreliable observations, for example station 1378A, with 70 m/s and 1433A with 78 m/s.

| Stnr | *H10* | *H10* | *H10* | *H10* | *H10* | *ERA* | *ERA* | *ERA* | *ERA* | *ERA* |
| | ME | MAE | RMSE | STDE | COR | ME | MAE | RMSE | STDE | COR |
|---|---|---|---|---|---|---|---|---|---|---|
| 1001 | 0.80 | 3.12 | 4.01 | 3.12 | 0.59 | 0.50 | 2.58 | 3.40 | 3.37 | 0.70 |
| 1003 | 0.46 | 2.32 | 3.15 | 3.11 | 0.73 | 0.43 | 2.79 | 3.70 | 3.68 | 0.61 |
| 1007 | 0.66 | 2.19 | 2.81 | 2.73 | 0.65 | 1.07 | 2.48 | 3.15 | 2.96 | 0.57 |
| 1007A | 0.43 | 2.01 | 2.59 | 2.56 | 0.68 | 0.81 | 2.26 | 2.92 | 2.81 | 0.60 |
| 1008 | -0.6 | 2.15 | 2.72 | 2.64 | 0.66 | -1.5 | 2.54 | 3.28 | 2.94 | 0.54 |
| 1010 | 0.48 | 1.78 | 2.30 | 2.25 | 0.77 | -0.2 | 1.86 | 2.40 | 2.39 | 0.74 |
| 1023 | 0.89 | 1.72 | 2.13 | 1.94 | 0.41 | 0.63 | 1.53 | 1.90 | 1.79 | 0.51 |
| 1025 | 0.51 | 1.92 | 2.40 | 2.34 | 0.68 | -0.0 | 2.00 | 2.48 | 2.48 | 0.63 |
| 1033 | 0.00 | 2.59 | 3.32 | 3.32 | 0.63 | -3.1 | 3.85 | 5.22 | 4.20 | 0.39 |
| 1055 | -1.1 | 2.93 | 3.78 | 3.63 | 0.65 | -2.7 | 3.22 | 4.20 | 3.24 | 0.74 |
| 1062 | 1.49 | 2.72 | 3.45 | 3.11 | 0.59 | 1.83 | 2.71 | 3.39 | 2.86 | 0.67 |
| 1078 | -0.2 | 2.47 | 3.19 | 3.19 | 0.65 | -1.3 | 2.52 | 3.22 | 2.95 | 0.70 |
| 1089 | -0.6 | 1.93 | 2.51 | 2.43 | 0.60 | -0.2 | 1.61 | 2.08 | 2.08 | 0.73 |
| 1092 | 0.58 | 2.16 | 2.77 | 2.71 | 0.74 | -0.0 | 2.20 | 2.83 | 2.83 | 0.71 |
| 1098 | 0.12 | 2.13 | 2.75 | 2.75 | 0.66 | 0.14 | 1.75 | 2.26 | 2.26 | 0.78 |
| 1102 | -1.1 | 2.04 | 2.62 | 2.38 | 0.86 | -2.9 | 3.23 | 4.03 | 2.78 | 0.82 |
| 1108 | -0.5 | 2.08 | 2.65 | 2.59 | 0.80 | -1.1 | 2.21 | 2.83 | 2.62 | 0.79 |
| 1113 | 1.22 | 2.26 | 2.78 | 2.50 | 0.46 | 2.03 | 2.80 | 3.40 | 2.72 | 0.42 |
| 1115 | 0.78 | 2.93 | 3.74 | 3.66 | 0.64 | -1.2 | 2.38 | 3.13 | 2.90 | 0.77 |
| 1152 | -1.2 | 2.55 | 3.24 | 3.02 | 0.59 | -2.2 | 2.79 | 3.55 | 2.76 | 0.63 |
| 1160 | -0.0 | 2.28 | 2.93 | 2.93 | 0.71 | -0.9 | 2.36 | 3.05 | 2.91 | 0.70 |

58

| | | | | | | | | | | |
|---|---|---|---|---|---|---|---|---|---|---|
| 1167 | 0.78 | 1.88 | 2.36 | 2.23 | 0.58 | 1.93 | 2.71 | 3.43 | 2.84 | 0.52 |
| 1200 | -1.0 | 2.02 | 2.68 | 2.47 | 0.86 | -1.2 | 1.88 | 2.50 | 2.17 | 0.90 |
| 1201 | 0.83 | 1.64 | 2.14 | 1.97 | 0.88 | 0.50 | 1.67 | 2.14 | 2.08 | 0.86 |
| 1202 | 0.15 | 1.69 | 2.28 | 2.27 | 0.87 | -1.2 | 2.09 | 2.83 | 2.55 | 0.83 |
| 1205 | -4.7 | 5.10 | 6.45 | 4.41 | 0.54 | -3.9 | 4.90 | 6.43 | 5.09 | 0.20 |
| 1210 | -3.4 | 3.53 | 4.33 | 2.66 | 0.59 | -1.5 | 2.8 | 3.65 | 3.34 | 0.21 |
| 1212 | -5.8 | 5.85 | 7.14 | 4.18 | 0.59 | -3.84 | 4.54 | 6.01 | 4.62 | 0.26 |
| 1228 | 0.48 | 2.37 | 3.15 | 3.11 | 0.78 | -4.1 | 4.62 | 6.23 | 4.67 | 0.31 |
| 1238 | 0.2 | 2.01 | 2.64 | 2.63 | 0.56 | 0.63 | 2.63 | 3.36 | 3.29 | 0.27 |
| 1240 | -0.2 | 2.48 | 3.28 | 3.27 | 0.75 | -5.06 | 5.37 | 6.79 | 4.52 | 0.38 |
| 1241 | 1.85 | 3.46 | 4.52 | 4.12 | 0.45 | -2.5 | 3.23 | 4.21 | 3.37 | 0.35 |
| 1259A | -0.9 | 1.96 | 2.53 | 2.37 | 0.84 | -3.1 | 3.36 | 4.21 | 2.89 | 0.77 |
| 1259 | -1.1 | 2.48 | 3.18 | 3.0 | 0.82 | -3.4 | 3.88 | 4.99 | 3.68 | 0.75 |
| 1262 | -1.5 | 2.50 | 3.17 | 2.78 | 0.81 | -4.1 | 4.33 | 5.16 | 3.10 | 0.80 |
| 1271 | -0.5 | 1.83 | 2.43 | 2.38 | 0.48 | -1.4 | 2.06 | 2.83 | 2.46 | 0.41 |
| 1300M | 0.64 | 1.49 | 1.97 | 1.86 | 0.91 | 0.51 | 1.57 | 2.05 | 1.98 | 0.90 |
| 1304 | 1.20 | 3.23 | 4.08 | 3.90 | 0.68 | 0.97 | 2.95 | 3.72 | 3.59 | 0.73 |
| 1317 | 5.23 | 5.49 | 6.61 | 4.05 | 0.38 | 4.83 | 5.05 | 6.01 | 3.58 | 0.52 |
| 1319 | 5.31 | 5.72 | 6.80 | 4.24 | 0.41 | 5.11 | 5.56 | 6.60 | 4.17 | 0.42 |
| 1321A | 0.52 | 1.21 | 1.53 | 1.44 | 0.47 | -0.1 | 1.12 | 1.46 | 1.46 | 0.31 |
| 1322 | 0.95 | 1.61 | 2.04 | 1.81 | 0.48 | 0.82 | 1.67 | 2.18 | 2.02 | 0.36 |
| 1350A | -1.3 | 2.37 | 3.09 | 2.80 | 0.80 | -3.6 | 4.0 | 5.28 | 3.81 | 0.45 |
| 1364 | 1.27 | 2.03 | 2.47 | 2.12 | 0.67 | -0.0 | 1.93 | 2.74 | 2.74 | 0.27 |
| 1366 | -0.4 | 1.86 | 2.45 | 2.42 | 0.77 | -1.9 | 2.59 | 3.69 | 3.18 | 0.35 |
| 1367 | 1.06 | 1.66 | 2.02 | 1.71 | 0.16 | 0.56 | 1.34 | 1.67 | 1.57 | 0.13 |
| 1378 | 1.22 | 1.60 | 1.95 | 1.52 | 0.48 | 1.15 | 1.68 | 2.07 | 1.72 | 0.31 |
| 1378A | 0.64 | 1.26 | 2.43 | 2.35 | 0.32 | 0.67 | 1.43 | 2.57 | 2.48 | 0.22 |
| 1382 | 0.9 | 1.48 | 1.85 | 1.62 | 0.54 | 0.52 | 1.38 | 1.76 | 1.69 | 0.45 |
| 1382A | -0.4 | 2.66 | 5.90 | 5.88 | 0.14 | -0.67 | 2.62 | 5.94 | 5.90 | 0.12 |
| 1384 | -0.13 | 1.44 | 1.85 | 1.84 | 0.52 | -0.21 | 1.43 | 1.82 | 1.81 | 0.53 |
| 1393 | 1.21 | 1.80 | 2.16 | 1.79 | 0.59 | 0.82 | 1.75 | 2.16 | 2.0 | 0.45 |
| 1397A | 1.35 | 1.57 | 1.93 | 1.38 | 0.59 | 0.91 | 1.44 | 1.83 | 1.58 | 0.44 |
| 1400M | 0.45 | 1.47 | 1.98 | 1.93 | 0.89 | -0.3 | 1.30 | 1.74 | 1.71 | 0.87 |
| 1401M | -0.1 | 1.73 | 2.38 | 2.38 | 0.88 | -0.6 | 1.80 | 2.55 | 2.47 | 0.87 |
| 1402M | 0.45 | 1.40 | 1.90 | 1.84 | 0.90 | -0.4 | 1.17 | 1.62 | 1.59 | 0.93 |
| 1415 | 0.19 | 1.97 | 2.51 | 2.50 | 0.66 | 1.05 | 1.95 | 2.47 | 2.23 | 0.75 |
| 1424 | 1.81 | 2.01 | 2.36 | 1.52 | 0.44 | 1.97 | 2.24 | 2.71 | 1.86 | 0.29 |
| 1427A | 0.41 | 1.67 | 2.14 | 2.10 | 0.83 | 0.22 | 1.76 | 2.27 | 2.26 | 0.80 |
| 1427 | 0.58 | 2.57 | 3.26 | 3.21 | 0.65 | 0.27 | 2.03 | 2.58 | 2.57 | 0.78 |
| 1432 | 1.47 | 1.89 | 2.29 | 1.75 | 0.61 | 2.02 | 2.54 | 3.10 | 2.36 | 0.44 |
| 1433A | -1.6 | 2.25 | 3.79 | 3.44 | 0.66 | -2.96 | 3.30 | 4.99 | 4.02 | 0.38 |
| 1433 | -1.5 | 2.27 | 3.07 | 2.71 | 0.76 | -2.9 | 3.31 | 4.48 | 3.39 | 0.44 |
| 1436 | 0.49 | 2.03 | 2.55 | 2.51 | 0.83 | -0.12 | 2.23 | 2.81 | 2.81 | 0.78 |

| St | | | | | | | | | | |
|---|---|---|---|---|---|---|---|---|---|---|
| 1441A | 1.38 | 1.75 | 2.18 | 1.68 | 0.67 | -0.4 | 1.43 | 1.87 | 1.83 | 0.50 |
| 1442 | -0.2 | 1.48 | 1.86 | 1.85 | 0.55 | 0.39 | 1.81 | 2.27 | 2.24 | 0.45 |
| 1448 | -0.05 | 1.71 | 2.18 | 2.18 | 0.81 | -0.93 | 2.11 | 2.68 | 2.52 | 0.73 |
| 1450 | 0.76 | 1.92 | 2.39 | 2.26 | 0.71 | -2.0 | 2.49 | 3.57 | 2.98 | 0.38 |
| 1455 | 2.06 | 2.33 | 2.71 | 1.77 | 0.53 | 1.50 | 1.94 | 2.40 | 1.87 | 0.45 |
| 1459 | 1.86 | 2.12 | 2.47 | 1.62 | 0.58 | 2.48 | 2.65 | 3.09 | 1.85 | 0.55 |
| 1465 | -0.8 | 1.88 | 2.43 | 2.30 | 0.79 | -2.4 | 2.92 | 3.68 | 2.76 | 0.68 |
| 1482 | -0.55 | 2.33 | 3.00 | 2.95 | 0.67 | -3.94 | 4.09 | 4.86 | 2.83 | 0.72 |
| 1490 | 0.03 | 1.47 | 1.90 | 1.90 | 0.57 | -0.5 | 1.54 | 2.07 | 2.00 | 0.49 |
| 1494 | 0.43 | 1.62 | 2.08 | 2.03 | 0.58 | -0.58 | 1.43 | 1.82 | 1.73 | 0.66 |
| 1495A | -0.5 | 1.61 | 3.15 | 3.11 | 0.68 | -3.0 | 3.18 | 4.60 | 3.50 | 0.60 |
| 1496 | 1.23 | 1.80 | 2.16 | 1.77 | 0.69 | 0.83 | 1.79 | 2.20 | 2.04 | 0.57 |
| **99090** | -0.9 | 2.5 | 3.23 | 3.1 | 0.75 | -1.0 | 1.4 | 1.9 | 1.6 | 0.94 |

| St | OBS T100 m/s | OBS T99 m/s | OBS T95 m/s | OBS T90 m/s | H10 T100 m/s | H10 T99 m/s | H10 T95 m/s | H10 T90 m/s | ERA40 T100 m/s | ERA40 T99 m/s | ERA40 T95 m/s | ERA40 T90 m/s |
|---|---|---|---|---|---|---|---|---|---|---|---|---|
| 1001 | 38.1 | 19.0 | 15.4 | 12.9 | 28.1 | 17.7 | 14.4 | 12.6 | 25.4 | 17.1 | 14.1 | 12.4 |
| 1003 | 50.9 | 18.5 | 14.4 | 12.3 | 22 | 15.6 | 13.1 | 11.4 | 21.4 | 16.2 | 13.2 | 11.4 |
| 1007 | 30.9 | 15.4 | 10.8 | 8.2 | 19.6 | 12.6 | 9.6 | 8.1 | 17.5 | 11.9 | 9.4 | 8.2 |
| 1007a | 22.7 | 15.4 | 10.9 | 8.8 | 19.2 | 12.9 | 9.8 | 8.2 | 16.1 | 12.1 | 9.6 | 8.3 |
| 1008 | 26.8 | 14.9 | 11.3 | 9.8 | 17.6 | 11.3 | 8.8 | 7.6 | 16.3 | 10.3 | 7.5 | 6.2 |
| 1010 | 29.8 | 16.5 | 12.3 | 10.3 | 23.6 | 14.8 | 11.9 | 10.5 | 21.6 | 14.2 | 11.3 | 9.8 |
| 1023 | 17.5 | 8.2 | 6.2 | 5.1 | 13 | 7.4 | 5.9 | 5.1 | 13.5 | 7.3 | 5.6 | 4.8 |
| 1025 | 21.6 | 12.9 | 9.8 | 8.2 | 16.7 | 10.4 | 8.4 | 7.4 | 16.9 | 10.4 | 8.2 | 7.1 |
| 1033 | 29.3 | 18.5 | 14.4 | 12.3 | 24.3 | 15.9 | 12.8 | 11.1 | 20.1 | 12.6 | 9.8 | 8.2 |
| 1055 | 35 | 21.6 | 17.5 | 14.9 | 27.4 | 17.7 | 14.2 | 12.5 | 20 | 13.4 | 11.2 | 9.9 |
| 1062 | 28.3 | 15.4 | 11.8 | 9.8 | 23.6 | 15.8 | 12.8 | 11.3 | 25 | 16.4 | 13.4 | 11.8 |
| 1078 | 31.4 | 19 | 14.9 | 12.9 | 25.1 | 16 | 13.1 | 11.6 | 20.4 | 13.7 | 11.4 | 10.2 |
| 1089 | 30.9 | 13.4 | 10.3 | 9.3 | 14.9 | 9.8 | 8 | 7.1 | 17.1 | 11.1 | 9.2 | 8.2 |
| 1092 | 28.8 | 18 | 13.4 | 12.3 | 23 | 15.6 | 12.6 | 11.2 | 19.3 | 13.8 | 11.6 | 10.3 |
| 1098 | 28.8 | 16.5 | 12.9 | 11.3 | 22.2 | 14.4 | 11.7 | 10.4 | 19.7 | 14.1 | 11.8 | 10.6 |
| 1102 | 31.4 | 21.6 | 17.5 | 15.4 | 27.4 | 18.3 | 14.8 | 13 | 23.6 | 14.5 | 11.7 | 10.2 |
| 1108 | 30.9 | 19 | 15.4 | 12.3 | 21.4 | 15.8 | 12.8 | 11 | 22.2 | 14.4 | 11.9 | 10.4 |
| 1113 | 22.6 | 12.3 | 6.7 | 4.6 | 12.4 | 8 | 6.2 | 5.4 | 16.2 | 10.3 | 8 | 6.9 |
| 1115 | 35 | 19 | 15.4 | 12.3 | 26.6 | 18.2 | 15 | 13.2 | 22.5 | 14.4 | 11.7 | 10.2 |
| 1152 | 19 | 16.5 | 12.9 | 11.3 | 21.2 | 13.8 | 10.9 | 9.3 | 18.6 | 11.4 | 8.7 | 7.4 |
| 1160 | 30.9 | 19 | 14.9 | 12.3 | 26.5 | 17.2 | 13.4 | 11.4 | 24.3 | 14.8 | 11.6 | 10 |
| 1167 | 26.2 | 11.3 | 8.2 | 7.2 | 16.9 | 11 | 8.7 | 7.5 | 22.9 | 14.6 | 11.6 | 10 |
| 1200m | 34 | 22.6 | 18 | 15.4 | 24.7 | 18.8 | 15.2 | 13.4 | 22.8 | 18.5 | 15 | 13.1 |
| 1201m | 29.8 | 19 | 14.9 | 12.9 | 24.7 | 19 | 15.7 | 13.7 | 24.2 | 18.3 | 15 | 13.3 |
| 1202m | 30.9 | 21.6 | 16.5 | 13.9 | 24.1 | 19.8 | 15.8 | 13.7 | 24.1 | 16.8 | 13.2 | 11.5 |
| 1205 | 32.9 | 22.6 | 17.5 | 15.4 | 12.2 | 8 | 6.5 | 5.8 | 14.8 | 9.6 | 7.8 | 6.9 |
| 1210 | 29.8 | 14.4 | 11.3 | 9.3 | 8.2 | 4.9 | 3.9 | 3.4 | 14.4 | 9.2 | 7.4 | 6.5 |
| 1212 | 35.5 | 21.6 | 17 | 14.4 | 8.2 | 4.9 | 3.9 | 3.5 | 14.4 | 9.3 | 7.6 | 6.6 |
| 1228 | 35 | 22.6 | 17.5 | 14.4 | 32.1 | 20 | 16 | 13.8 | 11.9 | 8 | 6.3 | 5.5 |
| 1238 | 30.9 | 14.4 | 9.8 | 7.7 | 13.1 | 8.7 | 7.2 | 6.4 | 15 | 9.7 | 7.9 | 7 |
| 1240 | 32.4 | 22.6 | 17.5 | 15.4 | 31.7 | 20.2 | 16.1 | 14 | 11.2 | 7.9 | 6.3 | 5.6 |
| 1241 | 31.4 | 16.5 | 12.3 | 10.3 | 31.6 | 19.6 | 15.7 | 13.5 | 11.8 | 7.9 | 6.3 | 5.5 |
| 1259 | 32.4 | 22.6 | 15.4 | 15.4 | 25.1 | 16.6 | 12.9 | 11.2 | 18.1 | 11 | 8.5 | 7.3 |
| 1259a | 25.6 | 19.2 | 15.6 | 13.5 | 22.8 | 16.6 | 12.9 | 11.2 | 17.5 | 11.7 | 9.1 | 7.8 |
| 1262 | 35 | 22.6 | 19 | 15.9 | 26.9 | 18.7 | 15.2 | 13.5 | 21.6 | 13.2 | 10.6 | 9.2 |
| 1271 | 24.7 | 12.9 | 8.7 | 7.2 | 13.2 | 7.7 | 6.1 | 5.4 | 14.3 | 6.7 | 5.1 | 4.2 |
| 1300 | 31.9 | 20.6 | 16.5 | 14.4 | 28.9 | 20.2 | 16.8 | 15 | 26 | 19.7 | 16.6 | 14.9 |
| 1304 | 35 | 22.6 | 16.5 | 15.4 | 30.1 | 20.3 | 16.9 | 15.1 | 26.6 | 19.6 | 16.5 | 14.8 |
| 1317 | 22.6 | 10.8 | 8.2 | 7.2 | 28.4 | 19.7 | 16.3 | 14.5 | 26.9 | 18.8 | 15.7 | 13.9 |
| 1319 | 26.8 | 15.4 | 9.8 | 9.3 | 28.6 | 19.8 | 16.4 | 14.5 | 26.4 | 19.2 | 16.1 | 14.3 |
| 1321a | 13.2 | 6.4 | 4.5 | 3.7 | 8.6 | 6.3 | 5.1 | 4.5 | 9.1 | 5.2 | 3.8 | 3.2 |
| 1322 | 19 | 9.8 | 4.6 | 4.6 | 8.5 | 6.2 | 5 | 4.3 | 10.6 | 6.6 | 5.2 | 4.4 |

| | | | | | | | | | | | | | |
|---|---|---|---|---|---|---|---|---|---|---|---|---|---|
| 1350a | 51 | 17 | 13.3 | 11.1 | | 11.8 | 9.4 | 7.8 | 6.8 | | 7.5 | 4.4 | 3.4 | 2.9 |
| 1364 | 26.8 | 12.3 | 6.7 | 4.6 | | 12.6 | 8.5 | 6.4 | 5.4 | | 7.3 | 4.5 | 3.5 | 3 |
| 1366 | 34 | 13.4 | 9.8 | 8.2 | | 9.3 | 7 | 5.7 | 5 | | 6.4 | 4 | 3.2 | 2.7 |
| 1367 | 11.8 | 5.1 | 3.6 | 3.1 | | 9.9 | 6.5 | 5.1 | 4.5 | | 9 | 5.4 | 4.2 | 3.6 |
| 1378 | 19 | 4.6 | 4.6 | 2.6 | | 10.3 | 6.2 | 5 | 4.4 | | 9.8 | 6.3 | 4.8 | 4.1 |
| 1378a | 70 | 7.1 | 4.6 | 3.6 | | 9.2 | 6.2 | 5 | 4.3 | | 11.2 | 6.7 | 5 | 4.2 |
| 1382 | 17 | 7.2 | 6.2 | 4.6 | | 10.4 | 6.9 | 5.5 | 4.8 | | 8.5 | 5.8 | 4.6 | 4 |
| 1382a | 27 | 27 | 27 | 5 | | 9.7 | 7 | 5.6 | 4.8 | | 11.9 | 6.9 | 5.1 | 4.3 |
| 1384 | 15.4 | 8.7 | 6.7 | 5.7 | | 9.6 | 6.6 | 5.3 | 4.6 | | 12.8 | 6.8 | 5.1 | 4.4 |
| 1393 | 15.4 | 9.8 | 6.7 | 4.6 | | 11.2 | 7.2 | 5.9 | 5.2 | | 11.3 | 6.5 | 5.2 | 4.6 |
| 1397a | 45.3 | 6.6 | 4.6 | 3.7 | | 10 | 7.2 | 5.8 | 5.2 | | 10.4 | 6.9 | 5.3 | 4.6 |
| 1400m | 33.4 | 19.5 | 15.9 | 13.9 | | 26.7 | 18.6 | 15.8 | 14 | | 26 | 17.7 | 14.6 | 12.9 |
| 1401m | 36 | 22.6 | 18.5 | 15.4 | | 27.1 | 19.8 | 16.6 | 14.7 | | 26.9 | 18.7 | 15.6 | 13.9 |
| 1402m | 28.8 | 19.5 | 15.9 | 13.9 | | 29.2 | 19.3 | 16.2 | 14.5 | | 24.2 | 17.9 | 14.8 | 13.2 |
| 1403 | 30.9 | 20.1 | 15.4 | 13.9 | | 26 | 18.1 | 14.8 | 13.1 | | 20.9 | 14.7 | 12 | 10.5 |
| 1415 | 27.3 | 13.4 | 10.3 | 9.3 | | 20.5 | 12.2 | 9.7 | 8.4 | | 20.2 | 13.8 | 11.3 | 9.9 |
| 1424 | 19 | 6.7 | 2.6 | 2.6 | | 10.2 | 6.7 | 5.2 | 4.5 | | 12.3 | 7.7 | 5.9 | 5 |
| 1427 | 34.5 | 17.5 | 13.4 | 11.8 | | 26.4 | 16.1 | 13.2 | 11.7 | | 23.2 | 15.3 | 12.6 | 11.2 |
| 1427a | 30.8 | 16.2 | 13.1 | 11.5 | | 24.6 | 15.8 | 13.1 | 11.7 | | 20.5 | 15.2 | 12.6 | 11.3 |
| 1432 | 22.6 | 9.8 | 6.7 | 4.6 | | 12.8 | 8.5 | 6.9 | 6.1 | | 15.7 | 10.6 | 8.5 | 7.4 |
| 1433 | 26.8 | 15.4 | 12.3 | 9.8 | | 11.8 | 8.1 | 6.4 | 5.6 | | 9.5 | 5.6 | 4.2 | 3.5 |
| 1433a | 78.4 | 16.2 | 12.1 | 10.1 | | 10.7 | 8.1 | 6.7 | 5.8 | | 9.7 | 6.2 | 4.5 | 3.8 |
| 1436 | 30.9 | 19 | 15.4 | 12.3 | | 25.3 | 16.4 | 13.5 | 12 | | 23.8 | 15.1 | 12.5 | 11.1 |
| 1442 | 19 | 9.8 | 6.7 | 6.7 | | 12.3 | 7.9 | 6.4 | 5.7 | | 15.5 | 10 | 8 | 6.9 |
| 1448 | 26.8 | 16.5 | 13.4 | 11.8 | | 21.6 | 15.1 | 12.5 | 11 | | 21.6 | 13.3 | 10.9 | 9.6 |
| 1450 | 22.6 | 12.3 | 9.8 | 9.8 | | 16.5 | 10.6 | 8.5 | 7.4 | | 8.5 | 5.2 | 4 | 3.4 |
| 1452 | 17 | 10.3 | 8.2 | 7.2 | | 14.5 | 9.7 | 7.9 | 7 | | 20.4 | 12.6 | 10.3 | 9.1 |
| 1455 | 26.8 | 9.8 | 4.6 | 3.1 | | 12.8 | 7.8 | 6.3 | 5.6 | | 12.5 | 7.4 | 5.7 | 4.9 |
| 1459 | 22.6 | 9.8 | 4.6 | 4.6 | | 11.7 | 7.5 | 6.1 | 5.4 | | 14.6 | 9.5 | 7.6 | 6.7 |
| 1465 | 31.4 | 17.5 | 13.9 | 12.3 | | 20.7 | 14.5 | 12 | 10.5 | | 17.1 | 11.1 | 9 | 7.9 |
| 1482 | 34 | 17 | 13.9 | 12.3 | | 24.1 | 15.7 | 12.8 | 11.3 | | 13.4 | 8.2 | 6.4 | 5.5 |
| 1490 | 19 | 9.8 | 6.7 | 6.7 | | 10.6 | 7.1 | 5.8 | 5.1 | | 8.9 | 6.1 | 4.8 | 4.2 |
| 1494 | 18 | 9.8 | 7.7 | 6.7 | | 16.3 | 10 | 7.8 | 6.8 | | 12.7 | 7.6 | 5.8 | 5 |
| 1496 | 15.4 | 9.8 | 6.7 | 4.6 | | 10.9 | 8.1 | 6.6 | 5.7 | | 12.3 | 8 | 6 | 5.2 |
| 99090 | 36 | 21.6 | 17.5 | 15.4 | | 26.8 | 19.3 | 15.9 | 14.1 | | 28.1 | 19.1 | 15.8 | 14 |
| | | | | | | | | | | | | | | |

Table A.4.2. T100, T99, T95 and T90 percentiles for observations, HIRLAM10 and ERA40.

| Station | Position | In work | | Type |
|---|---|---|---|---|
| 1001  Jan Mayen | 70.93 N,  08.00 W | 1957.09 | 2002.08 | Weather |
| 1003  Hornsund | 77.00 N,  15.50 E | 1995.11 | 2000.03 | Weather |
| 1007  Ny Ålesund | 78.92 N,  11.93 E | 1974.08 | 2002.08 | Weather |
| 1007  Ny Ålesund | 78.92 N,  11.93 E | 1994.09 | 2002.08 | Automat |
| 1008  Svalbard Airport | 78.25 N,  15.47 E | 1975.08 | 2002.08 | Weather |
| 1010  Andøya | 69.30 N,  16.15 E | 1958.06 | 2002.08 | Weather |
| 1023  Bardufoss | 69.07 N,  18.53 E | 1957.09 | 2002.08 | Weather |
| 1025  Tromsø - Langnes | 69.68 N,  18.92 E | 1964.10 | 2002.08 | Weather |
| 1033  Torsvåg lighthouse | 70.25 N,  19.50 E | 1957.09 | 2002.08 | Weather |
| 1055  Fruholmen lighthouse | 71.10 N,  24.00 E | 1957.09 | 2002.08 | Weather |
| 1062  Hopen | 76.50 N,  25.07 E | 1957.09 | 2002.08 | Weather |
| 1078  Sletnes lighthouse | 71.08 N,  28.23 E | 1957.09 | 2002.08 | Weather |
| 1089  Kirkenes airport | 69.73 N,  29.90 E | 1957.09 | 2002.08 | Weather |
| 1092  Makkaur lighthouse | 70.70 N,  30.08 E | 1957.09 | 2002.08 | Weather |
| 1092  Makkaur lighthouse | 70.70 N,  30.08 E | 1998.11 | 2002.08 | Automat |
| 1098  Vardø | 70.37 N,  31.08 E | 1957.01 | 2002.08 | Weather |
| 1102  Sklinna lighthouse | 65.20 N,  11.00 E | 1974.10 | 2002.08 | Weather |
| 1108  Vega-Vallsjø | 65.70 N,  11.85 E | 1991.07 | 2002.08 | Weather |
| 1113  Glomfjord | 66.80 N,  13.98 E | 1957.09 | 2002.08 | Weather |
| 1115  Myken | 66.77 N,  12.48 E | 1957.09 | 2002.08 | Weather |
| 1152  Bodø | 67.25 N,  14.40 E | 1957.09 | 2002.08 | Weather |
| 1160  Skrova lighthouse | 68.15 N,  14.65 E | 1957.09 | 2002.08 | Weather |
| 1167  Sortland | 68.70 N,  15.42 E | 1985.01 | 2002.08 | Weather |

| | | | | |
|---|---|---|---|---|
| 1200 Norne | 66.02 N, 8.08 E | 1998.02 | 2002.08* | Maritime |
| 1201 Heidrun | 65.30 N, 7.30 E | 1996.01 | 2002.08* | Maritime |
| 1202 Draugen | 64.35 N, 7.77E | 1993.01 | 2002.08* | Maritime |
| 1205 Svinøy lighthouse | 62.33 N, 05.27 E | 1957.09 | 2002.08 | Weather |
| 1210 Ålesund | 62.57 N, 06.12 E | 1958.07 | 2002.08 | Weather |
| 1212 Ona | 62.87 N, 06.53 E | 1978.09 | 2002.08 | Weather |
| 1228 Sula | 63.85 N, 08.47 E | 1975.01 | 1999.11 | Weather |
| 1238 Fokstua | 62.12 N, 09.28 E | 1968.06 | 2002.08 | Weather |
| 1240 Halten lighthouse | 64.28 N, 09.70 E | 1983.09 | 2002.08 | Weather |
| 1241 Ørland | 63.70 N, 09.60 E | 1957.09 | 2002.08 | Weather |
| 1259 Buholmråsa lighthouse | 64.40 N, 10.45 E | 1965.11 | 1994.06 | Weather |
| 1259 Buholmråsa lighthouse | 64.40 N, 10.45 E | 1994.10 | 2002.08 | Automat |
| 1262 Nordøyan lighthouse | 64.80 N, 10.55 E | 1957.09 - 2002.08 | | Weather |
| 1271 Værnes | 63.47 N, 10.93 E | 1957.09 | 2002.08 | Weather |
| 1300 Gullfaks | 61.20 N, 02.30 E | 1989.11 | 2002.08 | Maritim |
| 1304 Ytterøyane lighthouse | 61.57 N, 04.68 E | 1984.09 | 2002.04 | Weather |
| 1317 Bergen | 60.38 N, 05.33 E | 1957.09 | 2002.08 | Weather |
| 1319 Takle | 61.03 N, 05.38 E | 1957.09 | 2002.08 | Weather |
| 1321 Stryn | 61.88 N, 06.57 E | 1993.11 | 2002.08 | Automat |
| 1322 Førde | 61.47 N, 05.92 E | 1992.11 | 2002.08 | Weather |
| 1350 Finsevatn | 60.60 N, 07.53 E | 1993.11 | 2002.08 | Automat |
| 1364 Geilo | 60.52 N, 08.20 E | 1966.09 | 2002.08 | Weather |
| 1366 Sognefjell | 61.57 N, 08.00 E | 1978.12 | 1989.05 | Weather |
| 1367 Fagernes | 60.98 N, 09.23 E | 1982.07 | 2002.08 | Weather |
| 1378 Lillehammer | 61.08 N, 10.48 E | 1982.12 | 1994.11 | Weather |
| 1378 Lillehammer | 61.08 N, 10.48 E | 1994.11 | 2002.08 | Automat |
| 1382 Kiese | 60.77 N, 10.80 E | 1957.09 | 1980.12 | Weather |
| 1382 Kiese | 60.77 N, 10.80 E | 1994.01 | 2002.08 | Automat |
| 1384 Gardermoen | 60.20 N, 11.10 E | 1957.08 | 2002.08 | Weather |
| 1393 Drevsjø | 61.88 N, 12.05 E | 1957.09 | 2002.03 | Weather |
| 1397 Trysil | 61.50 N, 12.45 E | 1993.11 | 2002.08 | Automat |
| 1400 Ekofisk | 56.50 N, 03.20 E | 1980.01 | 2002.08 | Maritime |
| 1401 Frigg | 59.90 N, 02.10 E. | 1978.03 | 2002.08 | Maritime |
| 1402 Sleipner | 58.40 N, 01.90 E | 1993.10 | 2002.08 | Maritime |
| 1403 Utsira | 59.30 N, 04.88 E. | 1957.09 | 2002.08 | Weather |
| 1415 Sola | 58.88 N, 05.63 E | 1957.09 | 2002.08 | Weather |
| 1424 Sauda | 59.65 N, 06.37 E | 1957.09 | 2002.08 | Weather |
| 1427 Lista lighthouse | 58.12 N, 06.57 E | 1957.09 | 2002.08 | Weather |
| 1427 Lista lighthouse | 58.12 N, 06.57 E | 1994.09 | 2002.08 | Automat |
| 1432 Sirdal | 58.88 N, 06.85 E | 1974.09 | 2002.08 | Weather |
| 1433 Midtlæger | 59.83 N, 06.98 E | 1967.02 | 1995.10 | Weather |
| 1433 Midtlæger | 59.83 N, 06.98 E | 1994.11 | 2002.08 | Automat |
| 1436 Lindesnes lighthouse | 57.98 N, 07.05 E | 1957.09 | 2002.08 | Weather |
| 1442 Byglandsfjord | 58.67 N, 07.80 E | 1969.12 | 2002.08 | Weather |
| 1448 Oksøy lighthouse | 58.07 N, 08.05 E | 1957.09 | 2002.08 | Weather |
| 1450 Møsstrand | 59.85 N, 08.07 E | 1980.11 | 2002.08 | Weather |
| 1452 Sørlandet | 58.20 N, 08.07 E | 1957.09 | 2002.08 | Weather |
| 1455 Teitsund | 59.03 N, 08.52 E | 1957.09 | 2002.08 | Weather |
| 1459 Nelaug | 58.65 N, 08.63 E | 1966.07 | 2002.08 | Weather |
| 1465 Torungen lighthouse | 58.38 N, 08.80 E | 1957.09 | 2002.08 | Weather |
| 1482 Færder lighthouse | 59.03 N, 10.53 E | 1957.09 | 2002.08 | Weather |
| 1490 Tryvasshøda | 59.98 N, 10.68 E | 1957.09 | 1975.12 | Weather |
| 1494 Rrygge | 59.38 N, 10.78 E | 1957.09 | 2002.08 | Weather |
| 1495 Strømtangen lighthouse | 59.15 N, 10.83 E | 1994.05 | 2002.08 | Automat |
| 1496 Høland - Løken | 59.72 N, 11.45 E | 1991.10 | 2002.08 | Weather |
| 99090 Polarfront | 66.00 N, 2.00 E | 1999.06 | 2002.08 | Weather |

* Discontinuous dataset

Table A.4.3. List of stations with number and name, position, operational period and type of station.

# Appendix 2

## A2.1. Time series of qualified stations

**ME. Wind 10m. 22 qualified stations. 2002.09–2008.12**



**RMSE. Wind 10m. 22 qualified stations. 2002.09–2008.12**
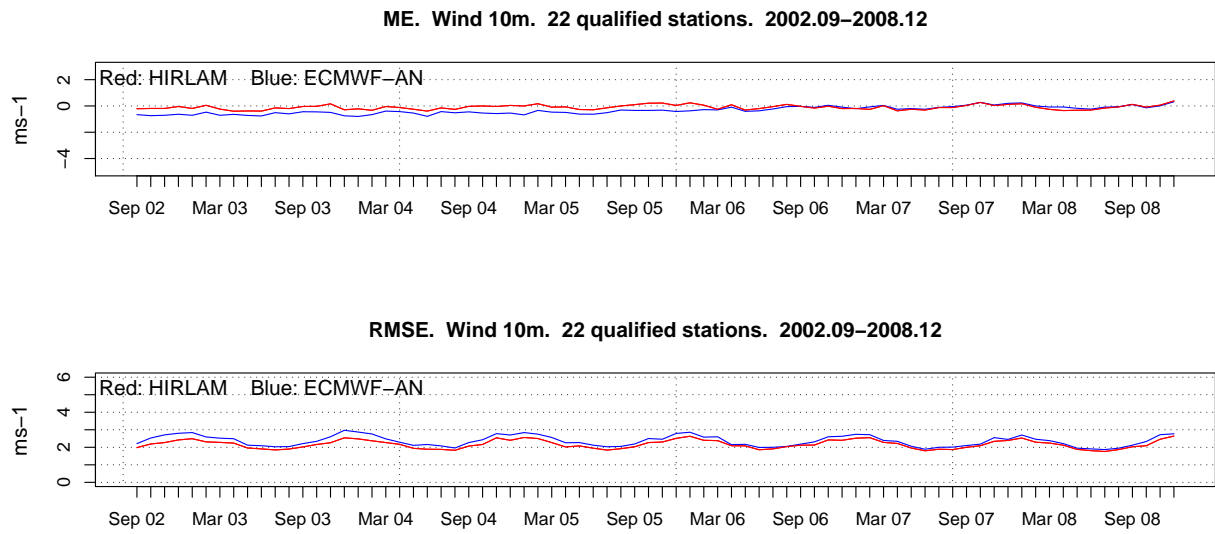


Figure A2.1.1. Time series (2002.09  2008.12) of respectively ME and RMSE for 10m wind speed based on 22 qualified stations.

**ME. Pressure. 22 qualified stations. 2002.09–2008.12**



**RMSE. Pressure. 22 qualified stations. 2002.09–2008.12**
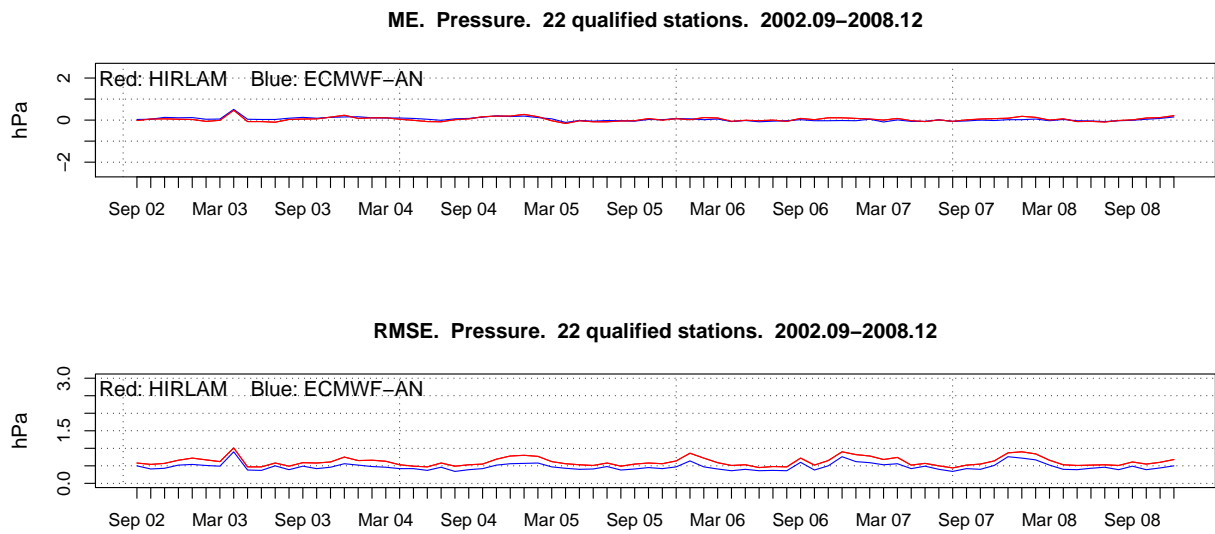


Figure A2.1.2. Time series (2002.09  2008.12) of respectively ME and RMSE for MSLP based on 22 qualified stations.

**ME. Temperature 2m. 22 qualified stations. 2002.09–2008.12**
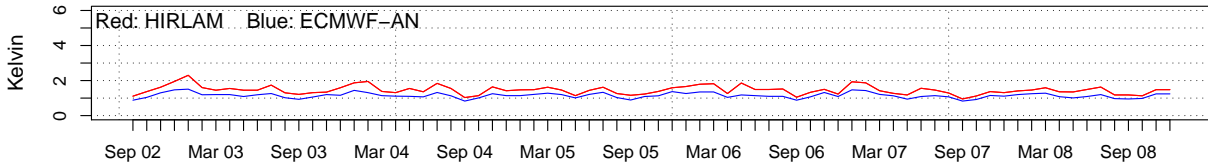
Figure A2.1.3. Time series (2002.09 2008.12) of respectively ME and RMSE for T2m based on 22 qualified stations.

## A2.2. Time series of all stations

**ME. Wind 10m. All stations. 2002.09–2008.12**
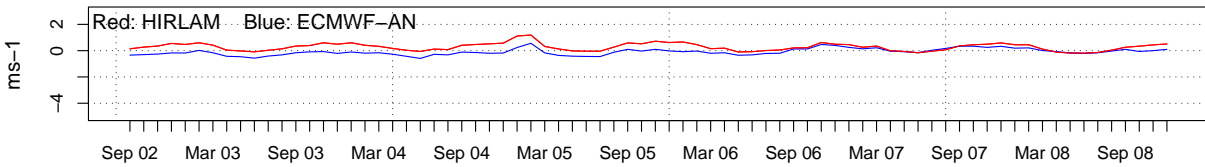
**RMSE. Wind 10m. All stations. 2002.09–2008.12**
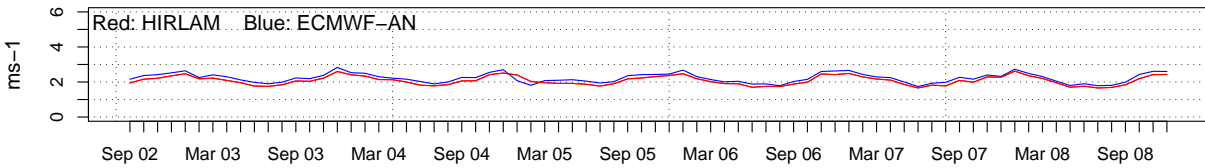
Figure A2.2.1 Time series (2002.09 2008.12) of respectively ME and RMSE for 10m wind based on 77l Norwegian stations.

**ME.  Pressure.  All stations.  2002.09–2008.12**
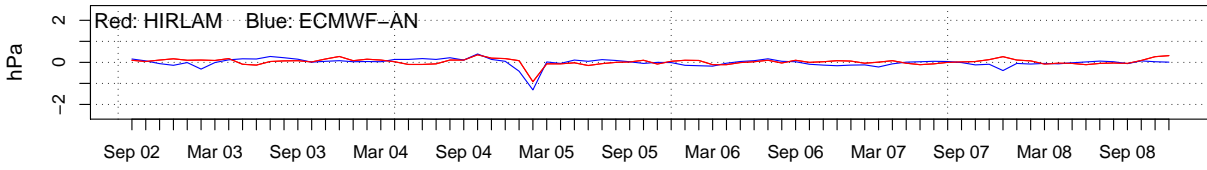


**RMSE.  Pressure.  All stations.  2002.09–2008.12**
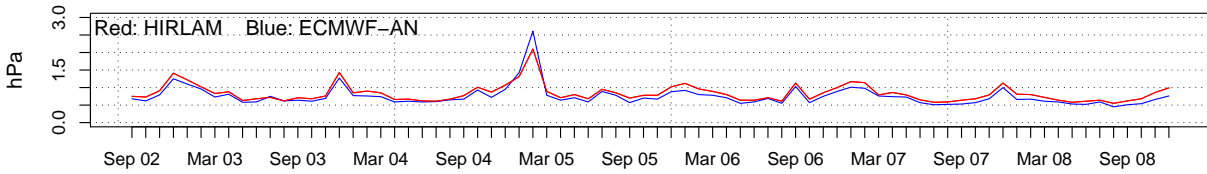


Figure A2.2.2 Time series (2002.09  2008.12) of respectively ME and RMSE for MSLP based on 77l Norwegian stations.

**ME.  Temperature 2m.  All stations.  2002.09–2008.12**
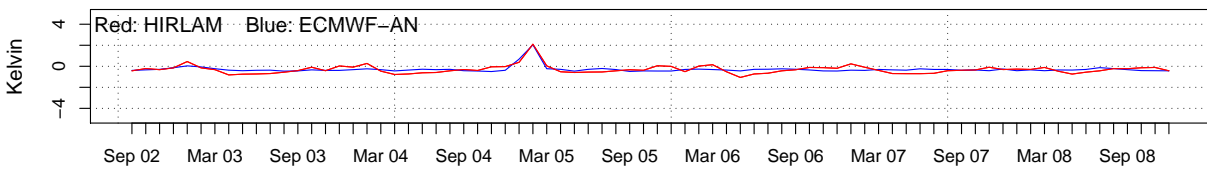


**RMSE.  Temperature 2m.  All stations.  2002.09–2008.12**
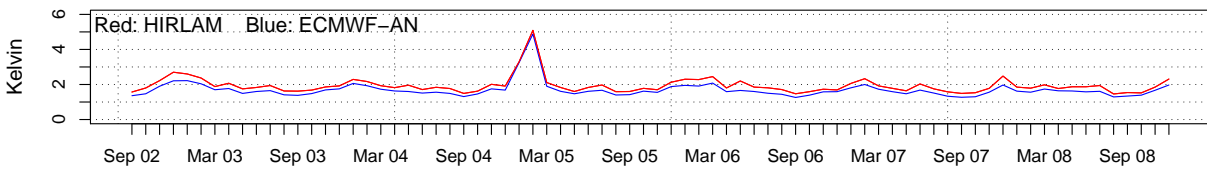


Figure A2.2.3 Time series (2002.09  2008.12) of respectively ME and RMSE for T2m based on 77 Norwegian stations.

## A2.3.  Time series coastal stations

**ME. Wind 10m. Coastal stations. 2002.09–2008.12**
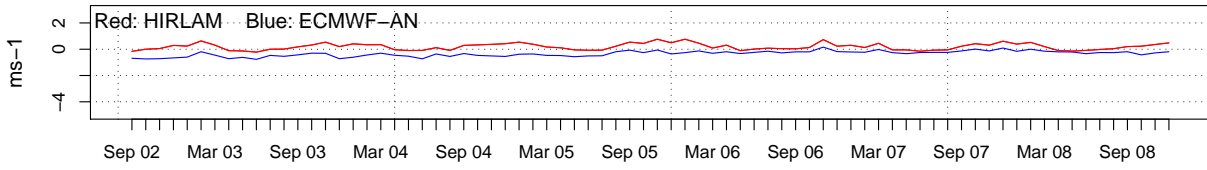


**RMSE. Wind 10m. Coastal stations. 2002.09–2008.12**
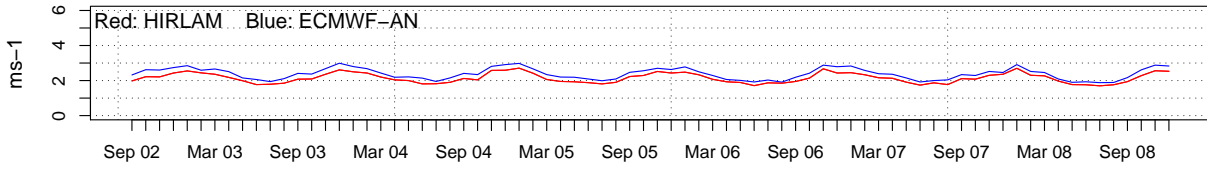


Figure A2.3.1 Time series (2002.09  2008.12) of respectively ME and RMSE for T2m based on coastal stations.

**ME. Pressure. Coastal stations. 2002.09–2008.12**
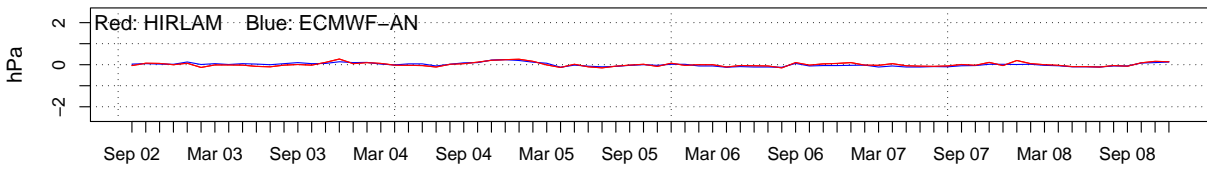


**RMSE. Pressure. Coastal stations. 2002.09–2008.12**
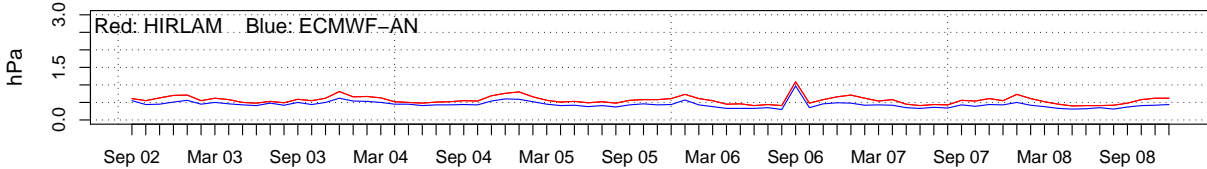


Figure A2.3.2 Time series (2002.09  2008.12) of respectively ME and RMSE for MSLP based on coastal stations.

**ME.  Temperature 2m.  Coastal stations.  2002.09–2008.12**
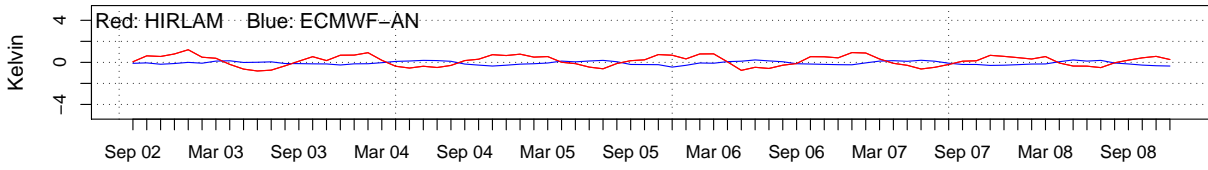


**RMSE.  Temperature 2m.  Coastal stations.  2002.09–2008.12**
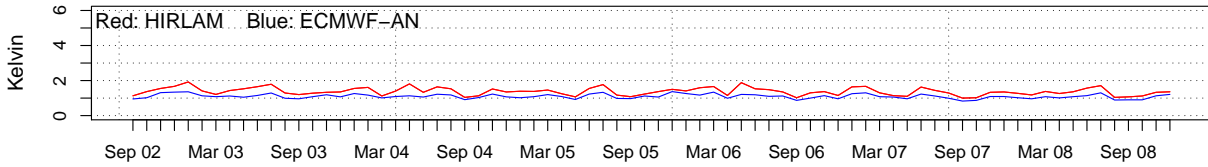


Figure A2.3.3 Time series (2002.09  2008.12) of respectively ME and RMSE for T2m based on coast stations.

## A2.4.  Time series of stations around Svalbard

**ME.  Wind 10m.  Svalbard.  2002.09–2008.12**
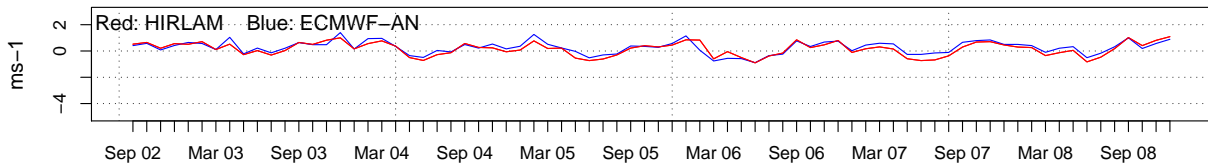


**RMSE.  Wind 10m.  Svalbard.  2002.09–2008.12**
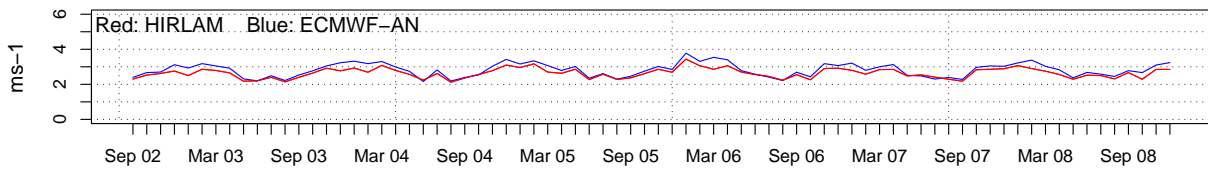


Figure A2.4.1. Time series (2002.09  2008.12) of respectively ME and RMSE for 10m wind speed based on stations around Svalbard.

**ME. Pressure. Svalbard. 2002.09–2008.12**
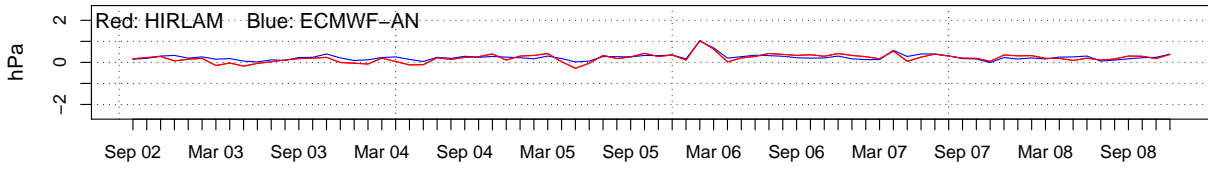


**RMSE. Pressure. Svalbard. 2002.09–2008.12**
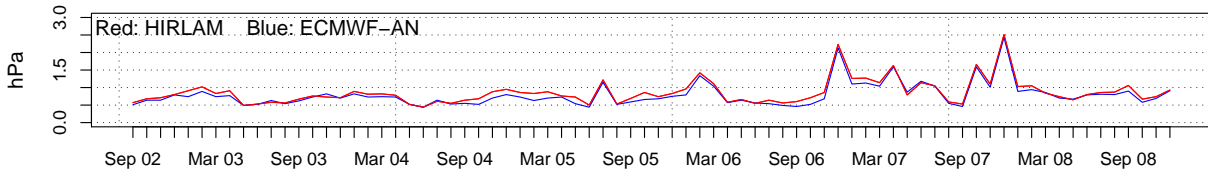


Figure A2.4.2. Time series (2002.09  2008.12) of respectively ME and RMSE for MSLP based on stations around Svalbard.

**ME. Temperature 2m. Svalbard. 2002.09–2008.12**
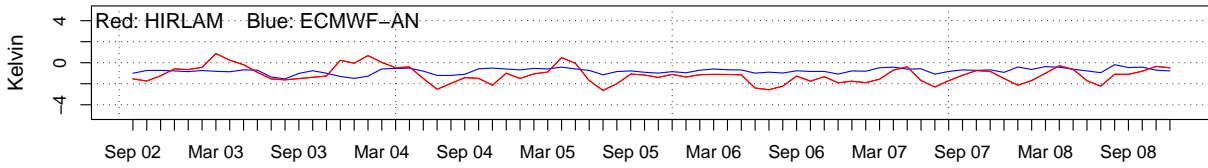


**RMSE. Temperature 2m. Svalbard. 2002.09–2008.12**
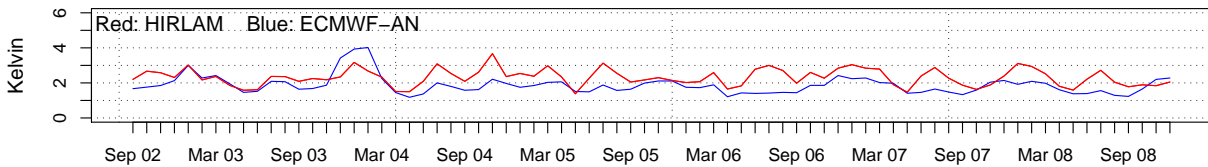


Figure A2.4.3. Time series (2002.09  2008.12) of respectively ME and RMSE for T2m based on stations around Svalbard.

## A2.5.  Time series of stations in the Eastern Norwegian Sea

68

**ME.  Wind 10m.  Draugen, Heidrun and Norne.  2002.09–2008.12**
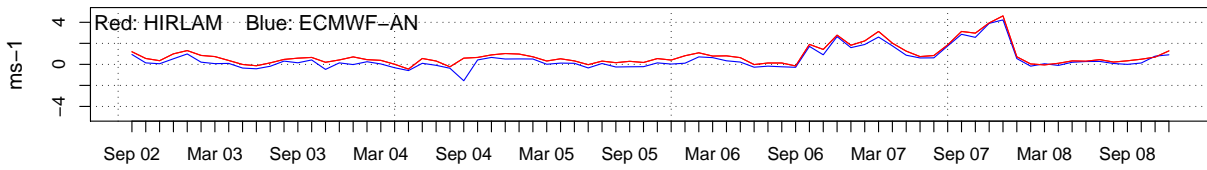


**RMSE.  Wind 10m.  Draugen, Heidrun and Norne.  2002.09–2008.12**
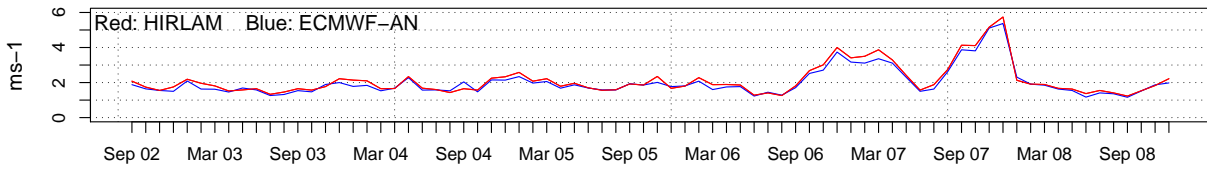


Figure A2.5.1. Time series (2002.09  2008.12) of respectively ME and RMSE for 10m wind speed based on the stations Draugen, Heidrun and Norne.

**ME.  Pressure.  Draugen, Heidrun and Norne.  2002.09–2008.12**
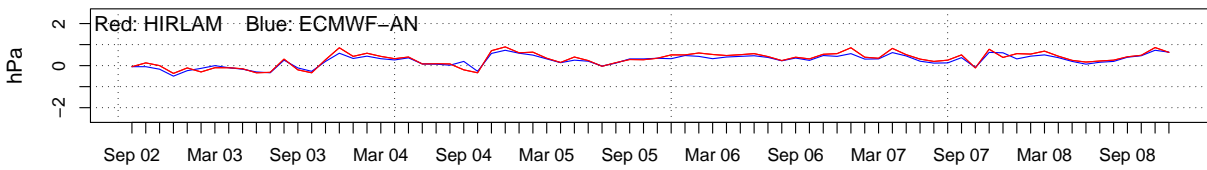


**RMSE.  Pressure.  Draugen, Heidrun and Norne.  2002.09–2008.12**
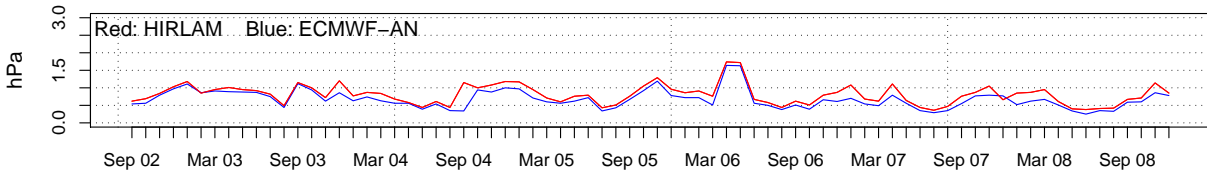


Figure A2.5.2. Time series (2002.09  2008.12) of respectively ME and RMSE for MSLP based on the stations Draugen, Heidrun and Norne.

**ME.  Temperature 2m.  Draugen, Heidrun and Norne.  2002.09–2008.12**

Red: HIRLAM    Blue: ECMWF–AN

Kelvin

Sep 02   Mar 03   Sep 03   Mar 04   Sep 04   Mar 05   Sep 05   Mar 06   Sep 06   Mar 07   Sep 07   Mar 08   Sep 08

**RMSE.  Temperature 2m.  Draugen, Heidrun and Norne.  2002.09–2008.12**

Red: HIRLAM    Blue: ECMWF–AN

Kelvin

Sep 02   Mar 03   Sep 03   Mar 04   Sep 04   Mar 05   Sep 05   Mar 06   Sep 06   Mar 07   Sep 07   Mar 08   Sep 08
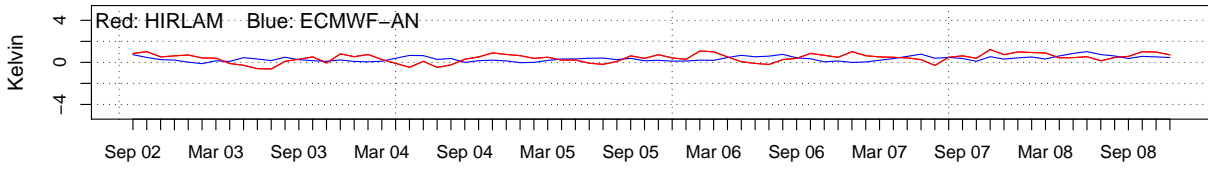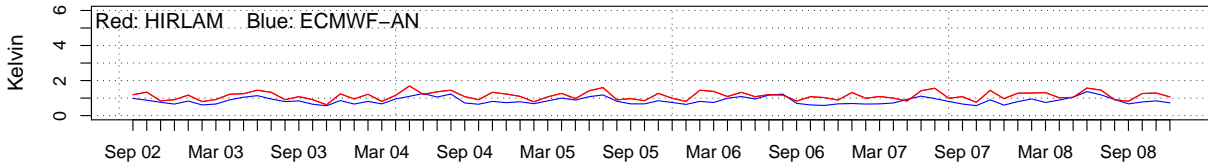
Figure A2.5.3. Time series (2002.09  2008.12) of respectively ME and RMSE for T2m based on the stations Draugen, Heidrun and Norne.

## A2.6.  Time series of North Sea stations

**ME.  Wind 10m.  North Sea.  2002.9–2008.12**

Red: HIRLAM    Blue: ECMWF–AN

ms−1

Sep 02   Mar 03   Sep 03   Mar 04   Sep 04   Mar 05   Sep 05   Mar 06   Sep 06   Mar 07   Sep 07   Mar 08   Sep 08

**RMSE.  Wind 10m.  North Sea.  2002.09–2008.12**

Red: HIRLAM    Blue: ECMWF–AN

ms−1

Sep 02   Mar 03   Sep 03   Mar 04   Sep 04   Mar 05   Sep 05   Mar 06   Sep 06   Mar 07   Sep 07   Mar 08   Sep 08
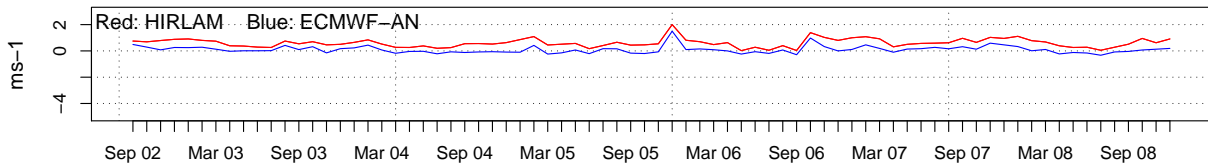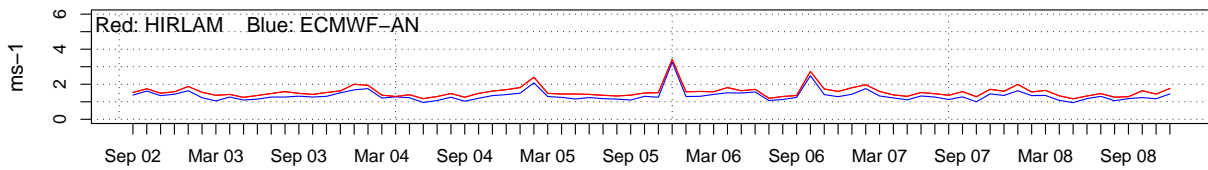
Figure A2.6.1. Time series (2002.09  2008.12) of respectively ME and RMSE for 10m wind speed based on the stations in the North Sea.

**ME. Pressure. North Sea. 2002.09–2008.12**
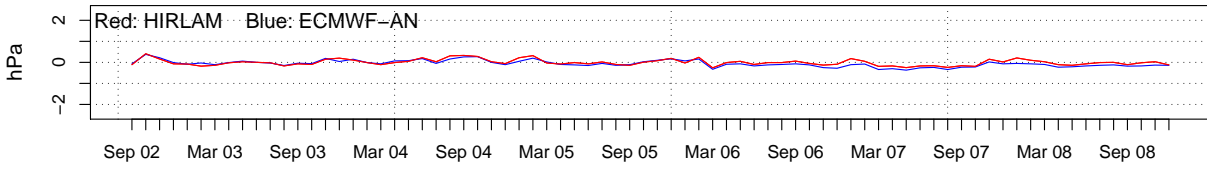


**RMSE. Pressure. North Sea. 2002.09–2008.12**
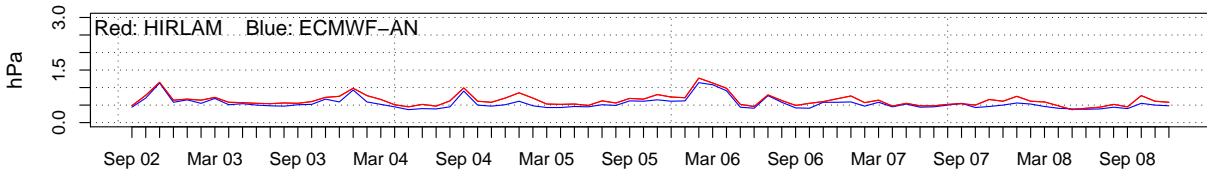


Figure A2.6.2. Time series (2002.09 2008.12) of respectively ME and RMSE for MSLP based on the stations in the North Sea.

**ME. Temperature 2m. North Sea. 2002.09–2008.12**
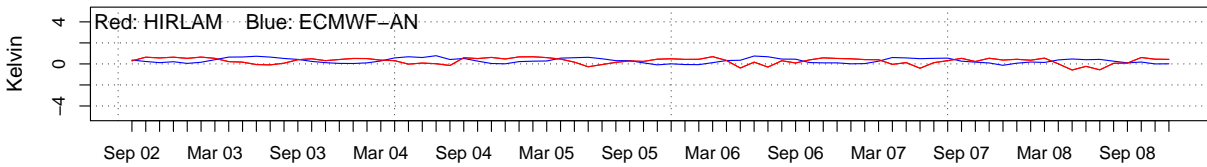


**RMSE. Temperature 2m. North Sea. 2002.09–2008.12**
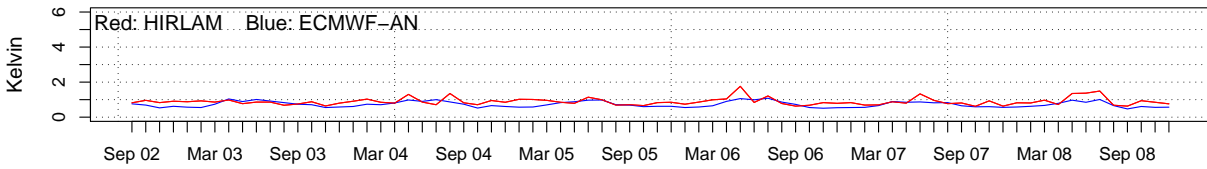


Figure A2.6.3. Time series (2002.09 2008.12) of respectively ME and RMSE for T2m based on the stations in the North Sea.

## A2.7. Statistical measures at selected stations

| *Stnr* | *H10* | *H10* | *H10* | *EC-analyse* | *EC-analyse* | *EC-analyse* |
|---|---|---|---|---|---|---|
| | ME | RMSE | COR | ME | RMSE | COR |
| 1001 | 1.19 | 3.20 | 0.75 | 0.77 | 3.01 | 0.75 |
| 1033 | 0.75 | 2.56 | 0.77 | 0.14 | 2.39 | 0.78 |

| | | | | | | |
|---|---|---|---|---|---|---|
| 1055 | -0.95 | 2.75 | 0.84 | -1.52 | 2.94 | 0.85 |
| 1078 | 0.02 | 2.28 | 0.83 | -0.73 | 2.49 | 0.82 |
| 1089 | 0.12 | 1.59 | 0.79 | -1.19 | 1.98 | 0.81 |
| 1098 | -0.88 | 2.35 | 0.79 | 0.35 | 2.10 | 0.81 |
| 1115 | -0.13 | 2.25 | 0.86 | -1.62 | 2.78 | 0.85 |
| 1152 | -1.87 | 3.08 | 0.71 | -2.04 | 3.24 | 0.69 |
| 1160 | -0.04 | 2.63 | 0.72 | -0.16 | 2.64 | 0.72 |
| 1205 | -0.28 | 2.79 | 0.84 | -4.69 | 6.85 | 0.19 |
| 1241 | 0.19 | 2.01 | 0.82 | -2.80 | 4.27 | 0.37 |
| 1262 | -1.36 | 2.64 | 0.87 | 2.37 | 3.28 | 0.88 |
| 1271 | -0.57 | 2.05 | 0.63 | -1.07 | 2.15 | 0.69 |
| 1384 | -0.19 | 1.33 | 0.73 | -0.11 | 1.39 | 0.69 |
| 1403 | -0.73 | 1.95 | 0.91 | -1.59 | 2.44 | 0.91 |
| 1415 | 1.05 | 2.07 | 0.82 | 1.07 | 2.20 | 0.79 |
| 1427 | 0.40 | 1.97 | 0.85 | -0.12 | 2.10 | 0.81 |
| 1436 | -0.96 | 2.55 | 0.85 | -1.23 | 2.87 | 0.82 |
| 1448 | -0.04 | 2.02 | 0.81 | -0.47 | 2.27 | 0.77 |
| 1200 | 0.20 | 1.77 | 0.91 | -0.19 | 2.07 | 0.88 |
| 1201 | 1.80 | 3.24 | 0.80 | 1.48 | 3.26 | 0.76 |
| 1202 | 0.65 | 1.94 | 0.91 | 0.15 | 2.14 | 0.88 |
| 1400 | 0.70 | 1.56 | 0.94 | 0.19 | 1.40 | 0.94 |
| 1401 | 0.58 | 1.60 | 0.94 | 0.01 | 1.38 | 0.95 |
| 1402 | 0.49 | 1.42 | 0.95 | -0.08 | 1.25 | 0.96 |

Table A2.1 Table given the statistical measures of mean error, root mean square error and the correlation for 10m wind speed at a selection of stations.

| St | OBS T100 | OBS T99 | OBS T95 | OBS T90 | H10 T100 | H10 T99 | H10 T95 | H10 T90 | EC T100 | EC T99 | EC T95 | EC T90 |
|---|---|---|---|---|---|---|---|---|---|---|---|---|
| 1001 | 25.7 | 19.0 | 14.4 | 12.3 | 24.3 | 19.1 | 15.1 | 13.3 | 22.7 | 18.1 | 14.4 | 12.7 |
| 1033 | 23.2 | 17.0 | 12.9 | 10.8 | 21.2 | 15.9 | 12.9 | 11.1 | 19.1 | 14.9 | 11.8 | 10.3 |
| 1055 | 31.9 | 21.1 | 17.5 | 15.4 | 25.5 | 18.1 | 14.8 | 13.0 | 22.9 | 16.4 | 13.8 | 12.1 |
| 1078 | 27.3 | 18.5 | 14.4 | 12.9 | 23.6 | 16.6 | 13.5 | 12.0 | 21.3 | 14.9 | 12.3 | 10.8 |
| 1089 | 22.1 | 12.9 | 9.8 | 8.2 | 14.7 | 10.9 | 8.8 | 7.7 | 11.7 | 8.3 | 6.6 | 5.8 |
| 1098 | 21.6 | 16.5 | 12.9 | 11.3 | 18.4 | 12.8 | 10.5 | 9.3 | 19.6 | 14.6 | 12.4 | 11.0 |
| 1115 | 28.3 | 19.5 | 15.9 | 13.9 | 25.2 | 19.0 | 15.3 | 13.5 | 20.0 | 16.0 | 12.8 | 11.3 |
| 1152 | 24.2 | 15.9 | 12.9 | 11.3 | 18.2 | 12.0 | 9.3 | 7.9 | 16.4 | 11.5 | 9.1 | 7.7 |
| 1160 | 25.7 | 17.0 | 12.9 | 11.3 | 24.6 | 17.2 | 13.0 | 10.9 | 23.7 | 16.4 | 13.3 | 11.1 |
| 1205 | 30.9 | 22.1 | 17.5 | 14.9 | 25.9 | 19.3 | 16.0 | 13.9 | 10.5 | 7.8 | 6.5 | 5.6 |
| 1241 | 24.2 | 16.5 | 12.3 | 10.8 | 23.4 | 15.8 | 12.2 | 10.7 | 12.3 | 7.7 | 6.2 | 5.5 |
| 1262 | 27.3 | 21.6 | 17.5 | 15.4 | 24.8 | 17.9 | 14.8 | 13.0 | 22.1 | 15.7 | 13.0 | 11.5 |
| 1271 | 19.0 | 12.3 | 8.7 | 7.2 | 12.1 | 7.6 | 6.1 | 5.3 | 11.0 | 7.0 | 5.6 | 4.8 |
| 1384 | 14.9 | 8.7 | 6.7 | 5.7 | 9.5 | 6.9 | 5.4 | 4.8 | 10.7 | 7.3 | 5.6 | 4.9 |
| 1403 | 26.8 | 20.1 | 15.9 | 14.4 | 22.8 | 17.7 | 14.8 | 13.2 | 20.6 | 16.2 | 13.6 | 11.9 |

| 1415 | 18.5 | 12.9 | 9.8 | 8.7 | 19.6 | 14.0 | 11.1 | 9.7 | 19.4 | 13.4 | 11.3 | 9.8 |
| 1427 | 21.1 | 15.9 | 12.9 | 11.3 | 19. | 15.2 | 12.7 | 11.3 | 17.5 | 13.6 | 11.7 | 10.5 |
| 1436 | 30.9 | 19.0 | 15.4 | 12.3 | 22.1 | 15.3 | 12.9 | 11.3 | 19.9 | 14.3 | 12.2 | 10.8 |
| 1448 | 19.5 | 14.9 | 12.3 | 10.8 | 19.1 | 14.0 | 11.7 | 10.5 | 18.9 | 12.9 | 10.8 | 9.8 |
| | | | | | | | | | | | | |
| 1200 | 24.8 | 19.7 | 16.2 | 14.5 | 25.6 | 19.7 | 16.4 | 14.7 | 22.5 | 18.4 | 15.7 | 14.0 |
| 1201 | 25.7 | 19.5 | 14.9 | 12.8 | 26.7 | 19.5 | 16.4 | 14.7 | 25.5 | 19.1 | 15.8 | 14.2 |
| 1202 | 26.5 | 19.4 | 15.8 | 14.1 | 26.4 | 19.1 | 16.3 | 14.6 | 24.4 | 18.3 | 15.5 | 13.8 |
| 1400 | 24.1 | 18.9 | 15.6 | 13.7 | 26.1 | 19.6 | 16.4 | 14.7 | 24.6 | 18.3 | 15.5 | 13.8 |
| 1401 | 24.2 | 19.5 | 15.9 | 13.9 | 27.7 | 19.9 | 16.5 | 14.6 | 25.8 | 18.5 | 15.5 | 13.5 |
| 1402 | 26.5 | 20.1 | 16.2 | 14.3 | 25.7 | 20.9 | 16.9 | 15.0 | 23.9 | 19.6 | 16.1 | 14.2 |

Table A2.2. 100, 99, 95 and 90 percentiles of 10 m wind speed at a selection of stations.

## A2.8. Quantile-quantile distributions
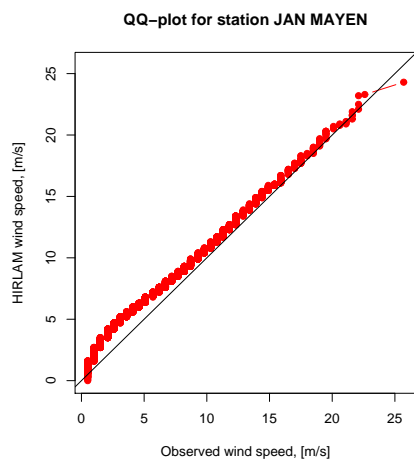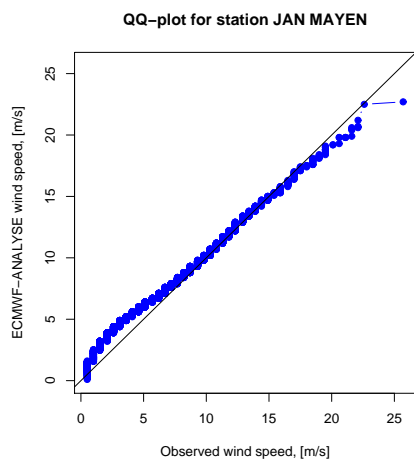
## QQ-plot for station FRUHOLMEN FYR
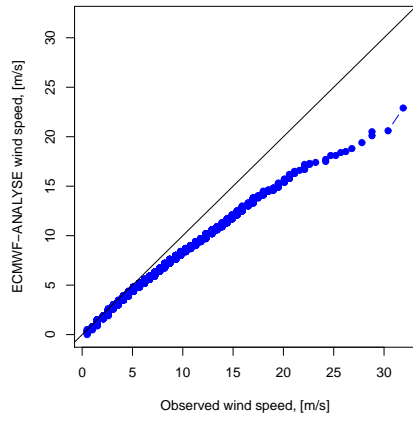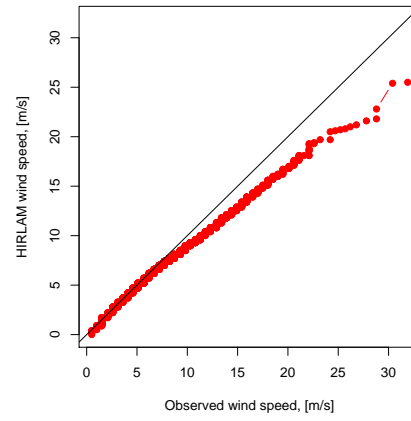
## QQ-plot for station FRUHOLMEN FYR

## QQ-plot for station NORNE
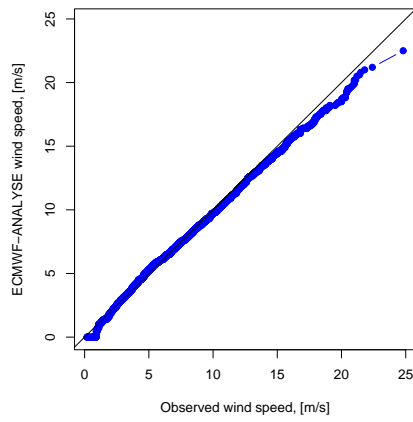
## QQ-plot for station NORNE
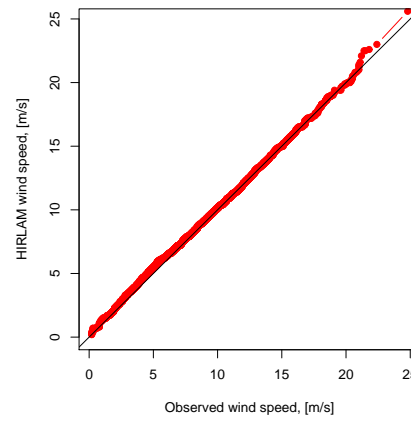
## QQ-plot for station DRAUGEN
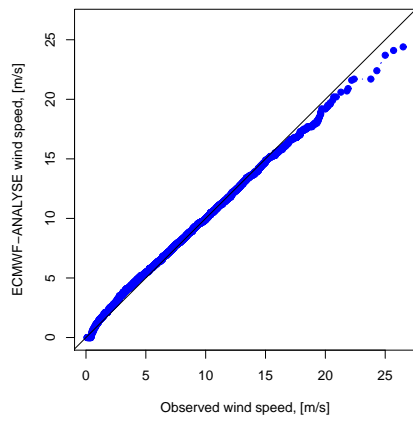
## QQ-plot for station DRAUGEN
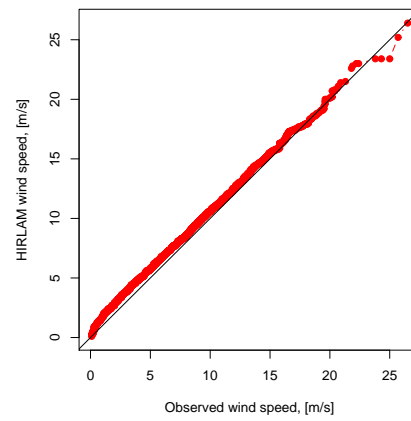
## QQ-plot for station EKOFISK
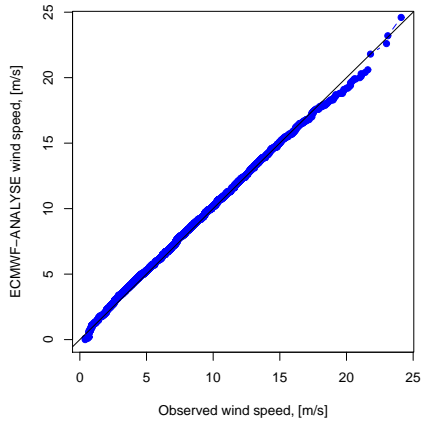
## QQ-plot for station EKOFISK
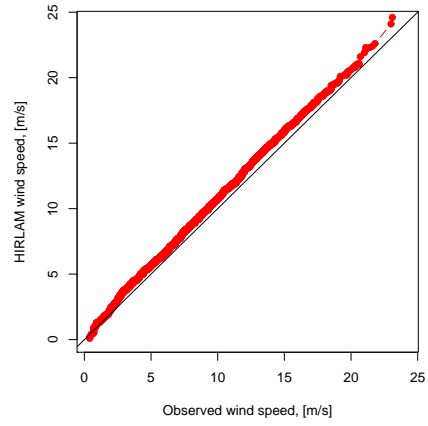
## QQ-plot for station SLEIPNER A

## QQ-plot for station SLEIPNER A